VOLUME 35 MARCH 1957 NUMBER 3

Canadian Journal of Physics

Published by THE NATIONAL RESEARCH COUNCIL
OTTAWA CANADA

CANADIAN JOURNAL OF PHYSICS

(*Formerly Section A, Canadian Journal of Research*)

Under the authority of the Chairman of the Committee of the Privy Council on Scientific and Industrial Research, the National Research Council issues THE CANADIAN JOURNAL OF PHYSICS and six other journals devoted to the publication, in English or French, of the results of original scientific research. Matters of general policy concerning these journals are the responsibility of a joint Editorial Board consisting of: members representing the National Research Council of Canada; the Editors of the Journals; and members representing the Royal Society of Canada and four other scientific societies.

Manuscripts for publication should be submitted to Dr. Léo Marion, Editor-in-Chief, Canadian Journal of Physics, National Research Council, Ottawa 2, Canada.

(For instructions on preparation of copy, see **Notes to Contributors** (inside back cover).)

Proof, correspondence concerning proof, and orders for reprints should be sent to the Manager, Editorial Office (Research Journals), Division of Administration, National Research Council, Ottawa 2, Canada.

Subscriptions, renewals, requests for single or back numbers, and all remittances should be sent to Division of Administration, National Research Council, Ottawa 2, Canada. Remittances should be made payable to the Receiver General of Canada, credit National Research Council.

The journals published, frequency of publication, and prices are:

Canadian Journal of Biochemistry and Physiology	Monthly	$3.00 a year
Canadian Journal of Botany	Bimonthly	$4.00 a year
Canadian Journal of Chemistry	Monthly	$5.00 a year
Canadian Journal of Microbiology	Bimonthly	$3.00 a year
Canadian Journal of Physics	Monthly	$4.00 a year
Canadian Journal of Technology	Bimonthly	$3.00 a year
Canadian Journal of Zoology	Bimonthly	$3.00 a year

The price of single numbers of all journals is 75 cents.

CORRECTION

Canadian Journal of Physics, Vol. 34.

p. 1151. In line 3, "$(\Delta B)_{\text{unperturbed}}$ a value *larger* than $(\Delta B)_{\text{perturbed}}$" should read "$(\Delta B)_{\text{unperturbed}}$ a value *smaller* than $(\Delta B)_{\text{perturbed}}$".

Canadian Journal of Physics, Vol. 34.

In *Nuclear magnetic resonance and electronic structure of conductors* by N. Bloembergen, pp. 1299–1314, a factor of one-half (1/2) has been erroneously omitted in the last term of equation (2). The discussion on page 1303 has to be modified correspondingly. The use of somewhat better values for the constants occurring in equations (2) and (3) leads to a vibrational change of the Knight shift between 200° K. and 350° K. of 0.6%, rather than 2.1% as quoted. The good agreement with the observed vibrational change of 1.5% is therefore lost.

The author is indebted to Dr. G. B. Benedek for calling his attention to the error.

Canadian Journal of Physics, Vol. 33.

In *Capture radiation and neutrons from the bombardment of C^{13} with protons* by G. A. Bartholomew, F. Brown, H. E. Gove, A. E. Litherland, and E. B. Paul, pp. 441–456, the following corrections should be noted. For the resonance at $E_p = 1.50$ Mev. in Table II the radiative yield should read 490 not 49 photons/10^{11} protons. The quantity θ_n^2 for the resonance at $E_p = 2.27$ Mev. in Table V should read 0.03 not 0.007. On page 452, in the 13th line from the bottom the first quantity in brackets should read $(\hbar^2/Ma^2)$ and in the 10th line from the bottom the first word should read Gordan.

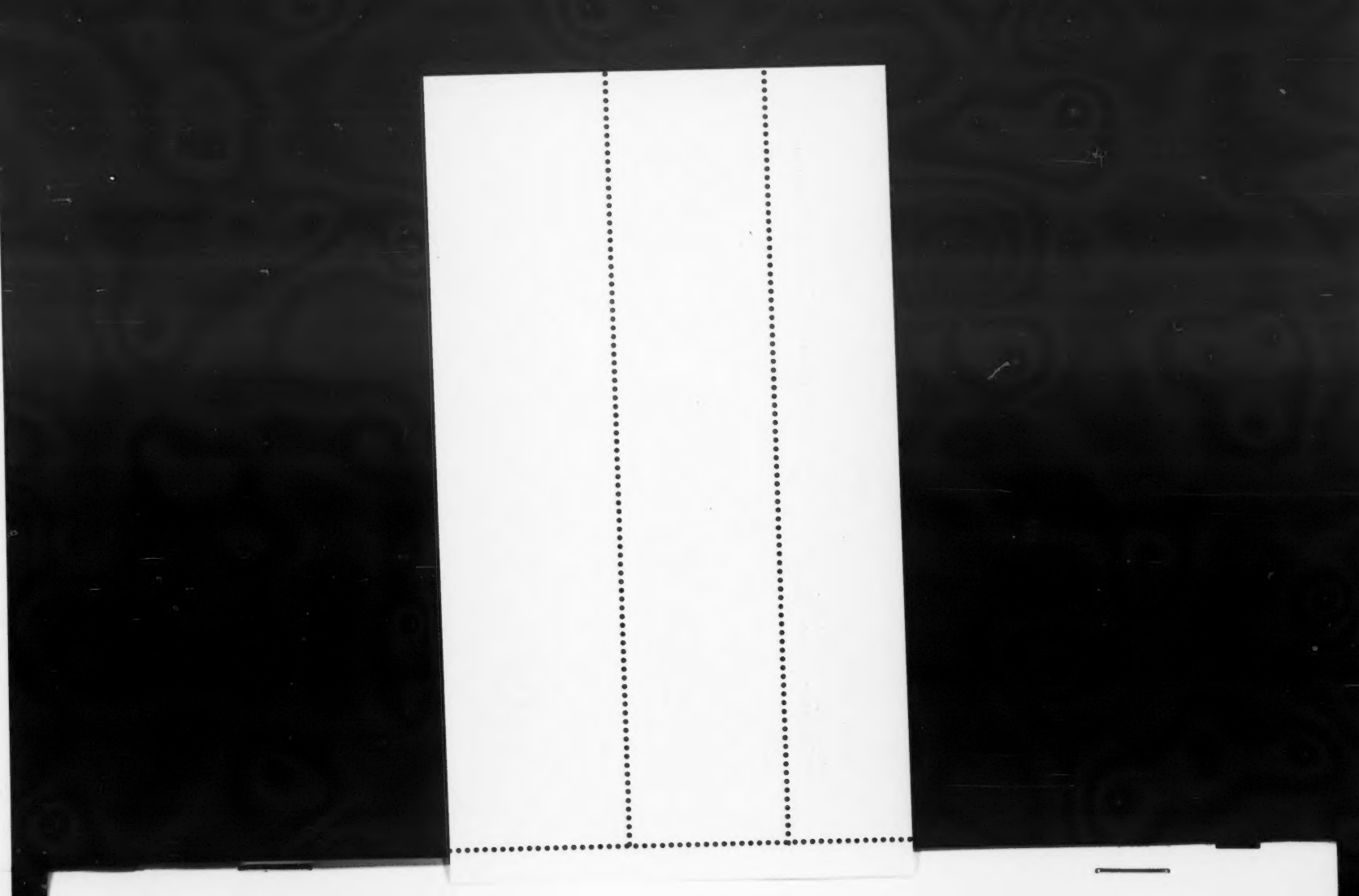

Canadian Journal of Physics

Issued by THE NATIONAL RESEARCH COUNCIL OF CANADA

VOLUME 35 MARCH 1957 NUMBER 3

A "FREE SPACE" ABSORPTION CELL FOR MICROWAVE SPECTROSCOPY[1]

C. C. COSTAIN

ABSTRACT

The absorption cell consists simply of a pyrex tube with a polystyrene lens and microwave horn at each end to couple to the standard microwave components. The lenses also serve as the vacuum windows. The attenuation at 8.5 mm. wavelength is 3.4 db. for a 250 cm. cell. Since there are no metal surfaces, this type of cell is very suitable for the investigation of reactive molecules. It can readily be employed in a high temperature microwave spectrometer for the investigation of corrosive substances with low vapor pressures, or in a Zeeman modulation spectrometer for the study of free radicals.

I. INTRODUCTION

Many polar molecules which decompose in contact with metal surfaces are comparatively stable in a glass vessel at the same temperature. The microwave spectra of a few of these molecules have been studied with microwave spectrometers using specially designed glass or quartz absorption cells. In the spectrometer used by Dousmanis, Sanders, and Townes (1955) to measure the spectrum of the OH radical, contact between the gas and metal surfaces was eliminated by inserting a liner of low-loss glass in the cylindrical waveguide absorption cell. A different design was employed by Meschi and Myers (1956), who used a quartz dielectric waveguide to obtain the microwave spectrum of the reactive S_2O molecule. In both of these designs, however, there is a considerable loss of power in the absorption cell, and the loss appreciably reduces the spectrometer sensitivity. This is particularly undesirable in a spectrometer used for the study of reactive molecules since, in general, the partial pressure of such molecules will be very low.

In this paper a new type of microwave absorption cell is described which is entirely free of metals and yet has less attenuation than the normal silver waveguide. Thus the cell may be employed in a microwave spectrometer without reducing the sensitivity and should be very useful for the investigation of reactive molecules.

II. CELL DESIGN

A photograph of the new microwave absorption cell is shown in Fig. 1. The body of the cell consists simply of a standard length of pyrex tubing.

[1]Manuscript received October 1, 1956.
Contribution from the Division of Pure Physics, National Research Council, Ottawa, Ontario.
Issued as N.R.C. No. 4194.

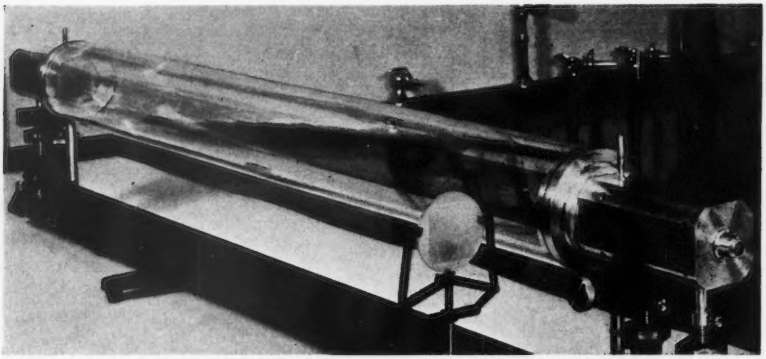

FIG. 1. A photograph of the "free space" absorption cell designed for the 8 mm. region.

The microwave energy is fed into one end of the pyrex tubing by means of a microwave horn and polystyrene lens and is taken from the tubing at the other end by a similar lens and horn. In addition to forming part of the microwave optical system, the lenses serve very conveniently as the vacuum windows of the cell (Fig. 2). The end flanges supporting the lenses may also be made of polystyrene.

The horns in the cell, which has been designed for the 8 mm. region, start with RG 96 waveguide (dimensions 0.280 in.×0.140 in.) and taper first for 1 in. to a 0.280 in.×0.280 in. square cross-section. From this point the horns taper symmetrically over a 6 in. run to a 2 in. square aperture.

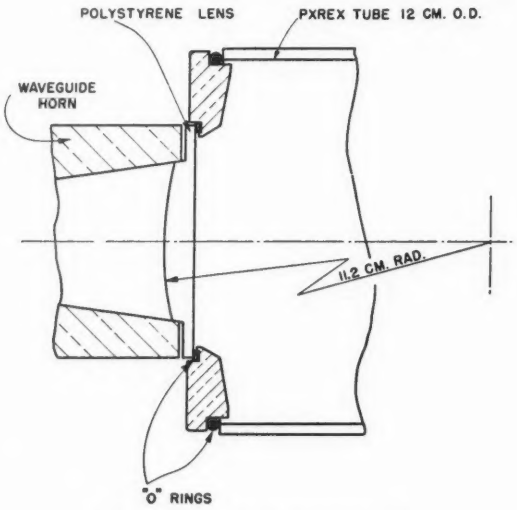

FIG. 2. End mount of absorption cell.

The polystyrene lenses are plano-convex. The convex surface is spherical and is shaped to fit into the square aperture of the horn. The radius of curvature R of the convex surface was calculated from the simple optical formula $1/f = (n-1)/R$, where f is the focal length and n the index of refraction. The focal length was made equal to the distance from the aperture to the convergence point of the symmetrical taper of the horn. The material used for the lenses is Polypenco Q–200, a form of polystyrene which is readily machined and which has a dielectric constant of 2.61.

The normal reflection of power from each of the lens's dielectric surfaces, which is about 5.5% for polystyrene, can be greatly reduced by a blooming technique described by Culshaw (1953) in which rectangular grooves are machined in the lens surface to make a quarter wavelength matching medium of intermediate dielectric constant. To bloom the lens for a wavelength of 8.5 mm., grooves 0.066 cm. wide and 0.165 cm. deep were milled in the faces of the lens at 0.107 cm. intervals. This makes a surface layer with an average dielectric constant of $\sqrt{2.61}$ and with a depth which is a quarter of the wavelength in this layer. The best performance is obtained with the grooves parallel to the electric vector of the r-f. field.

The tubing used is standard laboratory pyrex in approximately 125 cm. lengths, with the diameter selected to give maximum transmission. The optimum diameter for $\lambda = 8.5$ mm. was found to be 11.3 cm. (nominal 12 cm. O.D. tubing).

Throughout this paper reference is made only to pyrex tubing which has been used for the initial tests. There is no reason why other extruded glass tubing may not be used in applications where specific temperature or optical transmission requirements are to be met. It is necessary that the inside wall be smooth and that the tubing have a fairly uniform cross-section.

III. TRANSMISSION CHARACTERISTICS

The total attenuation, including that of the horns and lenses which contribute 0.8 db., is 2.4 db. for the 125 cm. cell. The transmission loss when the pyrex tube is removed is 15 db. The pyrex tube is therefore very effective in focusing the radiation into the receiving lens and horn. The distribution of the r-f. power at the end of the 125 cm. tube was measured using an RG 96 waveguide as a probe and is plotted in Fig. 3.

Since the image of the source is so well formed at the end of the cell, this image can act as a source for a second 125 cm. tube. This length was added to the cell and gave an attenuation for the 250 cm. cell of 3.4 db. Thus the additional length added an attenuation of only 1 db. The curves for the power distribution across the end of the 250 cm. cell in both the horizontal and vertical planes lie between the two curves in Fig. 3. Therefore, the cell may be made longer, if desired, without excessive loss. However, in order that the receiving horn may be placed at a node in the transmission pattern, the length must be increased in units of 125 cm. for the present cell. It is shown later that the choice of 125 cm. for the unit length is arbitrary but convenient.

The function of the horn and lens is to confine the radiation to a narrow

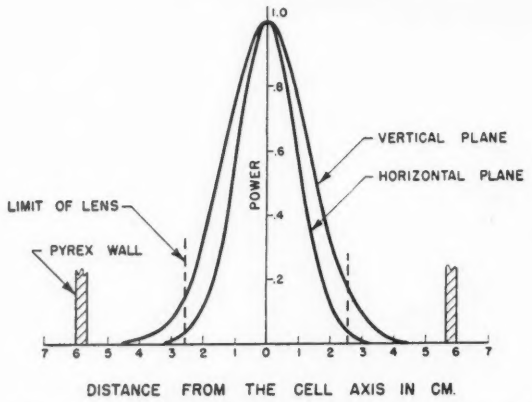

FIG. 3. Power distribution across the end of the 125 cm. cell.

beam and thus make the angle of incidence on the glass sufficiently close to grazing incidence to give a large reflection coefficient. Since the beam width is inversely proportional to the aperture, this requirement involves a compromise between the size of the components and a transmission that is acceptable. The following calculations show that the present cell is near the minimum size acceptable for 8.5 mm. waves.

The TE_{10} mode in the rectangular waveguide is retained in the horn, but the wavefront becomes spherical with an apparent source at the apex of the symmetrical pyramid. The lens in the aperture of the horn converts this front to a plane wave with a field uniform in the vertical direction (the plane of polarization) and having cosine distribution in the horizontal plane.

The diffraction pattern from an aperture with this illumination can be calculated for the far zone or Fraunhofer region.[2] The pattern characteristics are listed in Table I, in which $u = (\pi a/\lambda) \sin\theta$, a is the aperture, and θ the angle from the axis.

TABLE I

CHARACTERISTICS OF THE FRAUNHOFER DIFFRACTION PATTERN OF THE MICROWAVE HORN AND LENS

	Polar diagram	Total width at half power	First zero
Vertical plane	$\dfrac{\sin u}{u}$	$0.88\lambda/a$ radians $= 8.4°$	$\lambda/a = 9.5°$
Horizontal plane	$\dfrac{\cos u}{1-4u^2/\pi^2}$	$1.2\lambda/a = 11.4°$	$1.5\lambda/a = 14.3°$

The minimum distance from the aperture at which the field may be assumed to be in the Fraunhofer region is given by a^2/λ, and is approximately 30 cm. in this instance. At this distance in front of the lens, the pyrex tubing wall

[2]See, for example, Radiation Laboratory Series, Vol. 12 (McGraw-Hill Book Company Inc., 1948), p. 187.

subtends an angle of 10.5° at the center of the aperture. This angle of 10.5° is beyond the first zero of the Fraunhofer diffraction pattern in the vertical plane and below 1/10 power level in the horizontal plane. It is then reasonable to assume that the aperture is radiating into free space and that the Fraunhofer diffraction pattern is substantially correct. It was this characteristic that led to the designation of "free space" cell, which is admittedly a slight exaggeration as well as a contradiction in terms.

In a vertical plane through the cell axis the electric vector is perpendicular to the glass and the reflection coefficient is given by

$$R_v = \tan(i-r)/\tan(i+r)$$

where i is the angle of incidence and r is the angle of refraction. For a dielectric constant of the glass between 4 and 5, $R_v \approx 0.7$ for the half power angle of 4.2° (Table I). Since a fraction $(0.7)^2$ of the power is reflected, approximately half of the power is lost through the glass for this angle of incidence. For more oblique incidence R_v becomes larger so that less than one-half of the power incident in the vertical plane is lost.

In the horizontal plane with the electric vector parallel to the glass,

$$R_p = \sin(i-r)/\sin(i+r).$$

For the half-power angle of 5.7°, $R_p \approx 0.9$ so that less than one-fifth of the power incident in the horizontal plane is lost.

Since part of the power reaches the lens directly without reflection, less than one-quarter of the total power (1.25 db. attenuation) should be lost through the glass walls. This figure ignores the power in the side lobes beyond the first zero, which is incident at a more acute angle and will be almost entirely lost. This is consistent with a measured attenuation of 1.6 db. for the first 125 cm. length and 1.0 db. for the second.

The pyrex tube can be considered to act as a light guide, rather than a normal waveguide, with the symmetrical specular reflection of the diverging beam by the tube walls causing the radiation to converge into the receiving horn. Since the angle of incidence is greater than the Brewster angle, there is a phase reversal of the reflected wave which is independent of the polarization. Therefore, the field at the glass nearly vanishes when the reflection coefficient is large. When the diameter of the tube and the distance between the lenses is such that the path difference between the reflected and direct wave is $\lambda/2$, the waves reinforce at the lens. The tube diameter required to give this path difference of $\lambda/2$ for an axial ray is given by

$$D = \sqrt{\lambda L} \tag{1}$$

where L is the length of the tube. Experimentally it was found that the optimum diameter was given by

$$D = \sqrt{1.2\lambda L}. \tag{2}$$

Therefore, it is apparent that the concepts of a point source and polar diagram, which are characteristic of the Fraunhofer diffraction region, are not adequate to explain quantitatively the diffraction pattern that is produced. Since off-

axis effects and variations of the reflection coefficients have not been considered, it is not surprising that no quantitative agreement can be found. The approximate optical explanation does, however, serve as a very useful guide in the designing of this type of cell.

While the minimum attenuation is obtained with cell dimensions which satisfy equation (2), the attenuation does not vary rapidly when any of the parameters are changed. The performance of a cell of given dimensions is quite satisfactory over a 20% band of wavelengths. Therefore a 10% latitude in D is allowed, and a tube of suitable diameter may be selected from the stock sizes of large diameter tubing. The choice of 125 cm. for the unit length of the cell is, of course, arbitrary, but again it is very convenient to use the large tubing in the lengths normally available.

It is interesting to compare the transmission of the glass tube with that of a brass tube of the same diameter. The brass tube has an attenuation of 9 db. for a 125 cm. cell, and 3 db. for a 250 cm. cell. The difference in behavior can be explained by the fact that there is no phase reversal on reflection from a conducting surface for the perpendicular component of the electric vector. Therefore, a cell of twice the length with two reflections is required to give a path difference of λ.

The attenuation of the "free space" cell may be expected to decrease with decreasing wavelengths. For a constant aperture of the horn, the beam width is proportional to the wavelength. At more oblique incidence the reflection coefficients increase and less power will be lost through the glass. In one test made with the 250 cm. cell described previously, a loss of 2.9 db. was found for $\lambda = 8.0$ mm. as against the loss of 3.4 db. for $\lambda = 8.5$ mm.

IV. PERFORMANCE IN A MICROWAVE SPECTROMETER

The 125 cm. absorption cell has been tested in a source modulation spectrometer using a small 105 kc./sec. modulation voltage on the klystron reflector and a phase sensitive detector with 1 cycle/sec. bandwidth. The detector was followed by a differentiating circuit to filter out the low frequency signals arising from power reflections.

Several isotopic lines of the $J = 3 \leftarrow 2$ transition of OCS were recorded to measure the sensitivity of the spectrometer. A signal-to-noise ratio of 20 was obtained for the $O^{18}C^{12}S^{32}$ line. This line has an absorption coefficient of 3.2×10^{-7}/cm., so that a minimum detectable absorption coefficient for the spectrometer is about 3×10^{-8}/cm. The sensitivity of the present spectrometer can be increased by improvements in the display circuits and a large increase in sensitivity may be expected if molecular modulation is employed.

The large cross-section of the cell makes it possible to use a large input of microwave power without saturating the gas, but makes it impossible to apply large electric or magnetic fields. Molecular modulation methods are therefore limited either to molecules with a first-order Stark effect or to paramagnetic molecules with a "first-order" Zeeman effect. The latter class will include a large percentage of the molecules normally termed free radicals.

V. POSSIBLE APPLICATIONS

A high temperature spectrometer using a 250 cm. "free space" cell is being built in this laboratory for the study of corrosive substances with high boiling points. The substance to be studied will be introduced at the center of the cell and allowed to diffuse through a rare gas to the ends, which will be cooled. The sensitivity measurements indicate that it should be possible to obtain rotation lines with vapor pressures of about 10^{-2} microns.

The construction of another spectrometer is planned for the study of free radicals. Since the cell has no metal surfaces and has a large volume-to-surface ratio, conditions are very favorable for a long lifetime of the radicals. Almost any of the techniques used in the optical region for the continuous production of free radicals can be used with this cell. Flash photolysis or explosions are less suitable for the production of radicals for microwave studies since, for short-lived radicals, the wide bandwidth required drastically reduces the spectrometer sensitivity.

ACKNOWLEDGMENTS

The author is indebted to Dr. W. Culshaw and Dr. R. I. Primich for their advice on horn and lens design, and to Mr. B. W. Gibbs for many valuable suggestions during the course of this work.

REFERENCES

CULSHAW, W. 1953. Proc. Inst. Elect. Engrs. Pt. IIA, **100**, 3.
DOUSMANIS, G., SANDERS, T. M., and TOWNES, C. H. 1955. Phys. Rev. **100**, 1735.
MESCHI, D. J. and MYERS, R. J. 1956. Symposium on Molecular Structure and Spectroscopy, Ohio State University, Columbus, Ohio.

THERMAL AND ELECTRICAL CONDUCTIVITY OF RHODIUM, IRIDIUM, AND PLATINUM[1]

G. K. White and S. B. Woods

ABSTRACT

Measurements are reported of the thermal and electrical conductivities of the transition elements Rh, Ir, Pt in a state of high purity; the rapid rate of decrease of the "ideal" thermal and electrical resistivities with temperature, particularly in Rh and Ir, suggests that s–d transitions are not a dominant resistive mechanism at low temperatures in these metals, in contrast to palladium, iron, and nickel, which were studied previously. The electrical resistivity of platinum is in general agreement with the earlier results of de Haas and de Boer (1934); the quadratic dependence on temperature observed below about 10° K. suggests that electron–electron collisions may well be an important factor in this metal.

INTRODUCTION

Recent papers on the electron transport properties of palladium (Kemp *et al.* 1955), iron, nickel, zirconium, and titanium (Kemp, Klemens, and White 1956), have discussed the role of the unfilled d-band of the transition elements, which seems to be at least partially responsible for the particular temperature variation of the electrical resistance of these elements at low temperatures. It was reported that the ideal electrical resistivity, ρ_i, due to scattering by thermal vibrations varied approximately as T^3 for $T \ll \theta$, in contrast to the more rapid variation (T^5) expected and generally observed in simple monovalent metals at sufficiently low temperatures.

Mott (1935, 1936) suggested that the relatively high electrical resistance of the transition elements at room temperature was due to the electrons chiefly responsible for conduction, that is those in the s-band, being scattered not only within the s-band but also into the d-band by the lattice vibrations. Owing to the high density of states in the unfilled d-band these s–d transitions would be highly probable and would increase the resistance relative to that of the monovalent metals, which have filled d-shells. When de Haas and de Boer (1933–34) reported that in pure platinum, ρ_i was proportional to T^4 at $T \sim 20°$ K. and to T^2 at about 4° K., Baber (1937) calculated the effect of collisions between s and d electrons on the electrical resistance and showed that a term in T^2 would result, suggesting that for platinum $\rho_i = bT^2 + cT^5$ at sufficiently low temperatures. However Wilson (1938) argued that Baber was only able to achieve agreement with the experimental results by the use of rather unlikely values for parameters such as the effective electron mass. Wilson was therefore led to investigate the theory of s–s and s–d transitions.

When an electron with wave vector $\mathbf{k}$ undergoes a transition to a state where it has wave vector $\mathbf{k}'$, by interacting with a lattice wave of wave number $\mathbf{q}$, momentum is conserved if we exclude Umklapp processes, i.e.:

$$\mathbf{k}-\mathbf{k}'+\mathbf{q} = 0.$$

[1]Manuscript received September 24, 1956.
Contribution from the Division of Pure Physics, National Research Council, Ottawa, Canada.
Issued as N.R.C. No. 4203.

Wilson predicted that generally $\mathbf{k}_s \neq \mathbf{k}_d$ so that s–d transitions would be restricted to temperatures above a temperature θ_E below which only lattice waves of wave number $q < |\mathbf{k}_s - \mathbf{k}_d|$ would be excited. Hence at sufficiently low temperatures $\rho_i \propto T^5$, but he argued that at temperatures above θ_E, $\rho_i \simeq \rho_s = \rho_{ss} + \rho_{sd}$, where ρ_{ss} could be expressed by the Grüneisen–Bloch expression, i.e. proportional to $(T^6/\theta^5)J_5(\theta/T)$, but ρ_{sd} would vary as $(T/\theta)^3 J_3(\theta/T)$, where

$$J_n(\theta/T) = \int_0^{\theta/T} \frac{x^n dx}{(e^x-1)(1-e^{-x})}, \tag{1}$$

and thus

$$\rho_{sd} \propto \left(\frac{T}{\theta}\right)^3 \int_{\theta_E/T}^{\theta/T} \frac{x^3 dx}{(e^x-1)(1-e^{-x})}. \tag{2}$$

Since the measurements on palladium, nickel, and iron gave figures for ρ_i to temperatures as low as $\theta/20$ which seemed to follow equation (2), it seemed worth while to extend the experiments to other transition metals which could be obtained in a state of fairly high purity. As the thermal conductivity might also yield information about the scattering processes and there was a range of temperatures not covered by the measurements of Rosenberg (1955) and those recently made by Powell and Tye (1955), both properties were investigated on specimens of rhodium, iridium, and platinum.

EXPERIMENTAL METHOD

A cryostat similar to that described previously by White and Woods (1955) was used for the experiments, the thermal conductivity, K, being measured with the aid of gas thermometers and ρ with a galvanometer ampli-

TABLE I

DETAILS OF SPECIMENS AND RESULTS

Specimen:	Rh 1	Rh 2	Ir 2	Pt 1	Pt 2
Source	Baker Platinum Co.	Johnson-Matthey #8208	Johnson-Matthey #10371	Baker Platinum Co.	Pt 1 drawn
Quoted purity	>99.9%	>99.997% +0.002% Fe +0.0005% Cu	>99.98% +0.01% Rh +0.002% Pt +0.001% Cu	>99.99%	
Annealed at	1050° C.	1300° C.	1300° C.	1050° C.	1050° C.
Diameter (mm.)	1.5	1.5	2	1.5	0.5
$10^6\,\rho_0$ (ohm cm.)	0.44	0.0084	0.1034	0.0125	0.05925
$10^2\,\rho_0/\rho_{295}$	83	1.75	20.2	1.20	5.45
W_0T (cm. deg.^{2} watt^{-1})	16.1	0.348	4.13	0.53	—
$10^8 L_0$ (watt ohm deg.$^{-2}$)	2.73	2.41	2.50	2.35	—
n ($W_i \propto T^n$)	—	3.1	2.6	2.3	—
$10^3 B$ (at $\theta/10$)	—	5	9	50	—
θ (° K.)	350	350	290	225	225
W_∞	0.66	0.66	0.68	1.42	1.42
$\frac{W_i}{W_\infty}\left(\frac{\theta}{T}\right)^2$ (at $\theta/10$)	—	9	11	17	—

fier. In most of the experiments below 25° K., where ρ_i is small and generally much less than the impurity resistivity, ρ_0, the same current was passed through the specimen for each electrical resistance measurement and the voltage due to ρ_0 was cancelled by a method described by Woods (1956), so that only the voltage produced by ρ_i remained to be measured by the galvanometer amplifier.

The specimens in rod form (see Table I for details of source, purity, dimensions, etc.) were mounted in the cryostat with a non-superconducting Zn–Cd eutectic solder. All specimens were annealed in vacuum and were from 5 to 7 cm. in length.

RESULTS

Figures 1–4 show the results of the thermal conductivity measurements together with previous data of Rosenberg (1955) for Rh, Ir, and Pt, Powell and Tye (1955) for Rh and Ir, and Meissner (1915) for Pt. Graphs for the

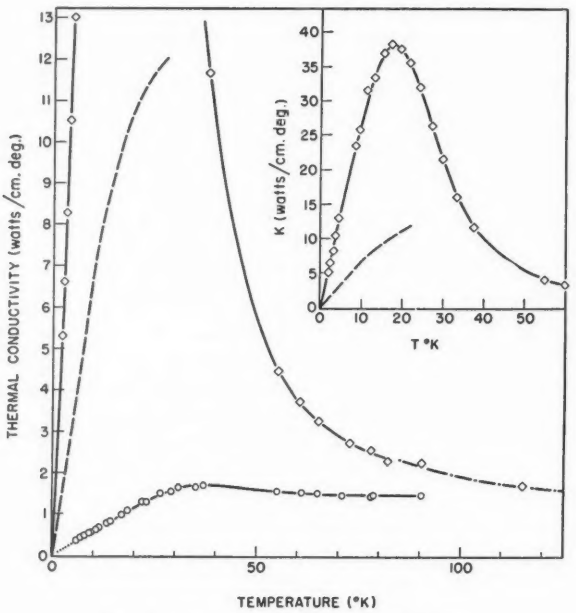

FIG. 1. Thermal conductivity of rhodium.
— ○ — Rh 1 — — — Rosenberg (1955)
— ◇ — Rh 2 ·—·— Powell and Tye (1955)

ideal thermal resistivity W_i—due to scattering of the electrons by thermal vibrations—are included and have been deduced (see for example White and Woods (1955) or reviews by Olsen and Rosenberg (1953), Klemens (1956)) assuming the validity of Matthiessen's rule, i.e., that the total thermal resistivity, W, is the sum of W_i and the impurity thermal resistivity, W_0.

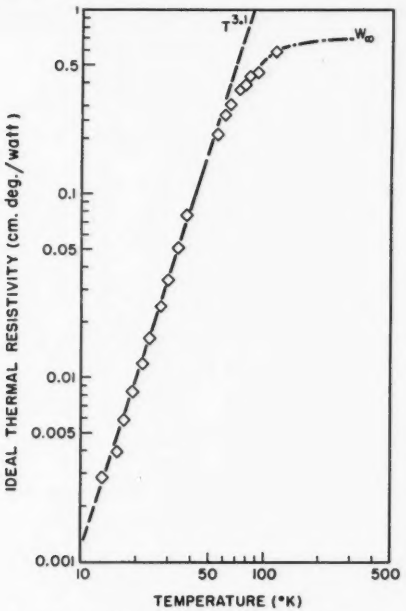

FIG. 2. Ideal thermal resistivity of rhodium.
◇ Rh 2 ·—·— Powell and Tye (1955)

W_0 varies inversely with temperature and the constant $A = W_0 T$ may be deduced from measurements in the liquid helium region where $W_0 \gg W_i$; then generally

$$W_i(T) = W(T) - W_0(T) = \frac{1}{K(T)} - \frac{A}{T}$$

where $K(T)$ is the observed thermal conductivity. As expected, it is found that W_i becomes sensibly constant ($= W_\infty$) at high temperatures ($T \sim \theta$). For $T \leqslant \theta/10$, $W_i \propto T^n$ where the values of n (Table I and figures) are rather higher than the theoretically predicted figure of ~ 2.0. In the case of the alkali metals and many other elements (MacDonald, White, and Woods 1956; Klemens 1956) it was found that $W_i \propto T^2$ rather closely. Since it has been predicted from approximate solutions of the Bloch equation that

$$W_i/W_\infty = CN^{2/3}(T/\theta)^2 \quad \text{for } T \ll \theta \quad (N = \text{no. of free electrons/atom}),$$

values for W_i at $T \simeq \theta/10$ have been used to determine the values of the constant $CN^{2/3} = (W_i/W_\infty)(\theta/T)^2$ shown in Table I. The theoretical expressions suggest that for metallic elements in which $N \simeq 1$, C should have a value in the vicinity of 60 to 70, but the experimental values found for most metallic elements, including those reported in this paper, are considerably lower, in the range $C = 15 \pm 5$. Values of the Debye characteristic temperature,

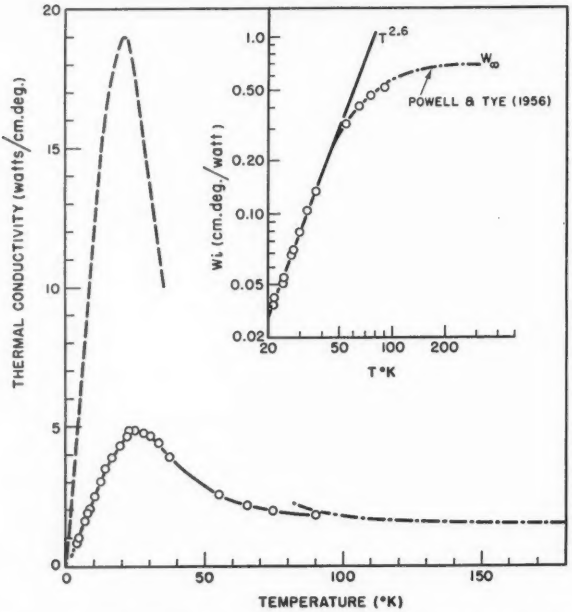

FIG. 3. Thermal conductivity and "ideal" thermal resistivity of iridium.
— O — Ir 2 — — — Rosenberg (1955) ·—·— Powell and Tye (1955)

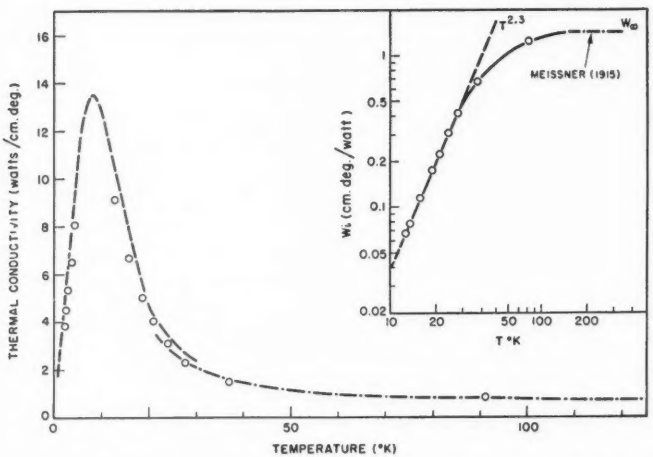

FIG. 4. Thermal conductivity and "ideal" thermal resistivity (inset) of platinum.
O Pt 1 — — — Rosenberg (1955) ·—·— Meissner (1915)

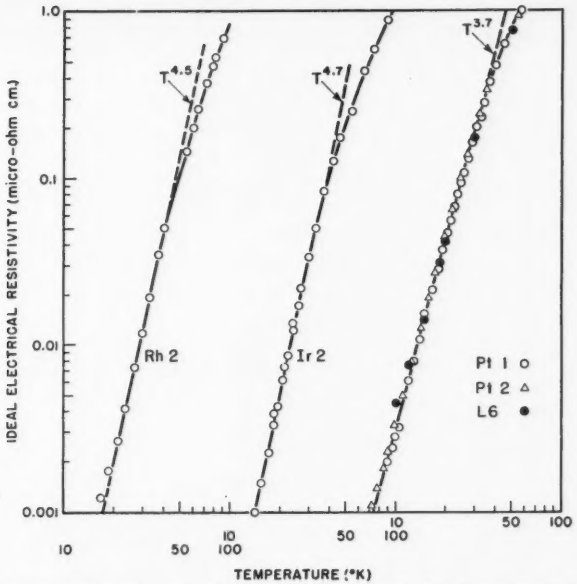

FIG. 5. Ideal electrical resistance of rhodium, iridium, and platinum at low temperatures.

θ, used in this calculation and subsequently have been taken from Clusius and Losa (1955) for Rh and Ir and Simon and Zeidler (1926) for Pt.

For the electrical resistance measurements, the validity of Matthiessen's rule has been assumed: that is, the temperature independent resistance due to impurities—ρ_0, as determined between 1.5° K. and 4.2° K.—has been subtracted from the total resistance to give the so-called "ideal" electrical resistivity, ρ_i, due to thermal vibrations alone. Values are plotted in Figs. 5 and 6 for the region below 100° K. and some smoothed values at various temperatures up to room temperature are tabulated in Table II.

TABLE II

VALUES OF "IDEAL" ELECTRICAL RESISTIVITY IN MICRO-OHM CM.

T, ° K.	Rh 2	Ir 2	Pt 1.Pt 2
θ	5.8	4.9_5	8.0
295	4.78	5.05	10.65
273	4.38	4.63	9.8_0
200	2.93	3.15	6.8_1
150	1.91	2.12	4.8_0
100	0.87	1.08	2.8_0
75	0.42	0.60	1.7_2
50	0.10_7	0.20	0.76
40	0.048	0.11	0.45
30	0.0124	0.034	0.180
20	0.0022	0.005_0	0.044
15	0.0007_5	0.0012_5	0.0155
10	—	—	0.0031
6	—	—	0.0006
Index m	4.5 (<40° K.)	4.7 (<35° K.)	3.7 (<30° K.)

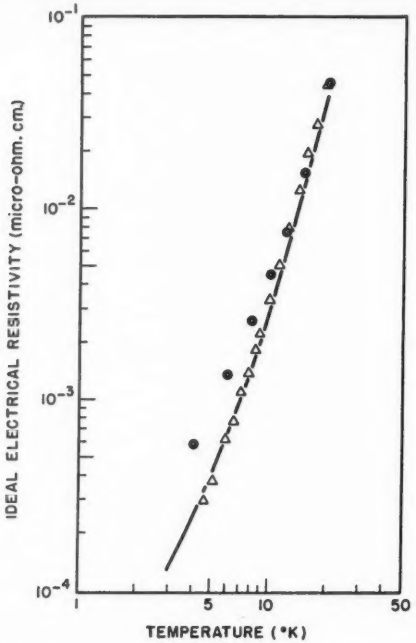

FIG. 6. Ideal electrical resistivity of platinum below 20° K.
——— de Haas and de Boer (1933–34)
△ Pt 2
● Calculated from constants for L6 (Hoge and Brickwedde 1939)

As may be seen, for $T \leqslant \theta/10$, $\rho_i \propto T^m$ for rhodium and iridium where $m = 4.5$ and 4.7 respectively, in fair agreement with the figure 5.0 which we would expect for the resistance due to scattering of electrons by thermal vibrations at temperatures sufficiently low that interband transitions are unlikely. For platinum, however, $m = 3.7$ appears to fit the data over a considerable range of temperature, but Fig. 6 shows that the index, m, becomes smaller at temperatures below 8° K. In Fig. 6 experimental data obtained by de Haas and de Boer (1933–34) for very high purity platinum and points calculated from the formulae given by Hoge and Brickwedde (1939) are also plotted. This latter formula,

$$R = a + bT^2 + CT^5,$$

with appropriate values of the constants was found by Hoge and Brickwedde to fit their data on a Pt electrical resistance thermometer, L6, between 10° and 15° K., but appears to give much too high a T^2 term to fit our results or those of de Haas and de Boer.

DISCUSSION

Mott (1935, 1936) has pointed out that for metallic elements the values of the parameter $M\theta^2\rho(T_1)$ (M = atomic weight, T_1 = room temperature) should be used for comparison when discussing the relative room temperature electrical resistivities, since the resistance is proportional to the mean square amplitude of thermal vibrations, that is to $T/M\theta^2$. The high values of this parameter for the transition metals may be understood in terms of scattering of s electrons into the d-band which leads to $\rho_{sd} > \rho_{ss}$. For transition metals such as Fe, Co, Ni, Mo, W, Rh, Pd, Ir, and Pt, this parameter has values between 50 and 100 compared with $\sim$10 for Cu, Ag, and Au, and 2.5 to 7.5 for the alkali metals. Despite this, there seems to be no uniform behavior among transition metals at low temperatures. Previous results on Pd, Fe, Ni, Cr (Kemp *et al.* 1957) led us to believe that for $T < \theta/10$, $\rho_i \propto T^3$ and thus the ideal resistivity could be well represented by the Wilson relation: $\rho_{sd} \propto (T/\theta)^3 \times J_3(\theta/T)$. However the present results on Rh, Ir, and Pt show that this is not always the case. Apparently in rhodium and iridium, we must suppose that the Fermi surfaces for s- and d-electrons do *not* overlap in **k**-space sufficiently for s–d transitions to be effective at very low temperatures, although there is no sudden marked decrease in ρ_i below a particular temperature (cf. temperature θ_E suggested by Wilson) which would correspond to a rapid fall in ρ_i from a value of $\rho_{ss}+\rho_{sd}$ to a value ρ_{ss}. Perhaps as Klemens (private communication) suggests, even at very low temperatures there may be sufficient points of contact between the s- and d-Fermi surfaces for s-conduction electrons to diffuse with a few small angle scatterings across the s-surface to a point of contact and then suffer an s–d transition. This would result in a complicated expression for ρ_i in which $\rho_i \propto T^m$ with $3 < m < 5$ as observed. The rather rapid decrease in W_i with temperature below about $\theta/5$ suggests that s–d transitions are becoming forbidden with decrease in temperature, since both contributions to W_i, viz., W_{ss} and W_{sd} due to s–s and s–d transitions, being single step phonon processes would normally be expected to fall as T^2.

The general significance of electron–electron collisions in producing a T^2 electrical resistivity term in the transition metals still seems uncertain. In platinum our results seem to confirm those of de Haas and de Boer and may be represented below 10° K. by

$$\rho_i = \{0.14\times10^{-10}T^2+0.8\times10^{-14}T^5\} \text{ ohm cm.}$$

At 10° K. the T^2 and T^5 terms are comparable but at higher temperatures the T^5 term rapidly becomes dominant and would lead to a much higher value of the resistivity at 20° K. than is observed. In fact over a wide range of temperature (see Fig. 5) $\rho_i \propto T^{3.7}$, which compares with the T^4 relation found by de Haas and de Boer at about 20° K. The results for rhodium and iridium are not accurate enough below 15° K. to distinguish with certainty the temperature dependence of the resistance. This was because the impurity resistivity of the iridium sample (and also Rh 1) was rather high, and because

the cross section of the Rh 2 sample was too large to allow very accurate measurement. Owing to the brittle nature of the Rh 2, we were unable to reduce its diameter by drawing. However, it is hoped that in the near future more samples of very high purity transition elements will be available in a form which will allow sufficiently accurate measurements of ρ_i to establish the temperature dependence where a T^2 term might be expected to be important.

As an illustration of the behavior of the "ideal" resistivity ρ_i for some of the transition elements, Fig. 7 shows ρ_i/ρ_θ plotted against T/θ. Rhodium

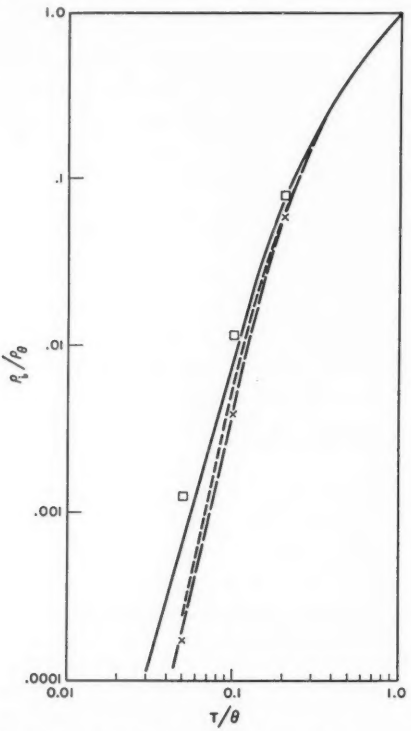

FIG. 7. Variation of ρ_i/ρ_θ with reduced temperature T/θ.
——— Pt using $\theta = 225$, $\rho_\theta = 8.0\times10^{-6}$ ohm cm.
– – – – Ir using $\theta = 290$, $\rho_\theta = 4.95\times10^{-6}$ ohm cm.
— — Rh using $\theta = 350$, $\rho_\theta = 5.0\times10^{-6}$ ohm cm.
□ Points from Pd (Kemp, Klemens, Sreedhar, and White 1955)
× Points from Cu (White 1953)

behaves very similarly to copper, whose resistance follows the Bloch–Grüneisen function down to very low temperatures. At the other extreme, palladium, for which three representative experimental points are shown, follows reasonably closely the function $(T/\theta)^3 J_3(\theta/T)$; platinum and iridium are intermediate in behavior.

ACKNOWLEDGMENTS

We are indebted to Drs. D. K. C. MacDonald and P. G. Klemens for interesting discussions, to Mr. J. Broome for his technical assistance, and to Mr. F. Anglin for his help with many of the experimental observations.

REFERENCES

BABER, W. G. 1937. Proc. Roy Soc. A, **158**, 383.
CLUSIUS, A. K. and LOSA, C. G. 1955. Z. Naturforsch. **10a**, 545.
DE HAAS, W. J. and DE BOER, J. 1933–34. Physica, **1**, 465.
HOGE, H. J. and BRICKWEDDE, F. G. 1939. J. Research Natl. Bur. Standards, **22**, 351.
KEMP, W. R. G., KLEMENS, P. G., SREEDHAR, A. K., and WHITE, G. K. 1955. Phil. Mag. **46**, 811.
KEMP, W. R. G., KLEMENS, P. G., and WHITE, G. K. 1956. Australian J. Phys. **9**, 180.
KEMP, W. R. G., KLEMENS, P. G., TAINSH, R. J., and WHITE, G. K. 1957. To be published.
KLEMENS, P. G. 1956. Handb. der Physik, **14**, 198.
MACDONALD, D. K. C., WHITE, G. K., and WOODS, S. B. 1956. Proc. Roy. Soc. A, **235**, 358.
MEISSNER, W. 1915. Ann. Physik, **47**, 1001.
MOTT, N. F. 1935. Proc. Phys. Soc. **47**, 571.
——— 1936. Proc. Roy Soc. A, **153**, 699.
OLSEN, J. L. and ROSENBERG, H. M. 1953. Phil. Mag. Suppl. **2**, 28.
POWELL, R. W. and TYE, R. P. 1955. Proc. IXth Intern. Congr. Refrig., Paris, Commission 2, p. 083.
ROSENBERG, H. M. 1955. Trans. Roy. Soc. **247**, 441.
SIMON, F. E. and ZEIDLER, W. 1926. Z. physik. Chem. **123**, 383.
WHITE, G. K. 1953. Australian J. Phys. **6**, 397.
WHITE, G. K. and WOODS, S. B. 1955. Can. J. Phys. **33**, 58.
WILSON, A. H. 1938. Proc. Roy. Soc. A, **167**, 580.
WOODS, S. B. 1956. Can. J. Phys. **34**, 223.

THE ENERGY OF ALPHA PARTICLES FROM U^{234}, U^{238}, AND Th^{232} [1]

B. G. HARVEY,[2] H. G. JACKSON,[2] T. A. EASTWOOD, AND G. C. HANNA

ABSTRACT

The α-particle energies of U^{234}, U^{238}, and Th^{232} have been measured with a grid ionization chamber. The electronic equipment was designed to provide low noise, high resolution, and good long term stability. Ra^{226}, Em^{222}, Po^{218}, Po^{214}, and Po^{210} were used as energy standards. An investigation was made of the corrections to the measurements due to variation in pulse rise-time, source thickness, and imperfect shielding of the collector by the grid. It was found that the experimentally observed resolution was satisfactorily accounted for by the combination of these factors and the noise and ionization straggling.

Alpha particle pulse heights were measured in terms of the output of a precision pulse generator. The corrected pulse heights were related to the energies of the standard sources by a two-parameter least squares calculation; the standard deviation was never greater than 5 kev. On extrapolating to zero ionization the line so obtained intercepted the energy axis at 83 kev. The α-particle energies deduced using this line were: U^{234} 4.768±0.003, U^{238} 4.195±0.005, Th^{232} 4.007±0.005 Mev.

INTRODUCTION

The α-particle energies of U^{238} and Th^{232} cannot be measured conveniently with a spectrograph because their specific activities are too low. An instrument of higher transmission is required and an ionization chamber with a large solid angle of particle collimation is suitable. When this work was started it appeared that the specific activity of U^{234} was also too low for spectrographic measurement and it was therefore included in this investigation, but since then its α-particle energy has been measured with a double-focusing spectrometer (Goldin *et al.* 1955). The most recently published measurements with an ionization chamber (Clark *et al.* 1944, 1945) were done with Po^{210} as an energy standard and it was assumed that the pulse-amplitude vs. α-energy calibration would be a straight line passing through the origin. It has since been found that this is not always the case (Cranshaw and Harvey 1948; Hanna 1950). The measurements have therefore been repeated, using five standards, and making no assumptions about the interception of the calibration curve.

APPARATUS

(*a*) *The Chamber*

The electrode arrangement of the grid chamber used in this work is shown in Fig. 1(*a*). The source disk of maximum diameter 3 cm. was at the center of a 10.2 cm. square brass plate. Alpha particles were collimated by a ring 0.3 cm. high with a diameter of 3 cm. which was concentric with the source disk. The solid angle (as a fraction of 4π) is then 40% for a central point and 32.5% for a uniform 3 cm. diameter source (Howlett and Whitehouse 1950).

The grid was 5.5 cm. away from the source disk. It consisted of a frame

[1]Manuscript received December 7, 1956.
Contribution from the Research Chemistry and Nuclear Physics Branches, Atomic Energy of Canada Limited, Chalk River, Ontario.
Issued as A.E.C.L. No. 400.
[2]Present address: Radiation Laboratory, University of California, Berkeley, California.

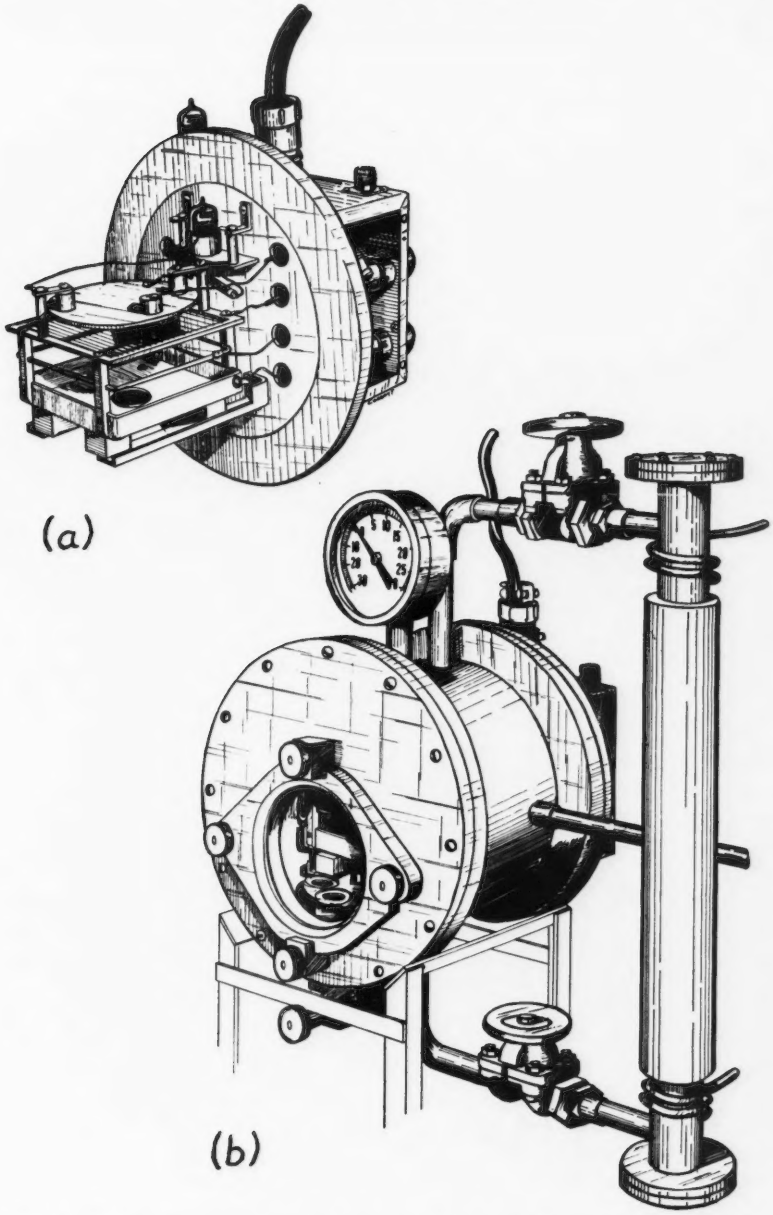

FIG. 1. The grid ionization chamber showing (*a*) the electrode assembly, (*b*) the complete assembly.

10.2 cm. square, strung with 0.005 in. copper wires, 0.9 mm. apart. A guard ring was used to improve the uniformity of the field lines between the collector and source; this was 3.5 cm. from the source. The collector was a brass disk of 10.2 cm. diameter, 6.5 cm. from the source disk. The calculated grid inefficiency, σ, is 0.0124 (Bunemann *et al.* 1949). Referred to the collector, which was at ground potential, the grid was at -800 v., the guard ring at -1.4 kv., and the source plate at -2.0 kv.

A calcium furnace operating at 350° C. was used to remove traces of oxygen or other electron-capturing impurities from the gas in the chamber. The furnace (shown in Fig. 1(*b*)) consisted of a thin-walled stainless steel tube packed with calcium turnings and joined to the top and bottom of the chamber; the counter gas was circulated by convection. It was then only necessary to change the gas filling when the chamber was opened to remove sources.

Within the chamber was a six position turntable, seen through the chamber window in Fig. 1(*b*). The radioactive sources used in the experiments were placed on the turntable, and by means of an external control, each source could be brought into the counting position. Therefore, all sources were counted under identical conditions of geometry and gas filling. It was determined experimentally that any gas introduced into the chamber when a source was brought into the counting position had a negligible effect on the peak height of the α-particle pulse distribution.

The chamber was filled to a pressure of 1.8 atm. with argon (99.6% pure) plus about 6% methane (96% pure). No thorough investigation was made of chamber gases and mixtures. It is, however, well known that methane is an excellent "moderating" gas in argon (English and Hanna 1953). The mixture used provided a very short collection time of the electrons in the chamber and saturation could be achieved at reasonable field strengths.

(*b*) *Electronic Equipment*

Fig. 2 shows a block diagram of the electronic equipment and Fig. 3 a circuit diagram of the preamplifier. It was realized that for this experiment a high signal–noise ratio from the input tube would be a great asset. Performance figures were therefore obtained for the 6AK5, 403B, 12AY7, 6BR7, and 404A tubes. While all these tubes showed a peak in the signal–noise ratio when the band width of the amplifier was set by equal rise and fall time

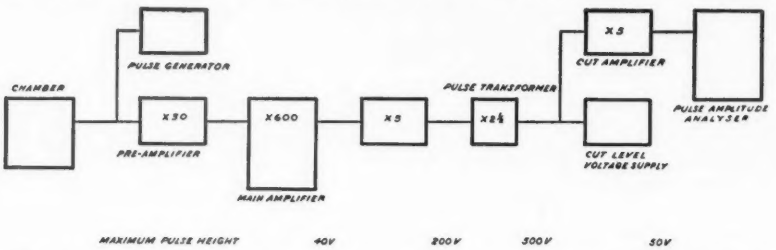

FIG. 2. Block diagram of electronic equipment showing the position of "cutting", the amplification at each stage, and the maximum pulse height after amplification.

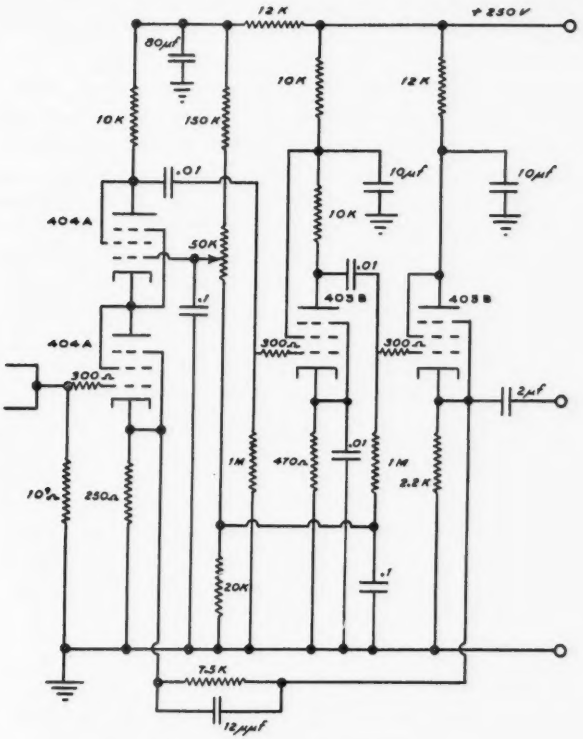

FIG. 3. Circuit diagram of preamplifier.

constants of 10 μsec., the figures clearly indicated that the 404A tube was to be preferred. Accordingly, this tube was used in the familiar "cascode" form of circuit. The input tube itself was mounted inside the chamber, thus reducing the loss of signal voltage due to stray capacities. Microphonics arising at the input were a problem until the whole chamber assembly, of which the preamplifier was a part, was mounted on a 1 in. thick sponge rubber pad, and the two 404A tubes changed from a horizontal to vertical mounting. The preamplifier itself was a negative feed-back ring of three having a gain of approximately 30, with a cathode follower output, which fed into the main amplifier. This was a linear amplifier type AEP 1444 (Moody and Howell 1950), which was used with a gain of ~600 and top and bottom cuts of 10 μsec. This band width was chosen because of the superiority of the signal–noise ratio: the time constants are sufficiently long compared to the collection time of the chamber.

The signal was further amplified by a gain of 5 and finally a pulse-transformer was used to bring the maximum signal up to 500 v. For good resolution, the pulses were then 'cut' and only their 'tops' further amplified and fed to

the pulse analyzer. It was necessary that the cut-level voltage supply be stable to 1 part in 10^4. An improved circuit was developed from one used at Chalk River by R. E. Bell. This consisted of the usual form of stabilized power supply, but by use of high precision resistors in a voltage divider system across the output a fraction of the voltage was compared with a Weston standard cell. The difference signal obtained from a Brown convertor was amplified by a Leeds and Northrup chopper amplifier, the output being rectified by a phase sensitive bridge rectifier and fed back to the grid of the regulator tube. The output of the supply was obtained from a 0.05% linear Helipot potentiometer controlled by a Duodial assembly.

After "cutting", the signal was again amplified by a negative feed-back amplifier with a gain of 5, and then fed to a 30 channel pulse amplitude analyzer type AEP 516 (Moody *et al.* 1951).

Artificial pulses were developed by a pulse generator. This again was a stable supply (1 part in 10^4) with a circuit similar to the cut-level voltage supply. The output was chopped by a Western Electric mercury relay 276E, and shaped by a resistor–condenser combination to approximately simulate an alpha-pulse from the ionization chamber. This is characterized by a fast rise-time of about 1.0 μsec. and a long exponential decay of some 20 msec. Actually the pulse generator pulses had a decay time of about 200 μsec., but this is of little consequence. These artificial pulses were fed to the grid of the input tube through a 1 μμf. condenser. The amplitude of the pulses was varied by using a 0.05% linear Helipot potentiometer and Duodial assembly. The linearity of the potentiometer was checked using a standard cell, Leeds and Northrup Type K potentiometer and galvanometer. To achieve the necessary stability the equipment was located in a room where the temperature was kept constant to within 1° C. Also all amplifying equipment was stabilized against line voltage fluctuations by a Sorenson 1001 voltage regulator. The pulse-size produced from a given α-particle emitter then usually varied by less than 0.1% during the course of an experiment, provided that the chamber gas was at least 12 hours old, and that none of the electronic equipment had been switched off during the previous 48 hours.

EXPERIMENTAL

(*a*) *Preparation of Sources*

(i) Th^{232}.—A solution of $Th(NO_3)_4.4H_2O$ in absolute ethanol (containing about $\frac{1}{2}$ mg. Th/ml.) was placed two or three drops at a time on a smooth platinum disk and allowed to dry slowly in still air. The disk was then ignited at red heat for a few seconds, and the addition repeated until sufficient Th^{232} had been deposited. It was found that the ThO_2 tended to accumulate at the edge of the disk, giving a deposit of varying thickness. This difficulty was avoided by using oversize disks which were then trimmed to their final size after the ThO_2 had been deposited.

The source which was used for the energy measurements had an average thickness of 18 μg. $Th^{232}/cm.^2$ over an area of 7 $cm.^2$ The ThO_2 layer appeared uniform to the eye.

(ii) U^{234} and U^{238}.—Uranium sources were prepared by electrodeposition from an ammonium oxalate solution onto platinum disks (Hufford and Scott 1949). The thinnest deposits (of high specific activity U^{234}) were quite invisible. Thicker deposits were a clear golden yellow color. The source used for the energy measurements of U^{238} was of intermediate thickness, 23 μg./cm.^{2}

(iii) Po^{210}.—These sources were prepared by placing a solution of Po^{210} in very dilute (<0.1 *M*) hydrochloric acid onto a clean, smooth silver disk. After 30 seconds, the solution was rinsed off, and the disks washed with a sodium thiosulphate solution to remove traces of silver chloride which might have been formed. The disks were flushed with water and dried by rinsing with absolute ethanol.

(iv) Ra^{226}.—Radium sources were prepared by volatilization of $RaCl_2$ from a wolfram filament heated to 2000° C. in vacuum. The radium was condensed onto a smooth platinum disk supported about 8 mm. above the filament. The deposits were invisible.

(*b*) *Choice of Chamber Operating Conditions*

As stated previously, the chamber was operated at 1.8 atm. pressure and 2.0 kv. The choice of these conditions was dictated by the following considerations: the pressure must be such that the most energetic α-particles, those from Po^{214}, are stopped before reaching the grid and that saturation is achieved at a conveniently low voltage. The minimum pressure required to meet the first condition is 1.3 atm., but at this pressure the correction to be made for the positive ion effect, discussed in detail below, is undesirably large (35 kev. for Po^{214}). The positive ion induction correction is reduced by increasing the pressure, but at pressures above 1.8 atm. another effect becomes apparent which widens the α-pulse distribution very slightly. The nature of this effect is not understood, but experiments showed that it is not associated with inefficient operation of the calcium purifier and is present at methane concentrations from 3 to 6% in the counting gas. Therefore, a chamber pressure of 1.8 atm. was chosen. The voltage plateau at this pressure had a slope of less than 0.1% per 100 v. over the range 1 to 3 kv. and the operating voltage used was 2 kv.

(*c*) *Experimental Method*

For the determination of the α-particle energies, all sources both standard and unknown were counted long enough for 400 counts to be recorded in the peak channel of the pulse analyzer. Counting times varied from 7 minutes for the Po^{210} source to about 4 hours for the Th^{232} source.

After counting each source, two counts were made using the pulse generator in such a way that the peak of the pulse generator pulse distribution fell, first slightly below, and then slightly above, the peak of the α-pulse distribution. By a simple interpolation, the α-pulse could thus be measured in pulse generator scale divisions. The pulse generator scale was calibrated in this way with the standard sources of known α-particle energy (Po^{210}, Ra^{226}, and its daughters Em^{222}, Po^{218}, and Po^{214}). By this method any small non-linearity in the amplifying system was obviated.

The change in the position of the Po^{210} α-pulse distribution on the pulse analyzer was nearly always less than 5 kev. during the course of an experiment lasting 12 hours.

Seven determinations of the α-particle energies of each of the sources being investigated were made in a series of five runs.

RESULTS

The observed width of an α-pulse distribution is always greater than that obtained with artificial pulses from a pulse generator. The width of the pulse generator distribution is due entirely to amplifier noise. The width of the α-pulse distribution, however, is increased by other effects such as source thickness, the charge on the collector induced by positive ions, ionization straggling, and possibly lack of saturation. These contributions to the width of the α-pulse distribution can be calculated and combined with the noise as measured by the pulse generator distribution.

The full width at half-maximum of an α-pulse distribution varied from 27 kev. for the low energy α-particle emitters such as Ra^{226} to 42 kev. for the higher energy α-particle emitters such as Po^{214}. The width of the distribution obtained with artificial pulses was about 21 kev.

I. Corrections

Both amplifier noise and ionization straggling, by their nature, form a symmetrical pulse distribution so that their effect is merely to increase the width of the α-pulse distribution without shifting its peak to higher or lower energies. However, other factors such as source thickness and the variation of the charge induced by the positive ions can only decrease the pulse size. Hence their effect is to shift the distribution to a lower energy, and therefore corrections must be applied to the observed α-particle energies.

Such factors fall into two groups: (*a*) those inherent in the ionization chamber and therefore to be considered for all α-particle emitters, and (*b*) those inherent in the source of α-particles. These will now be considered in further detail.

A. Corrections for All α-Particle Sources

(*i*) *Rise-time Correction*

It can be shown (Wilkinson 1950) that when pulses are fed through an amplifier limited by equal rise and fall time constants of T μsec. the fractional loss in output pulse height due to a finite input pulse rise-time of t μsec. is $t^2/24T^2$. The maximum pulse rise-time at the collector (for Po^{214}) was calculated to be 1.1 μsec. from the drift velocity curves given by English and Hanna (1953); a direct measurement gave 1.0 μsec. Since $T = 10$ μsec., the maximum loss of pulse height from this cause is 0.04%, i.e. about 3 kev. for Po^{214}. This is much smaller than the effect of imperfect grid shielding, and since the latter effect is somewhat uncertain, the effect of rise-time has been neglected.

(*ii*) *Positive Ion Induction Correction*

The positive ions left in the chamber after collection of the electronic component of the ionization induce a charge on the collector electrode. Its

magnitude is proportional to σ, the shielding inefficiency factor of the grid, and depends on the length and orientation of the α-particle track. The observed α-pulse distribution is therefore broadened and its maximum shifted to lower energies. The maximum energy shift is expected to be $E_\alpha \bar{R}\sigma/sD$ Mev., where $\bar{R}$ is the range of the center of ionization in standard air at one atmosphere pressure (and is taken as $0.6 \times$ the total range), s is the stopping power of the chamber filling, and D the distance from source to grid. When $s = 1.72$, $D = 5.5$ cm., and $\sigma = 0.0124$, this reduces to $1.31 \times 10^{-3} E_\alpha \bar{R}$.

The collimator restricts the angle of the emergent tracks by an amount that depends on the area and uniformity of the source. For the radium source (i.e. for the α-emitters Ra^{226}, Em^{222}, Po^{218}, and Po^{214}) which was more concentrated near the center of the disk we have taken 0.3 as the effective value of $\cos \theta_{max}$. The induction effect is therefore expected to produce a rectangular distribution of width

$$2\Delta = 1.31 \times 10^{-3} E_\alpha \bar{R}(1-0.3) \tag{1}$$

and a mean shift in energy of

$$\delta = 1.31 \times 10^{-3} E_\alpha \bar{R}(1+0.3)/2. \tag{2}$$

The Po^{210} source was more uniform but the same value of $\cos \theta_{max}$ has been used. The numerical values of Δ from equation 1 are given by the straight line of Fig. 4.

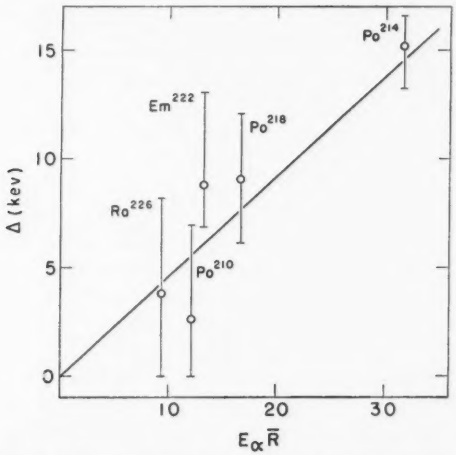

FIG. 4. Effect of positive ions. The line is the expected relation between Δ and $E_\alpha \bar{R}$ from equation 1. The points are derived from the width of the observed α-pulse distributions. The errors shown are the maximum deviation from the average of 10 observations.

A comparison of the expected value of Δ from equation 1 and that deduced from the observed width of the pulse height distribution can be made for Po^{210} and Ra^{226} where source thickness effects are negligible. In this case the observed width is the result of the symmetrical distributions due to amplifier

noise and ionization straggling and the rectangular distribution due to the positive ions. The half-width of the rectangle, Δ, deduced from the observed width assuming that the standard deviation of the ionization straggling is 7 kev. (Fano 1947; Engelkemeir and Magnusson 1955), is plotted in Fig. 4. It was found that the value of Δ vanished for Ra^{226} and Po^{210} if the standard deviation of ionization straggling was increased to 8 kev.

B. Corrections for Specific α-Particle Emitters

(i) Recoil Correction

Nuclei of Em^{222}, Po^{218}, and Po^{214} formed from decay of Ra^{226} are driven by recoil into the platinum source mount. The observed energy of α-particles from these decay products must be corrected for the energy loss that occurs in the platinum. An exact calculation of the effect of source thickness is complicated (Milton *et al.* 1956) and for the present purpose an approximate method, described below, seems adequate.

According to Briggs (1933) the range of recoil atoms, R, is about 4×10^{-7} cm. in platinum. An approximate calculation gives effective source thicknesses for Em^{222}, Po^{218}, and Po^{214} of respectively R, $3R/2$, and $2R$. Since the stopping power of platinum for α-particles is 3.7 mg./cm.^{2} equivalent to 1 cm. of air (Livingston and Bethe 1937), it may be calculated that the source thicknesses in terms of α-particle energy lost were 2.0, 2.8, and 3.9 kev. for Em^{222}, Po^{218}, and Po^{214}.

The magnitude of shift of the α-particle distribution depends not only on source thickness, but also on the amount of collimation. The effect of collimation has been treated by Howlett and Whitehouse (1950), and by approximate numerical integration of the distribution curves given in this reference it was calculated that the apparent reduction in energy of the α-particle spectrum was 1.6 kev. for Em^{222}, 2.3 kev. for Po^{218}, and 3.1 kev. for Po^{214}.

The observed α-pulse distribution was then analyzed as has been described for Ra^{226} and Po^{210}. The rectangle thus obtained was attributed to the combined effect of source thickness and positive ions. By subtracting the energy loss due to source thickness given in the last paragraph the half-width of the rectangle due to the positive ion effect alone was deduced and these values are plotted in Fig. 4. Although the agreement between the points and the line in Fig. 4 is good it cannot be regarded as an adequate check because the effect of source thickness has been treated in an approximate manner only. There remains, in consequence, some uncertainty in the value of δ (the mean peak shift). However, the effect of a complete neglect of δ would be to change the calculated α-particle energies of U^{238} and Th^{232} by about 2 kev. and of U^{234} by a negligible amount.

(ii) Source Thickness Correction

The U^{238} and Th^{232} sources were made as thin as possible, consistent with satisfactory counting rates. However, small corrections for source thickness were still required.

The correction for the U^{238} source was measured directly by comparing the

α-particle energy of a high specific activity U^{234} source with the apparent α-particle energy of U^{234} in the U^{238} source. A mean difference of 5 kev., with a standard deviation of 3 kev., was measured in seven experiments. The difference calculated from the (known) thickness of the source was 6 kev.

The measured α-particle energy of U^{238} was therefore increased by 5 kev. to correct for source thickness.

The correction for the Th^{232} source was not measured directly. It was calculated from the measured correction for U^{238} and the known mass thickness of the two sources. The correction was 4 kev.

(iii) Fine Structure Correction

The α-particle spectra of U^{234}, U^{238}, and Th^{232} all have a short-range group of approximately 25% abundance at an energy of about 50 kev. lower than the main group (Hollander *et al.* 1953). The short-range α-groups of U^{238} and Th^{232} have not before been observed directly. In the present work, these fine structure components were not completely resolved. Typical spectra are given in Figs. 5 and 6.

However, the excited nuclei following emission of low energy α-particles decay almost entirely by the emission of L-conversion electrons (accompanied by soft X-rays and Auger electrons). In a chamber of high solid angle, coincidences between short-range α-particles, and conversion and Auger electrons, will cause the spectrum of the short-range α-group to spread upward to higher energies. This effect has been observed with the present apparatus with Ra^{226},

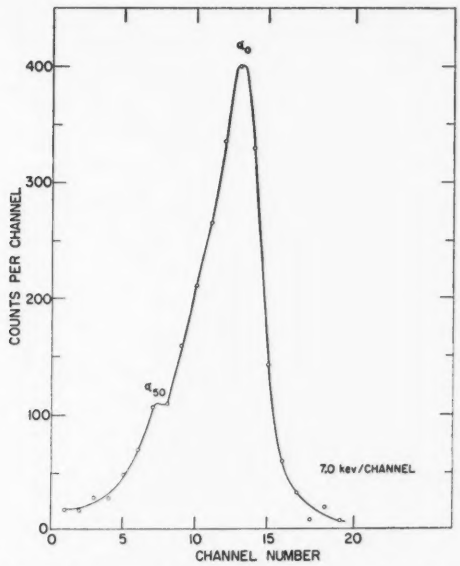

FIG. 5. Typical α-particle spectrum of U^{238}. The energy difference between the short-range α-particle group, α_{50}, and the main group, α_0, is about 50 kev.

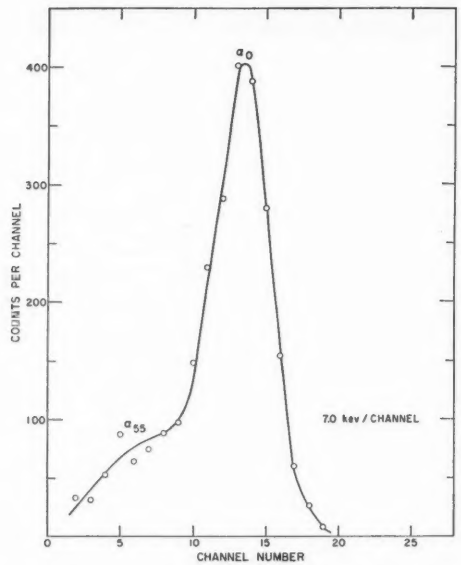

FIG. 6. Typical α-particle spectrum of Th^{232}. The energy difference between the short-range α-particle group, α_{55}, and the main group, α_0, is about 55 kev.

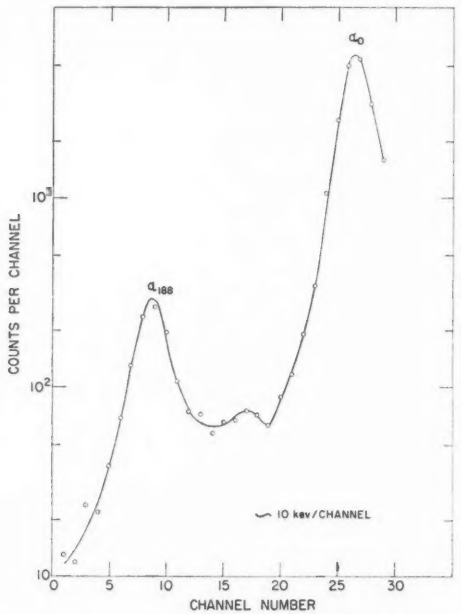

FIG. 7. Typical α-particle spectrum of Ra^{226}. Coincidences between the short-range α-particle group, α^{188}, and the conversion electrons which accompany this transition produce the broadening on the high energy side of the α_{188} peak. The small peak between the α_{188} and the α_0 groups is due to coincidences between the α_{188} group and K-conversion electrons.

which has a readily resolved short-range α-group 188 kev. lower than the main group (Hollander *et al.* 1953). Another maximum due to coincidences between the short-range group and K-conversion electrons can be distinguished in Fig. 7.

The effect of these coincidences on the apparent energy of the main α-group was investigated with a source of Cm^{242}, which has a fine structure component very similar to those of U^{234}, U^{238}, and Th^{232} (Hollander *et al.* 1953). By varying the amount of collimation, the frequency of α-conversion electron coincidences was varied at will. It was found that reducing the counter solid angle from 30% to 20% produced no significant increase in the observed α-particle energy (less than 1 kev.).

(*iv*) *Base-line Shift Correction*

All pulse amplifiers will exhibit some base-line deflection due to the condenser coupling between stages, and the magnitude of this deflection will be dependent upon the pulse repetition rate.

It was convenient to use standard calibrating sources whose counting rates were considerably higher than those of the U^{238} and Th^{232} sources. The effect of counting rate on the apparent energy of an α-group was therefore measured with a series of Po^{210} sources and shown to be negligible (less than 1 kev.).

II. Calculation of Results

After all necessary corrections for the five calibrating sources had been made, a straight line fit of observed energy (in pulse generator divisions) vs. E_α was made by a least squares calculation, using the E_α values given in Table I.

TABLE I

α-Particle energies of standard sources (Briggs 1954)

Nuclide	E_α (Mev.)
Ra^{226}	4.7790
Po^{210}	5.3007
Em^{222}	5.4861
Po^{218}	5.9982
Po^{214}	7.6804

It was found that the five points could be fitted to a straight line with a standard deviation which was never greater than 5 kev. From this line the apparent α-particle energies of U^{234}, U^{238}, and Th^{232} were calculated, and then corrected in the case of U^{238} and Th^{232} for source thickness, as described in I. B(ii). The values given in Table II were obtained.

TABLE II

α-Particle energies of U^{234}, U^{238}, and Th^{232}

U^{234}	4.768±0.003 Mev.
U^{238}	4.195±0.005 Mev.
Th^{232}	4.007±0.005 Mev.

The probable error, being an indication of the reproducibility of these results, was only 1 kev., but a review of the corrections and errors involved leads to the errors quoted above.

The value for U^{234} is in good agreement with 4.7683 ± 0.001 Mev. obtained by Goldin *et al.* (1955) using a double-focusing spectrometer. A recent measurement of Philbert *et al.* (1954) using a photographic emulsion technique gave 4.004 ± 0.020 Mev. for the α-particle energy of Th^{232}.

III. Chamber Calibration Curve

Upon extrapolation of the pulse height versus energy curve, an intercept on the energy axis was observed. An average of five values for the intercept was 83 kev. with a probable error of 4 kev. This agrees with a value of 85 kev. obtained by Cranshaw and Harvey (1948).

REFERENCES

Briggs, G. H. 1933. Proc. Roy. Soc. (London), A, **139**, 646.

——— 1954. Revs. Mod. Phys. **26**, 1, 472.

Bunemann, O., Cranshaw, T. E., and Harvey, J. A. 1949. Can. J. Research, A, **27**, 191.

Clark, F. L., Spencer-Palmer, H. J., and Woodward, R. N. 1944. British Report, BR522.

——— 1945. British Report, BR584.

Cranshaw, T. E. and Harvey, J. A. 1948. Can. J. Research, A, **26**, 243.

English, W. N. and Hanna, G. C. 1953. Can. J. Phys. **31**, 768.

Engelkemeir, D. W. and Magnusson, L. B. 1955. Rev. Sci. Instr. **26**, 295.

Fano, U. 1947. Phys. Rev. **72**, 26.

Goldin, L. L., Novikova, G. I., and Tretyakov, E. F. 1955. Conf. Acad. Sci. USSR on Peaceful Uses of Atomic Energy, Phys. Math. Sci., p. 226.

Hanna, G. C. 1950. Phys. Rev. **80**, 530.

Hollander, J. M., Perlman, I., and Seaborg, G. T. 1953. Revs. Mod. Phys. **25**, 469.

Howlett, J. and Whitehouse, W. J. 1950. Harwell Report, AERE N/R 473.

Hufford, D. L. and Scott, B. F. 1949. The transuranium elements, National Nuclear Energy Series, Vol. 14B (McGraw-Hill Book Co., Inc., New York), p. 1149.

Livingston, M. S. and Bethe, H. A. 1937. Revs. Mod. Phys. **9**, 272.

Milton, J. C. D., Rutledge, A. R., and Lennox, P. I. K. 1956. Chalk River Report, CRP–632.

Moody, N. F. and Howell, W. D. 1950. Chalk River Report, IM–8.

Moody, N. F., Battell, W. J., Howell, W. D., and Taplin, R. H. 1951. Rev. Sci. Instr. **22**, 551.

Philbert, G., Génin, J., and Vigneron, L. 1954. J. phys. radium, **15**, 16.

Wilkinson, D. H. 1950. Ionization chambers and counters (Cambridge University Press), p. 103.

THE ELECTRICAL RESISTANCE OF SOME METALS AND ALLOYS BELOW 1° K.[1]

J. S. Dugdale and D. K. C. MacDonald

ABSTRACT

Measurements of electrical resistance below 1° K. are described, including experiments to estimate the thermal contact resistance between the paramagnetic salt and gold wires which were subsequently used as secondary thermometers. The resistance of a dilute copper alloy, a lithium–magnesium alloy, and a sodium specimen was measured. No change was found in the resistance of sodium which might be correlated with the specific heat anomaly previously reported by Rayne. The resistance below the minimum in the gold and copper specimens showed a marked contrast in behavior below 1° K. No minimum was found in the resistance of the lithium–magnesium alloy.

1. INTRODUCTION

These experiments were intended in the first place to investigate the behavior of the resistance below 1° K. of certain metals and alloys whose behavior is of theoretical interest; in the second place to establish whether any of these materials could be used as a secondary thermometer in this temperature region.

At temperatures below about 0.1° K. to 0.2° K. it becomes very difficult to know whether thermal equilibrium exists between the cooling salt and the specimen to be cooled (e.g. cf. Mendoza (1948) and the pioneer work at Leiden (de Haas, Casimir, and van den Berg 1938; van den Berg 1938)). Since the thermal conductivity of the paramagnetic salt itself becomes poor, and the effective thermal resistance between the salt and the specimen is difficult to estimate, we have tried to measure this thermal resistance directly.

We were able to establish how the resistance of some specimens of fine gold wire varied from 1° K. down to about 0.06° K., and in subsequent experiments one of these specimens was used as a secondary thermometer to measure the temperature of the specimen being studied.

In this way we have examined several of the alkali metals and shown that at any rate down to about 0.2° K. their residual resistance is "normal", that is, it remains constant and shows no minimum. We have also confirmed that the resistance of copper specimens which show a minimum of resistance at higher temperatures becomes constant below about 0.8° K. in marked contrast to the gold specimens, whose resistance continues to rise down to the lowest temperatures. The minimum in the copper used is known to be due to the presence of iron, and in the gold this is also believed to be the case.

2. APPARATUS

2.1. The Cryostat

The cryostat has already been described by White (1955). The only important change since made has been to bring all electrical leads to the specimen

[1]Manuscript received October 10, 1956.
Contribution from the Division of Pure Physics, National Research Council, Ottawa, Canada.
Issued as N.R.C. No. 4206.

through the liquid helium in the inner chamber (whose temperature is about 1.2° K. during and after the demagnetization). For this purpose platinum–soft-glass seals have proved perfectly reliable over a long period; "Kovar" seals were unsatisfactory.

2.2. The Salt and Its Thermal Contact with the Specimen

For measurements on gold samples, several different arrangements have been used. These were as follows:

(1) Powdered potassium chrome alum compressed as a pill with different "binders" onto copper fins, to which the gold specimen was soldered externally;

(2) Iron ammonium alum crystallized from solution directly onto the gold wire;

(3) A two-pill method with both salts of iron ammonium alum;

(4) A two-pill method with the gold in a pill of cerium magnesium nitrate.

In the two-pill method all the leads to the specimen came via silver wires on which was grown salt A (Fig. 1).

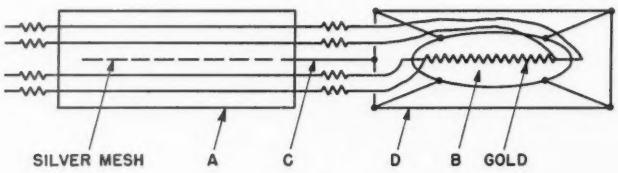

FIG. 1.

The second salt, B, was grown directly onto the gold specimen, which was connected by superconducting leads of high thermal resistance to the silver leads in A. A also contained a silver mesh to which the shield D was connected by a copper rod C. In this way a shield consisting of copper-plated German silver was maintained around salt B at the same temperature as salt A. This arrangement was suggested to us by the experiments of Nicol (1955).

When the two salts A and B were both of iron ammonium alum the heat influx into B could be reduced to about 2 ergs per minute as compared with about 60 ergs per minute for a single pill, although it was evident that the amount of residual exchange gas left before demagnetization was also a vital factor.

To cool other materials such as the alkali metals onto which the salt could *not* be directly grown, a pill of paramagnetic salt was crystallized onto a silver wire mesh, to which the specimen was afterwards soldered at one end (see, for example, Dabbs *et al.* 1955). The other end was then soldered to a gold thermometer so that the temperature of the specimen could be estimated independently of the salt temperature (see Fig. 2).

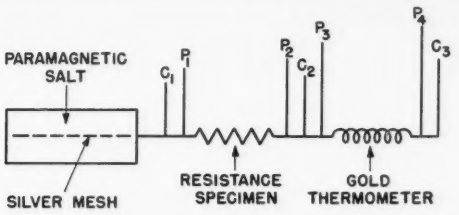

FIG. 2.

2.3. Temperature Measurement

The measurements of the susceptibility of the paramagnetic salt which was used as the primary thermometer were made by a ballistic method as already described by White (1955).

2.4. The Resistance Measurements

The resistance was measured by means of a galvanometer amplifier (MacDonald 1947). The measuring currents were varied to determine whether any significant heating of the specimen occurred and it was found that, in general, currents of less than 1 ma. produced no appreciable heating effect. Usually, currents of 250 μa. or less were employed. In a specimen of 1/10 ohm, typical of the gold wires used, this current dissipates less than 4 ergs per minute; a normal measuring time did not exceed 20 seconds.

3. EXPERIMENTAL RESULTS

3.1. Gold Specimens

Gold specimens from three different sources have been tested and the behavior of all of them is qualitatively similar: the resistance rises as the temperature is reduced from 4.2° K. (the highest temperature of the measurements) down to the lowest temperatures reached (about 0.05° K.). A number of samples of gold were measured using the techniques described in paragraphs 2.1 and 2.2 above. In all these measurements it was difficult to know whether the gold specimen and paramagnetic salt were in effective thermal equilibrium, since we were ignorant of the magnitude of the thermal contact resistance between salt and specimen. An experiment was accordingly made to measure this specifically and the details are described in the appendix: only the results are given here. The conclusions to be drawn from this experiment, however, are subject to some doubt as explained there.* If, nevertheless, we accept the results, we deduce that the thermal resistance between the gold wire and the salt at about 0.1° K. was about 1/10° C. sec./erg,† so that with a heat influx of about 6 ergs/min. this would give rise to about 1/100° temperature

*However, later experiments (Dugdale, MacDonald, and Croxon 1957) have satisfied us as to the validity of our conclusions.

†This value appears to agree roughly with the predictions of an equation (quoted by Kürti *et al.* (1956)) referring to the heat contact between copper fins and a paramagnetic salt compressed around them.

difference between wire and salt. The relaxation time of the thermometer *in situ* was calculated to be about 10^{-2} to 10^{-3} seconds. This agrees with the fact that no relaxation effects were observed. Hence it seems reasonable to suppose that the salt and the wire as used in the double pill arrangement were very closely in thermal equilibrium and the experimental results are shown in Fig. 3 (curve A). It is seen from this figure

(*a*) that the accuracy of the resistance measurements themselves appears to be quite adequate even with currents as low as 50–100 μa., and

(*b*) that the specimen obeys quite closely the law $R/R_1 = \ln(T_0/T)$ between 2° K. and 0.1° K.

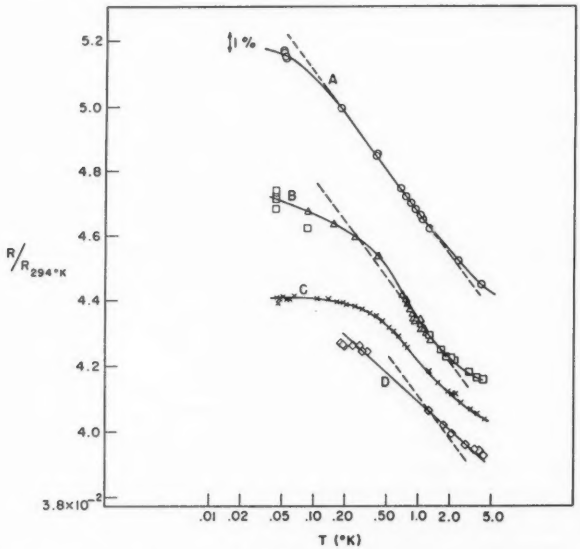

FIG. 3. Resistance of samples of gold wire used on various occasions as thermometers.
A: Experiment of March 19, 1956 (double "pill" arrangement–both iron ammonium alum—gold thermometer embedded in lower pill inside case).
B: Experiment of March 6, 1956 (measurement of resistance of Na(+K) specimen; silver mesh in salt).
C: Experiment of January 19, 1956 (measurement of resistance of Cu+0.056% Fe alloy; silver mesh in salt).
D: Experiment of January 31, 1956 (measurement of resistance of Li+Mg alloy; silver mesh in salt).
Temperatures: above ~1° K., determined from helium vapor pressure.
below ~1° K., determined from cooling salt (iron ammonium alum) after correction to absolute temperature scale (following Cooke 1949).

This type of relationship was found by Croft *et al.* (1953) to represent approximately their results from 4° K. to ~0.006° K. The deviation from the law at temperatures above 2° K. in our work is much too large to be accounted for by lattice scattering, which is quite negligible below 5° K.; the departure

at the lowest temperatures is presumably due to failure of the proposed law for the resistance. The suggested relationship is in any case still without theoretical foundation.

The gold wires we have used behaved in a sufficiently consistent and reproducible fashion to make useful secondary thermometers of very low heat capacity.

In the remaining curves (B, C, and D) in Fig. 3 the resistance of these wires used as thermometers in the single pill set-up of Fig. 2 is also plotted against salt temperature. It appears evident that the gold specimens are now markedly out of equilibrium with the salt at the lower temperature. There may be a number of causes:

(*a*) greater thermal load,

(*b*) increased thermal resistance of the contact between salt and silver mesh,

(*c*) enhanced mechanical vibration.

The temperature of the specimens may, however, be taken with some confidence from the gold thermometers to which they are soldered.

3.2. Copper–Iron Dilute Alloy

The results of measuring a copper specimen containing 0.056 weight per cent of iron are shown in Fig. 4 (curve B). Curve A in the same figure shows the resistance of a gold specimen (mentioned earlier) which was attached to the copper. A spectroscopic estimate of the impurities in the gold specimen gave Ag ~0.001%, Pt ~0.001%, Fe ~0.01%, from which it appears reasonable to conclude that iron is the dominant impurity in this case also. The contrast in the behavior of these two alloys is evident and the results for the

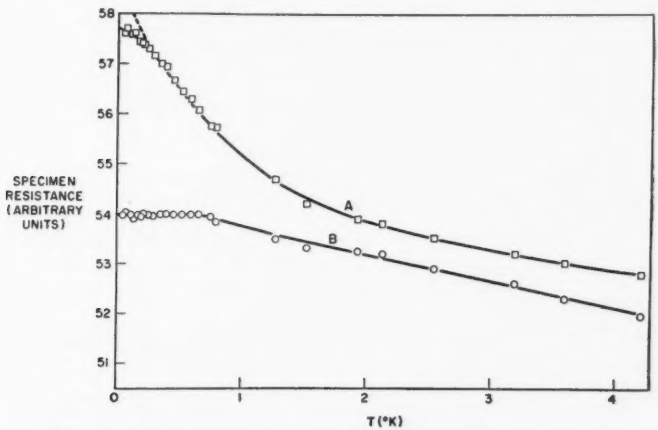

FIG. 4. Resistance of A: gold wire; B: copper+0.056% Fe alloy.
Temperatures: above ~1° K., determined from helium vapor pressure.
below ~1° K., determined from cooling salt (iron ammonium alum) after correction to absolute temperature scale (following Cooke 1949).

copper alloy confirm the finding of White (1955) that the resistance below 1° K. is practically independent of temperature, at least down to about 0.1° K.

3.3. Sodium

The resistance of sodium was measured as a function of rising temperature from about 0.1° K. up to about 1.3° K. with special concentration on the region around 0.8° K. at which a specific heat anomaly was reported by Rayne (1954). If a specimen were made directly of high purity sodium, the residual resistivity would be so low ($\sim 10^{-9}$ ohm cm.) that to measure it would demand either a very large measuring current (which we naturally wished to avoid) or an undesirably thin specimen. We therefore added deliberately a small percentage of potassium to our sodium specimen, raising the residual resistivity to about 2×10^{-7} ohm cm. With such a specimen cast in a glass mold of reasonable diameter we were then able to make quite accurate measurements below 1° K. with a measuring current of only 1 ma. If, as seemed most likely, the specific heat anomaly were associated with a primary change of electron properties, then this augmented residual resistance due to the potassium impurity would enable such a change to be observed readily.

We paid particular attention to the temperature region between 0.7° K. and 1.3° K., but no abnormal behavior could be found in the resistance of the sodium which might be associated with the specific heat anomaly. The results of the experiment are shown in Fig. 5.

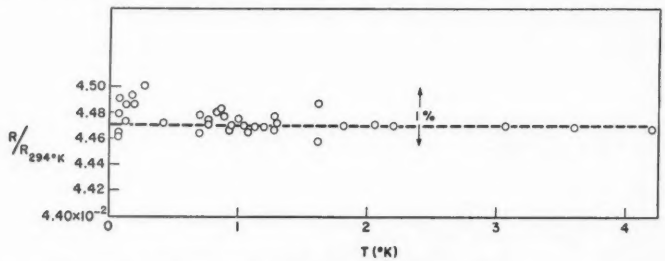

FIG. 5. Resistance of sodium (+small percentage of potassium).
Temperatures: above ~1° K., determined from helium vapor pressure.
below ~1° K., determined from cooling salt (iron ammonium alum) after correction to absolute temperature scale (following Cooke 1949).

3.4. Lithium–Magnesium Alloy

The alkali metals in general will not take up elements of other groups into solution, but magnesium in lithium forms a rare exception to this rule. Thus we were able to make a specimen from pure lithium with the addition of magnesium to test whether this might produce a minimum in the resistance temperature curve. The residual resistance ratio ($R_{4°K.}/R_{294°K.}$) was raised from about 2×10^{-3} to about 2×10^{-1} showing that a very significant amount of magnesium was present in solid solution. As Fig. 6 shows, no minimum was observed.*

*Recent experiments in this laboratory by W. B. Pearson show, however, that magnesium in copper produces no resistance minimum.

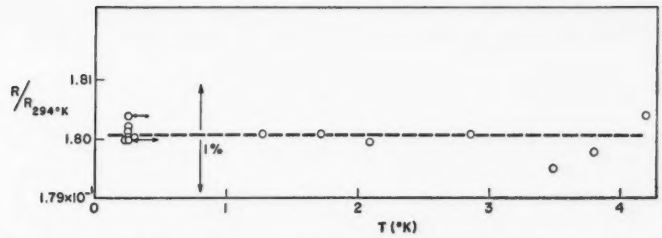

FIG. 6. Resistance of lithium+(nominal 1/10–1%) magnesium alloy.
Temperatures: above ~1° K., determined from helium vapor pressure.
below ~1° K., determined from gold thermometer (horizontal arrows indicate possible range of temperature).

4. CONCLUSION

Apart from the specific points discussed above two conclusions from these experiments appear to be of interest. Fig. 4 shows the resistance of gold and copper specimens each with a small amount of iron in solution. The difference in their behavior at very low temperatures is immediately evident; the gold resistance continues to rise while the resistance of the copper stays constant below about 1° K. Other differences between the resistive behavior of dilute copper and gold alloys may exist (cf. MacDonald and Pearson 1955).

In the alkali metals, no sign of a minimum has been found down to the lowest temperatures; apart from the measurements reported above on sodium this has also been found so in other experiments which we have made on rubidium and cesium, although in these cases we are less certain about the lowest temperatures attained. We believe they were cooled to at least 0.2° K.

ACKNOWLEDGMENTS

We wish to thank Mr. A. A. M. Croxon for his enthusiastic technical assistance in these experiments, Mr. F. W. Richardson for liquefaction of helium, and Mr. W. Stockdale for impurity analyses; we are also grateful to Dr. W. B. Pearson for supplying us with some of the specimens.

APPENDIX

In the experiments in which the salt pill was crystallized directly onto the gold specimen we were not able to estimate the magnitude of the effective thermal resistance between the bulk of the salt and the gold wire. We, therefore, modified the apparatus in an attempt to determine this experimentally (see Fig. 7, the arrangement being similar in many respects to that used by Mendoza (1948)).

In the experiment both salts were demagnetized from the same field and the thermal drift rate was then established by temperature measurements every minute. A current was next passed through the heater for a fixed time (several minutes) and then switched off. This procedure was repeated several times, the two pill temperatures being recorded at frequent intervals. From the temperature–time dependence we estimated approximately the contact resistance between the salt and the gold and hence the thermometer relaxation time, the results being given in the text. This estimate may, however, be

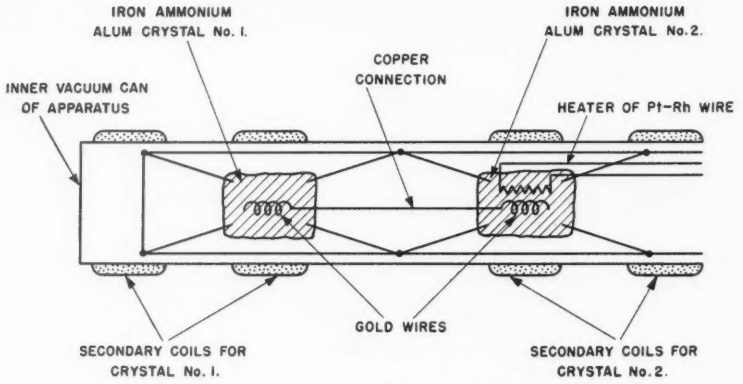

FIG. 7.

incorrect if the mechanism responsible for the anomalous thermal behavior (see below) plays a significant role in providing heat conduction between the pills.*

Temperature Oscillations

Under certain conditions, Mendoza (1948) observed oscillations in the apparent temperature of two salt pills connected by a copper rod. In some of our experiments we have also found rather similar oscillatory behavior in a system composed of a salt pill connected to a phial containing about 10 gm. of sodium metal. A carbon resistance thermometer was attached to the sodium and in one experiment the temperature registered by the carbon thermometer oscillated with a period of about 10 minutes, the first oscillation covering about 0.36° K. to 0.43° K. The apparent salt temperature also showed oscillations in approximately opposite phase.

In the present experiments a phenomenon apparently related to these oscillations was discovered. This is illustrated in Fig. 8, which shows the

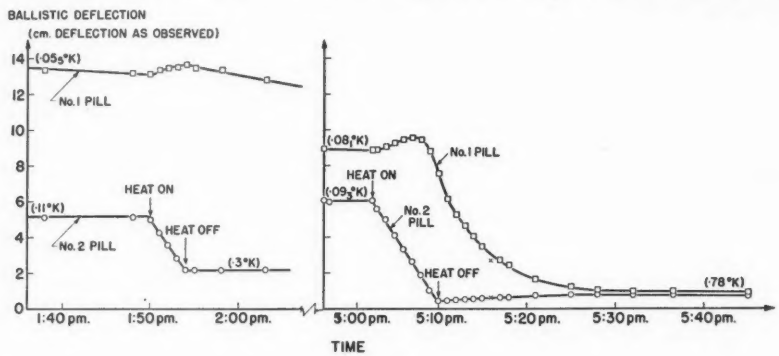

FIG. 8.

*But see Dugdale, MacDonald, and Croxon (1957).

actual ballistic deflections obtained from the two salts in two typical experiments. Ballistic deflections are shown, rather than temperatures, to bring out more detail. One sees the remarkable feature that *immediately* heat is supplied to pill No. 2, the apparent temperature of pill No. 1 falls. Moreover this happened *every* time heat was supplied. If this apparent temperature drop is real it implies that about 1000 ergs of energy has been lost from the "cold" pill. Now from our series of measurements we could estimate roughly the heat capacity of the "hot" pill, over a considerable temperature range, ignoring the anomalous thermal behavior, and these values agreed roughly with the published data of Cooke *et al.* (1956).* Generally speaking, however, they were found to be low, but if we assume an additional heat input to the hot pill of the magnitude of that lost by the "cold" one, our data can be brought into reasonable agreement with those of Cooke. This consequently gives support to the belief that a real heat transfer from the cold to the hot pill took place when the heater was switched on.

It is perhaps significant that when in action the heater was supplying about 5000 ergs/minute to pill No. 2, because Mendoza (1948) remarked that he only observed the temperature oscillations when the parasitic heat influx was large (about 1000 ergs/minute in his case instead of a more usual 100 ergs/minute) These effects are quite remarkable and seem to call for further detailed study.

REFERENCES

VAN DEN BERG, G. J. 1938. "De electrische Weerstand van zuivere metalen . . ." (Thesis, University of Leiden).
COOKE, A. H. 1949. Proc. Phys. Soc. A, **62**, 269.
COOKE, A. H., MEYER, H., and WOLF, W. P. 1956. Proc. Roy. Soc. A, **237**, 395.
CROFT, A. J., FAULKNER, E. A., HATTON, J., and SEYMORE, E. F. W. 1953. Phil. Mag. **44**, 289.
DABBS, J. W. T., ROBERTS, L. D., and BERNSTEIN, S. 1955. Phys. Rev. **98**, 1512.
DUGDALE, J. S., MACDONALD, D. K. C., and CROXON, A. A. M. 1957. Can. J. Phys. (In press).
DE HAAS, W. J., CASIMIR, H. B. G., and VAN DEN BERG, G. J. 1938. Physica, **5**, 225.
KÜRTI, N., ROBINSON, F. N. H., SIMON, F. E., and SPOHR, D. A. 1956. Nature, **176**, 450.
MACDONALD, D. K. C. 1947. J. Sci. Instr. **24**, 232.
MACDONALD, D. K. C. and PEARSON, W. B. 1955. Acta Met. **3**, 392.
MENDOZA, E. 1948. "Les phénomènes cryomagnétiques", Hommage National à Paul Langevin et Jean Perrin. Collège de France, Paris.
NICOL, J. 1955. Programme of N.S.F. Conference on Low Temp. Phys. and Chem., Louisiana State University, p. 39.
RAYNE, J. 1954. Phys. Rev. **95**, 1428.
WHITE, G. K. 1955. Can. J. Phys. **33**, 49.

*We are grateful to Dr. A. H. Cooke for correspondence and for letting us see his results before publication.

A FAST AURORAL CAMERA[1]

R. MONTALBETTI

ABSTRACT

A movie camera is described which photographs an auroral display at a speed of one or more frames per second. The fast optical system and wide angular field of view are obtained with an $f/0.71$ objective and a spheroidal mirror. The camera has been found very useful in the study of auroral motions.

INTRODUCTION

Series of photographs taken in rapid succession and covering as large a portion of the sky as possible are desirable for studying the development and decay of auroral displays and for correlating position, intensity, movement, and type of aurora with geomagnetic and ionospheric phenomena. Several types of camera consisting essentially of a spheroidal mirror and a movie camera have been developed for these purposes during recent years (Strofregen 1955). These image all, or nearly all, of the sky on each frame and require exposure rates for all except the brighter aurora of about one frame per 30 seconds. A series of photographs with one of these cameras is exceedingly useful for examining changes of position of an auroral display relative to the photographic station and for identifying types of aurora that change slowly with time. Details concerning types that develop and decay rapidly or that move rapidly across the sky are usually lost because of the relatively long exposure rates.

This note reports the development of a spheroidal mirror, movie camera combination that will take a series of satisfactory photographs at the rate of one frame per second or faster. While there is some loss in angular field (150° instead of 180°) in this camera it is not serious since details concerning auroral structure and movements at low angular altitudes can seldom be recorded by a camera because of the long distances involved.

DESIGN OF 16 MM. CAMERA

A design of a camera was undertaken which would photograph aurora of average brightness at a speed of at least one frame per second using a system basically similar to all-sky cameras. Previous experience with an $f/1.5$ lens and fast film indicated that the purchase of a commercially available $f/0.71$ coated objective[2] would make this a definite possibility. This lens also had the advantage that it could be used with 16 mm. film, thus keeping the size of the camera and its mechanical components reasonably small.

The one factor which necessitated a complete design of a 16 mm. camera was the extremely small distance between the back of the lens and its focal plane. For objects at infinity this distance was measured as 0.076 inch and

[1]Manuscript received December 4, 1956.
Contribution from the Radio Physics Laboratory, Defence Research Board, Ottawa, Ontario.
[2]The lens is available from the Wray Optical Works Ltd., Ashgrove Road, Bramley, Kent.

no commercial camera was found that could be readily adapted to the lens. The corresponding distance in many of the cameras on the market is approximately 1.5 inches.

Because of the variation in auroral brightness and the desire to make the camera as versatile as possible an additional mechanism was designed to give a rather wide range of exposure times. The camera was also designed bearing in mind the requirements that it was to be operated outdoors during severe weather conditions where the temperature could reach −40° C. and that it was to be built in a laboratory machine shop with materials on hand.

A complete description of the 16 mm. camera is given in a report having limited circulation (Mar 1955), but is available to anyone wishing to construct a similar one. Detailed drawings and complete sets of photographs showing the various stages of assembly are also available. For this reason, only the essential features of the construction are presented here.

(1) Claw mechanisms of the "D-motion" type, which are commonly used in commercial cameras, were eliminated in the present design because of the space limitation and the difficulty in machining the parts. Instead intermittent rotation-motion sprockets were used which require only gear trains and a transformation from continuous to intermittent motion. The latter was achieved by an eight-position Geneva stop mechanism having a very low inertia to reduce vibrations. One complete revolution of a main shaft revolves the film transport and loop sprockets one pitch distance, which is made equal to one 16 mm. frame.

(2) Since a pressure backing plate and a shutter were to be placed within the distance of 0.076 inch, a very thin shutter was cut from 0.010 inch bronze plate. This meant that the pressure plate could be machined to a thickness of 0.031 inch and still leave a clearance of 0.017 inch either side of the shutter. To ensure that the design was satisfactory the shutter was tested in a precision lathe up to speeds of 3000 r.p.m. with no aerodynamic instability in the way of flutter being observed. The pressure backing plate was milled from stainless steel stock and mounted as an integral part of the casing.

(3) To position the film at all times against the back pressure plate and to allow uniform film transport a polished stainless steel pressure plate was fitted to adjustable spring-loaded plungers.

(4) The various components of the camera were inserted in a machine-screw assembled case made from aluminum and mild steel. A cover fitted with a centrally controlled four-lug locking mechanism made it easy to unload and reload the camera. The interior compartment containing the film and the inside surface of the cover were blackened to reduce any possible film fogging.

(5) Several types of camera drives were considered but for a number of reasons it was decided to build a separate unit consisting essentially of a Geneva stop and a variac controlled motor. The unit gives a range of exposure times from 1 frame per 10 seconds to 16 frames per second, and is easily coupled to the main shaft of the camera. It is, thus, possible to operate the camera by hand, or set it up for unattended operation or control it from a remote site.

COMPLETE ALL-SKY MOVIE CAMERA

Although the use of the 16 mm. camera alone is rather limited by its narrow field of view (approx. 10°), it is readily converted to an all-sky type of camera by combining it with a spheroidal mirror. In special circumstances where small regions of an auroral form are to be investigated the narrow field of view is an advantage. However, the combination is most often desired, since the main studies deal with the development and decay of auroral displays and the correlation of movement and position with geomagnetic and ionospheric disturbances. The use of a 4-inch diameter, front-surfaced spheroidal mirror (radius of curvature 3.55 inches) placed a distance of 29.7 inches in front of the camera lens gives an angular field of view of some 150°.

In Fig. 1 the all-sky camera is shown mounted on a simple wooden turntable. Both the mirror, which can be turned about a horizontal axis, and the camera are fixed to a small optical bench. Thus, rotation of the turntable and the mirror allows any auroral display to be centered in the field of view of the camera. This films the aurora as it would be seen by an observer in a standing position. Both have some value when the film is projected—especially for viewers who are unfamiliar with aurora. This particular arrangement is also more convenient for hand operation of the camera. (Moreover, a minimum of the sky coverage is lost by the shadow cast on the mirror by the camera and operator.)

For unattended operation, or for operation from a remote site, the optical bench can be placed in a vertical position with the automatic exposure unit coupled to the camera.

RESULTS AND DISCUSSION

A number of short movies of aurorae were taken at Fort Churchill, Manitoba, between January and March, 1956, with no mechanical difficulties being encountered during cold weather. Flaming and pulsating aurorae and rayed forms were successfully photographed at a speed of one frame per second, which corresponds to an actual exposure of 0.57 second per frame. A series of 15 successive frames of an auroral display which occurred during the night of March 4, 1956, is shown in Fig. 2. Flaming aurora is clearly seen above the illuminated buildings. A number of features are observed to develop and decay during the 15-second interval. An important feature is the small difference between successive frames, although the difference between the first and the last frames is very noticeable. A full appreciation of the complexity of the motions and of the development and decay of displays, such as this one, is possible only by viewing a projection of the entire film.

Although the movements and forms of aurorae are registered very well at a speed of one frame per second there are types such as pulsating arcs which could be photographed at higher speeds to some advantage. A number of laboratory tests on the Tri-X film, which has been used to date, have shown that overdevelopment in D-19 developer could result in a film speed of some six times its rated value. As a result, it now appears that auroral movies are possible at speeds of the order of five frames per second.

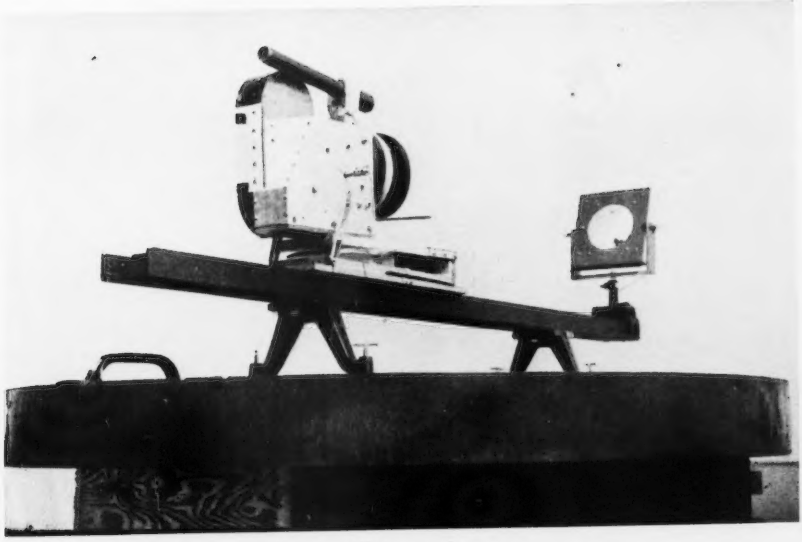

FIG. 1. All-sky movie camera.

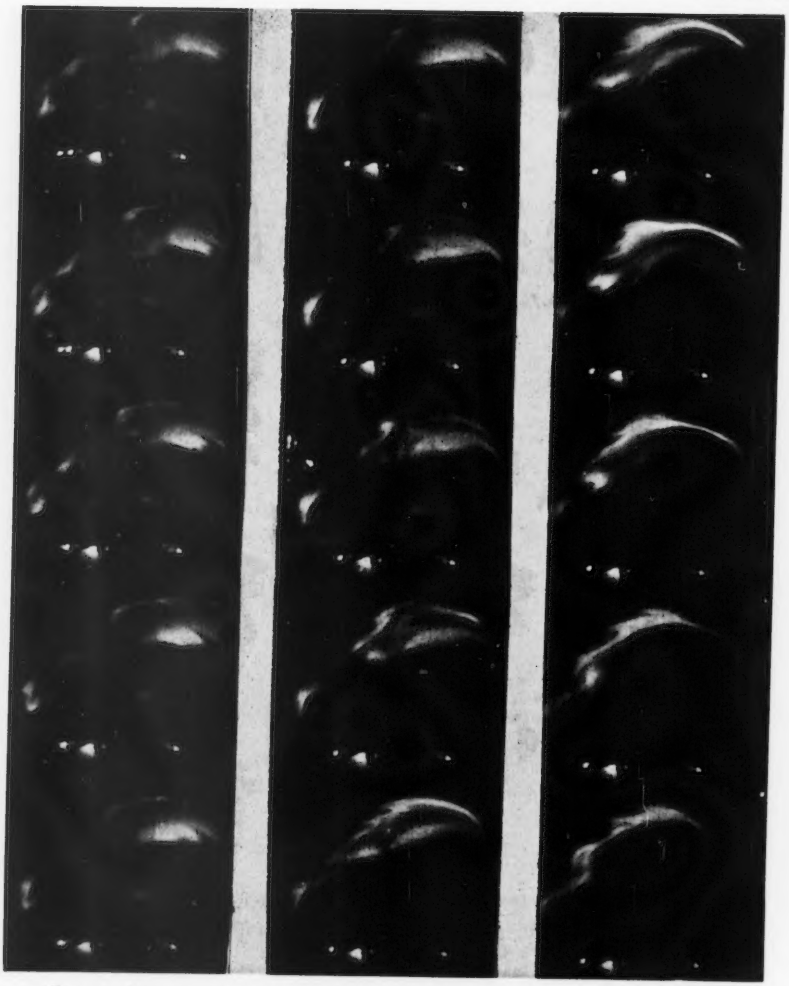

FIG. 2. Successive frames taken at 1-second intervals of an auroral display.

It is planned to use the present camera to supplement the auroral radar program of the University of Saskatchewan by photographing the aurora present in a selected region of the sky where radar echoes appear to originate. A detailed picture of types, forms, intensity, and motion of aurora is needed to correlate visual aurora with auroral radar echoes.

ACKNOWLEDGMENTS

The author wishes to express his thanks to Mr. J. Mar, who did a major portion of the design work of the 16 mm. camera, and to Mr. A. Pennie for his interest in the project.

REFERENCES

MAR, J. 1955. Defence Research Northern Laboratory Technical Note No. 35.
STROFFREGEN, W. 1955. Tellus, 7, 509.

ON THE PRODUCTION OF SINGLE CRYSTALS OF NAPHTHALENE AND ANTHRACENE[1]

F. R. LIPSETT

ABSTRACT

Furnaces for the growth of naphthalene (m.p. 80° C.) and anthracene (m.p. 217° C.) crystals from the melt by the Bridgman method are described and discussed. The advantages of long furnaces are emphasized. A seeding technique may be used to produce long crystals, and has been successful in producing naphthalene crystals 2½ feet long. A technique for polishing the crystals which gives flat, smooth surfaces is described. Methods of determining the orientation of the crystals by cleavage and by examination of the isogyres or birefringence in a polarizing microscope are given. A simple method for producing anthracene crystals by recrystallization from solution in N,N-dimethylformamide is given, and apparatus for producing very thin sublimation crystals of anthracene is described. The procedures may also be employed to produce mixed crystals.

INTRODUCTION

In general, the method selected for the growth of crystals depends on the melting point, crystal structure, and chemical properties of the material. Many methods have been devised for growing crystals of various materials (Buckley 1951; Johnson 1951; Neuhaus 1956), and in some cases theories have been developed to account for some of the phenomena observed, especially in the case of crystals grown from seeds in solution and metal crystals. The theories, however, are not necessarily of use to an experimenter who wishes to produce crystals in the laboratory. Methods suitable for growing crystals of one material may be quite useless for another because of differences in melting points or chemical properties.

Crystal growth is thus often more an art than a science, and many trials are often necessary before good crystals of a given material may be produced. Or, as Buckley (1951, p. 44) has elegantly put the matter, "It should be remembered that, in the preparation of large crystals, the touch of the artist is about as important as the application of established scientific principles". The author has for some time experimented with the growth of naphthalene and anthracene crystals, and the increasing amount of interest in these materials both for spectroscopic and for other investigations has prompted the preparation of these notes. While the methods described are not the only ones available (Menzies and Skinner 1949; Sidman 1956; Leninger 1952) and are not even necessarily the best, they should prove to be of use to other research workers.

GROWTH FROM THE MELT BY THE BRIDGMAN METHOD

One of the most successful methods for the growth of crystals is that devised by Bridgman (1925). Although first used for metals, the method is also

[1]Manuscript received November 5, 1956.
Contribution from the Division of Radio and Electrical Engineering, National Research Council, Ottawa, Canada.
Issued as N.R.C. No. 4233.

suitable for the growth of inorganic crystals (Stockbarger 1936) and for crystals of naphthalene and anthracene (Feazel and Smith 1948; Pimentel and McClellan 1952; Mohorčič 1953 *a*, *b*; Sangster and Irvine 1956). The principle of the method is illustrated in Fig. 1. A specially shaped container

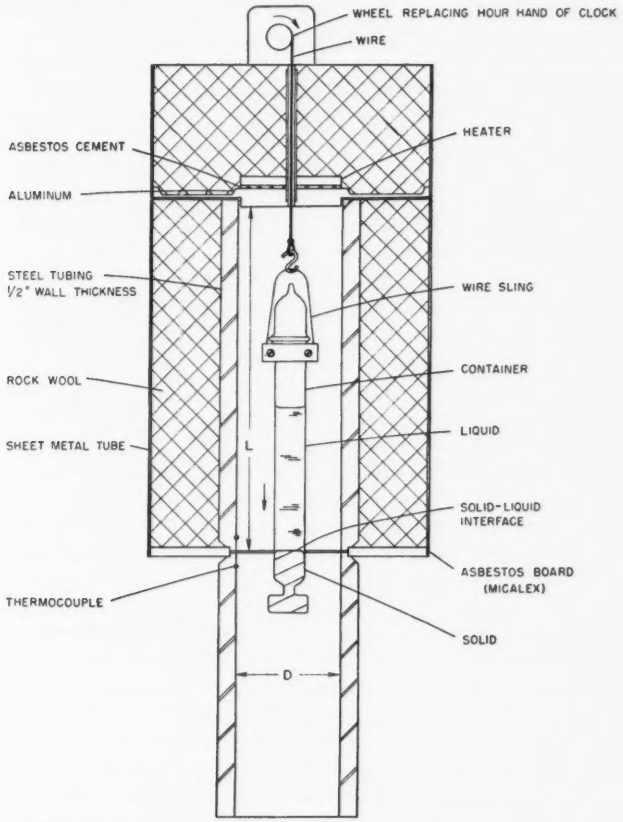

FIG. 1. Diagram of a furnace for the growth of crystals from the melt by the Bridgman method.

(of Pyrex in the present application) filled with the material to be grown into a crystal is suspended in the top section of a furnace. When the material is molten the container is slowly lowered. The furnace is designed in such a way as to have a large temperature gradient along the path of the moving container. In the furnace of Fig. 1 this is at the level of the asbestos board. As the container passes through the temperature gradient the molten material solidifies progressively upwards from the bottom of the container. If the thermal conditions in the furnace, the shape of the container, and the purity of the material are suitable, a single crystal may be obtained.

Design of Furnaces

Two considerations must be borne in mind when furnaces for crystal growth by the Bridgman method are designed: establishment of the correct temperature distribution within the furnace, and convenience in operation. The best form of temperature gradient is shown schematically in Fig. 2.

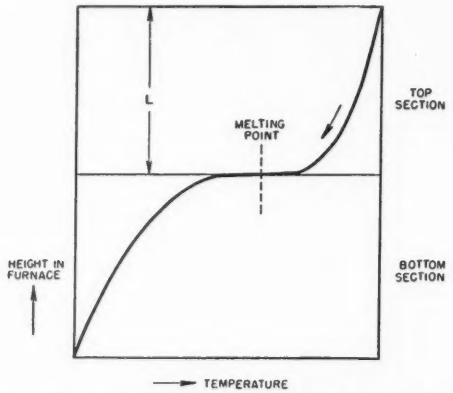

FIG. 2. Diagram showing the temperature gradient desired in a Bridgman furnace.

The temperature at the top of the furnace is in the upper right-hand corner of the diagram. This should not be high enough to cause any decomposition of the material. The temperature in the top section of the furnace should decrease fairly gradually until the lowest part of the top section is reached, and then should abruptly drop. The heat input to the furnace should be adjusted so that the melting point of the material is approximately in the mid-point of the sharp temperature drop. In the bottom section of the furnace the temperature may fall off more rapidly than in the top, provided the fall is not so large as to interfere with the annealing of large crystals, and if convenient the temperature at the bottom of the furnace may be that of the room. If the design of the furnace establishes a temperature gradient of the type shown in Fig. 2 very little regulation of the temperature will be required, since an increase or decrease in the temperature of the furnace as a whole will leave the solid–liquid interface of the crystal almost unmoved.

In contrast to the vertical temperature gradient, the temperature in any horizontal plane within the furnace should be uniform, that is to say, the isothermals should be horizontal. Whether or not this condition is obtained depends upon the dimensions and type of construction employed in the furnace. If the material to be grown into a crystal is sensitive to photochemical reactions (as might under some conditions be the case for anthracene), the crystal container should be shielded from light.

The convenience of operation of a furnace involves the insertion and removal of the crystal container, inspection of the material in the container during melting and growth, and maintenance. These in turn depend upon

the design of the furnace and its length, and may best be illustrated in connection with three types of furnace employed by the author.

The first type of furnace is shown schematically in Fig. 1. The heat is supplied by a heating element of the type commonly used for coffee percolators. The heater is insulated electrically from an aluminum plate by a layer of asbestos cement, and the interior of the furnace is heated by conduction along the thick steel tubing and by radiation from the tubing. A sharp temperature drop is obtained at the asbestos board, and the isothermals are closely horizontal because of the position of the heater at the top. The crystal container is suspended by a fine heat-resistant wire which is wound around a wheel replacing the hour hand of an electric clock. The diameter of the wheel is selected so as to give a rate of descent of 0.1 in. per hour, a rate which has proved convenient for naphthalene and anthracene and which has been employed in all the furnaces described here. The uppermost section of this furnace, that containing the heating element and supporting the clock, may be lifted from the lower sections of the furnace in order to insert or remove a crystal container.

Several furnaces of this type have been made with a diameter D of $2\frac{3}{4}$ in. and a heated length L of 8–10 in. The temperature distribution within the furnace is favorable, and the relatively high heat capacity obviates the need for careful voltage regulation. Many excellent crystals of both anthracene and naphthalene have been grown in furnaces of this type. The furnace nevertheless has a number of disadvantages. During melting the condition of the material may only be ascertained by lifting the uppermost section of the furnace from the rest and thus lifting the container momentarily out of the furnace. During growth the crystal may not be examined at all. The lifetime of the heater is fairly short and repairs are inconvenient to make. Perhaps the most serious disadvantage is that the heated length L cannot be made greater than about 12 in. and this sometimes makes the design of containers difficult, in addition to limiting the maximum length of the finished crystals to 3–7 in. When crystals of this length are adequate, however, the furnace may be very useful.

The cross-section of a second type of furnace is shown in Fig. 3. The heating element in this furnace consists of a length of resistance wire over which ceramic beads are strung to provide electrical and thermal insulation. The beaded wire is wound around a piece of Pyrex tubing on which the ends have been ground square, and the ends of the wire are secured to transite end pieces. The furnace as shown will attain a temperature sufficiently high for the growth of naphthalene crystals, and with a wrapper of asbestos paper or sheet metal as thermal insulation will attain a temperature of about 235° C. (with 500 watts applied), which is adequate for the growth of anthracene crystals. Two furnaces of this type have been constructed, the first with a diameter of 3 in. and a heated length L of 10 in., the second with a diameter of 5 in. and a length of 9 in. These furnaces have been very successful in growing crystals, although it is necessary to shield photosensitive materials from the light. They are remarkably easy to construct, and the entire process

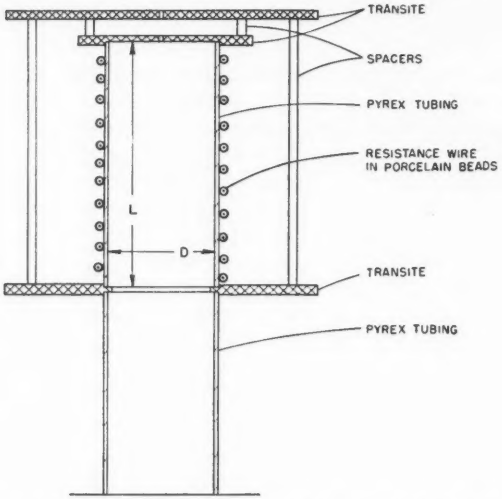

FIG. 3. Diagram of a glass furnace for the growth of crystals.

of crystal growth may be viewed through the gaps in the heating element. The furnaces have incidentally proved to be very useful for general laboratory use. This design is therefore strongly recommended.

After the furnaces so far described had been in operation for some time two aspects of the production of crystals came to light. In the first place it was found that no matter how carefully the operations involved in growing a crystal are carried out one is never certain of obtaining a good crystal on a given run, but only has a certain expectation of obtaining one. Also the growth process, at 0.1 in. per hour, is a slow one, and a day or two may pass before one can ascertain whether a given run is going to succeed or fail. It is therefore advisable to start the growth of two crystals when one is wanted, and to have more furnaces available than are normally needed. Secondly, it was found that the lengths of the above furnaces were much shorter than was desirable. There are a number of reasons for using longer furnaces. One is obviously that longer crystals may be obtained in longer furnaces. Another is that the growth of materials like anthracene is facilitated. Anthracene may not be melted in air without serious charring, so the starting material for a crystal is usually anthracene flakes which are sealed off in vacuum in a long container. When melted in a furnace the anthracene fills only a small section of the container, so that the production of long crystals is difficult and inconvenient. Finally and perhaps most important, the use of long containers greatly increases, for causes discussed below, the chances of obtaining a good crystal on any particular run. For these reasons the construction of four furnaces with heated sections 2–4 ft. long (total height of the furnaces 5–9 ft.) was undertaken. It was desired to make the furnaces of large bore Pyrex tubing as shown in Fig. 3, but at the time the quantities of tubing required

were not available and the furnaces were therefore constructed of sheet metal. The design employed was not so successful as was hoped, but quite a number of good crystals have been grown, especially very long crystals of naphthalene, and much useful experience has been gained, so these furnaces will be briefly discussed.

A schematic diagram of a sheet metal furnace is given in Fig. 4. The heated section consists of three concentric tubes of 6 in., 7 in., and 8 in. diameter.

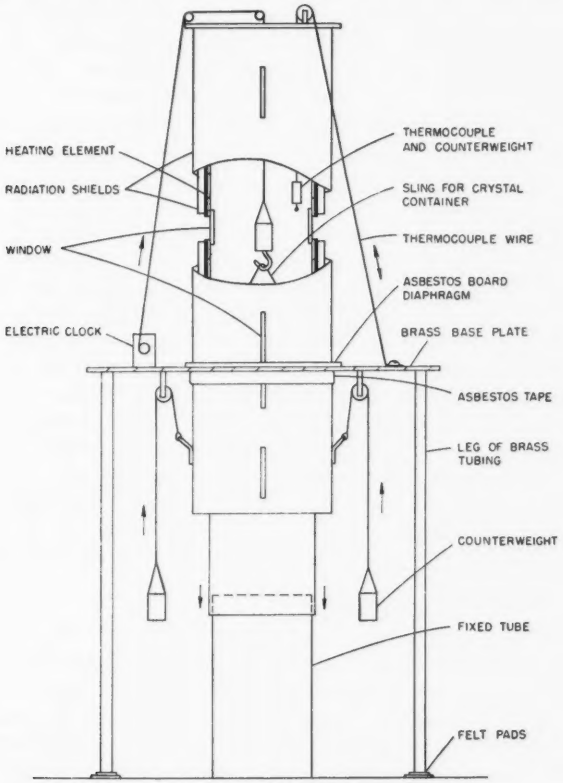

FIG. 4. Diagram of a sheet metal furnace.

The heating element is wound on the innermost tube, while the outer two provide thermal insulation. The hot section rests on an asbestos board diaphragm placed on a brass base plate. The base plate is in turn supported by four legs of brass tubing. The legs stand on felt pads, which serve both to prevent excessive building vibration from reaching the crystal and to level the furnace. The bottom section of the furnace is held against the base plate by means of two lead counterweights, and may be lowered outside of a fixed tube like a

telescope barrel. When a container is to be placed in the furnace the bottom is lowered, the counterweights detached, and the bottom tilted so that the container may be placed in the bottom. The bottom is then set upright again, the sling supporting the container is placed on the counterweighted hook, and the wire supporting the crystal is wound up on the wheel on the clock.

Slots are cut at intervals in the sheet metal tubes to serve as windows which allow observation of the progress of melting and growth. Small pieces of glass are placed over the slots in the innermost tube, while the slots in the outer two tubes are left open. The crystal may readily be viewed by holding a light against a window and looking in at the opposite window. The heating elements on the inner tube are wound on asbestos paper and cemented in place with water glass, a method which gives elements of low heat capacity but capable of withstanding fairly high temperatures. The elements were divided into sections one foot long, and the resistance was chosen to be 20 ohms. The voltage to each section is controlled by a variable voltage transformer.

In operation, it has proved difficult to control the temperature within these furnaces. In spite of the asbestos board diaphragms the brass base plate conducts a large amount of useful heat away from the furnace, and convection currents of air in the slotted outer tubes tend to cool excessively the part of the heated section adjacent to the base plate. It has been found necessary to install an auxiliary heater in the bottom of the furnace adjacent to the base plate, and furthermore to regulate the voltage applied to this heater with a Sorenson regulator. Repair of the heaters is difficult.

In spite of the above disadvantages these furnaces are in regular use and have clearly shown the advantages of long furnaces. It has proved possible to grow naphthalene crystals up to three feet long, and the design of crystal containers is made comparatively easy. An incidental benefit of the long furnaces is their use in the purification of naphthalene. This is discussed below.

Laboratory Procedures and Container Design

When growing naphthalene and anthracene crystals by the Bridgman method it is essential to use only materials of the highest purity, and various procedures were used in these experiments in order to purify the original materials. For naphthalene the procedure first used was to evaporate the material (supplied by the Eastman Kodak Co.) in air. This method is satisfactory but slow, and is applicable only to materials which do not react with air. A second method is made possible by the long Bridgman furnaces. A quantity of naphthalene is placed in a Pyrex tube of about 1 in. bore and $3\frac{1}{2}$ ft. length and melted to fill the tube. The tube is then evacuated, sealed off, and placed in a Bridgman furnace. When the naphthalene is molten the container is lowered at 1 in. per hour, and purification due to normal freezing takes place. Impurities heavier than naphthalene settle to the bottom while those lighter than or soluble in naphthalene go to the top of the tube. Adsorbed gases, which may seriously impede the growth of clear crystals, are removed, and the material in the central region of the tube is excellent for

crystal growth. This purification process naturally takes place during normal crystal growth as well. (It should be noted that Wolf and Deutsch (1954) purified naphthalene by zone melting with excellent results.) The purification of anthracene has been discussed in detail by Sangster and Irvine (1956) and their methods have been employed by the author. Anthracene (of "scintillation grade" supplied by the Reilly Tar and Chemical Corp.) was either recrystallized from solution in N,N-dimethylformamide or purified in a chromatographic column.

One can never be certain of obtaining a good crystal in a given run, and when growing crystals it is advisable, in order to have the greatest probability of getting a good crystal, to proceed in two stages:

1. Production of seed crystals.
2. Production of long or large crystals from seeds.

Once a stock of seed crystals is on hand the further production of crystals is greatly simplified. A number of types of container, illustrated in Fig. 5, may

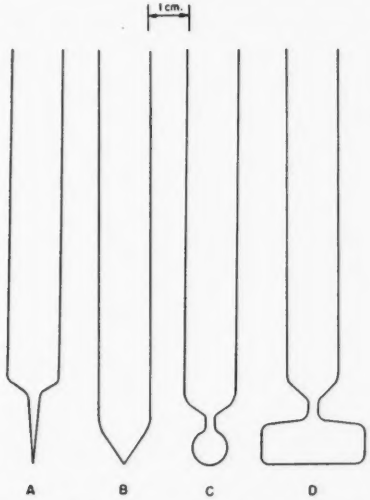

FIG. 5. Containers employed by various authors for the growth of crystals.

be employed for producing seed crystals. Type 5A was used by Huber and his associates (1949) and later by Leninger (1952), who also employed containers of rectangular cross-section, type 5B is that used by Stockbarger (1936), type 5C by Bridgman (1925) and later researchers, while type 5D is a modification of Bridgman's design employed by the author. In each case the object is to initiate the growth of a single crystal at a point or constriction. All the types shown in the diagram have been tried by the author. One of the difficulties encountered with types 5A and 5B is that the latent heat of fusion of naphthalene and anthracene can be conducted away initially only with

considerable difficulty. The situation is improved in type 5C, where the heat of formation may flow into the bulb, and in type 5D the bulb has been increased in size and altered in shape so as to provide a large "sink" into which the latent heat may flow for eventual dissipation by radiation. Type 5D has proved to be very successful, provided the constriction is not smaller than about 2–3 mm. An unexpected result is that very often a large clear crystal is produced in the bulb, and these crystals are sometimes more useful than those in the top section of the container.

When crystals are grown in containers of the type shown in Fig. 5D the growth may proceed in a variety of ways, as illustrated in Fig. 6. Crystals of

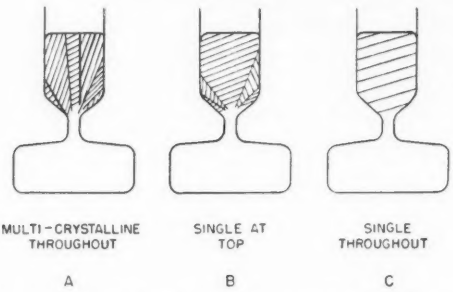

FIG. 6. Diagram illustrating the progress of crystal growth in various cases.

type 6A are fortunately unusual, while those of type 6B are quite common. Those of type 6C are less often obtained. The chances of obtaining a good crystal are increased if the wall of the container above the constriction slopes fairly gradually outwards to the full diameter, rather than abruptly. It will be observed that if a crystal grows in the manner indicated in Fig. 6B the growth of a single crystal is assured provided the container is sufficiently long. The advantages of long furnaces and crystal containers are thus emphasized.

When a single crystal is obtained it may be used as a source of seeds for further growth. These should be oriented in the same way as the source crystal since the direction of growth of the latter has presumably been a favorable one and the seeded crystal will have a high probability of growth in the same direction. This is a great aid in obtaining crystals. The growth of a crystal from a seed is carried out by fitting a length of 2–4 in. of the seed crystal into a flat-bottomed container and adding new material above the seed. The container is placed in the furnace at such a height that the solid–liquid interface is initially in the center of the seed crystal. Growth then proceeds from this level to produce additional crystals.

The crystal containers are prepared in the following manner. The containers are made of Pyrex with a ground cone fitted at the top. After they have been cleaned and filled a constriction is blown at a convenient position and the container is connected to a vacuum system by means of the cone.

The container is then evacuated, care being taken at the start that powdered material or flakes are not drawn out of the container, until a pressure of about 10 μ is attained. The container is then sealed off and placed in a furnace in the manner indicated in Fig. 1.

In order to remove finished crystals from their containers a glass cutter with a water-cooled wheel is first used. The crystal and container are first cut into a number of lengths. Each length is then placed in another cutting machine in which cuts parallel to the axis of the container may be made. Two or three cuts are then made along the length of the container until the glass falls away.

The methods described above have been used with very good success to produce crystals with diameters of $\frac{1}{2}$–$\frac{3}{4}$ in., and somewhat less success for crystals of 1 in. diameter or more. Various attempts have been made to produce crystals of 2–4 in. diameter. The chief difficulty in producing such crystals appears to be in conducting the latent heat of formation away from the interface. This may be facilitated by suspending a coil of wire wound like a spring in the center of the container, to increase the effective thermal conductivity in this region. This subterfuge has been successful in producing several good naphthalene crystals of 2 in. diameter. Another possibility might be to decrease the rate of descent of the container from 0.1 in. per hour to, say, 0.01 in. per hour. Up to the present the author has not had the patience necessary to carry out this experiment.

Orientation

When the crystal has been removed from its container it is first examined for any clues showing the location of the principal cleavage plane. Both naphthalene and anthracene have a monoclinic crystal structure, with the *ab* plane a perfect cleavage plane (Winchell 1954; Robertson 1953), and very often a stress crack or grain boundary gives an idea of the location of the *ab* plane. If this is not the case, however, a section about $\frac{1}{2}$ in. long is gently sawed from the end with a coping saw fitted with a fine-toothed blade. A razor blade is now grasped between the thumb and forefinger of each hand and carefully brought to bear upon the short length of crystal. If the cleavage plane is not found the blade may be pressed fairly firmly against the crystal and nothing will happen. If the blade is approximately aligned with the cleavage plane a fair amount of pressure will be required to cleave the crystal and the break will probably be irregular. If after a few trials, however, the blade is carefully aligned with the cleavage plane, the crystal will cleave with almost no pressure. The crystal may now be cleaved as required. The sections cannot be cleaved less than about 1.5 mm. thick, since the crystals also cleave along the *ac* plane and tend to crumble if thinner cleavages are attempted. This procedure may readily be carried out after a little practice with chips of crystals not required for experiments.

Once the *ab* plane is located it remains to determine the direction of the *b*-axis within this plane. Crystals grown from solution or by sublimation usually take the form of plates with the *ab* plane lying in the plane of the plate, and

the method described here therefore applies to them as well. The crystal is placed on a microscope slide or a suitable mount on the stage of a polarizing microscope. As the stage is rotated, the uniformity of extinction can be observed, and gives an idea of the perfection of the crystal (Pimentel and McClellan 1952). Crystals showing a mosaic pattern may be discarded in favor of more perfect ones. The procedure now followed depends upon the thickness of the crystal under examination. If the crystal is sufficiently thin (up to about 0.2 mm.) a conoscope and Bertrand lens are used and an interference pattern typified by dark regions or isogyres appears (Winchell 1947). The type of isogyre appearing with naphthalene or anthracene is shown in Fig. 7. The *b*-axis lies along the isogyre, and after the specimen has been

FIG. 7. Diagram illustrating the appearance of the isogyre of a thin crystal of naphthalene or anthracene as seen in the field of a polarizing microscope with a conoscope and Bertrand lens.

turned so that the isogyre is aligned with one of the cross hairs of the microscope eyepiece the specimen or its mount may be suitably marked.

If the specimen is too thick to show an isogyre, as is usually the case with cleaved sections, the *b*-axis may be located by observation of the birefringence of the crystal. The crystal is placed on the stage over a piece of thin graph paper or a thin piece of paper with a few dots marked on it, with both polarizer and analyzer in the optical path. As the stage is rotated the birefringence will vanish at two positions 180° apart. The *b*-axis now lies along either the north–south or the east–west axis of the microscope, depending on the arrangement of the microscope. If the polarizer is aligned with the east–west axis the *b*-axis is parallel to the microscope north–south axis, and vice versa.

Polishing

It is often desirable to polish a surface on a large crystal grown from the melt, and this may be done by the following procedure. The surface in question may, if necessary, first be ground approximately flat on a piece of number 00 emery paper or a fine-toothed flat file. The crystal is then ground with abrasive powders. A small quantity of abrasive powder is placed on a piece of plate glass and enough water mixed with it to produce a thin suspension. The crystal is then gently rubbed on the abrasive suspension with a circular motion. This process leaves a matte surface on the crystal, which may be removed as follows. A piece of tissue paper is placed on a separate piece of plate glass and thoroughly soaked with benzene. The crystal is rubbed on the soaked paper until the surface becomes clear. The surface of the crystal may then be examined, and polishing with the abrasion suspension resumed as necessary. The abrasive powder should be renewed frequently. When the coarsest abrasive powder has been employed sufficiently long to produce a flat surface the crystal should be cleaned in flowing water and by rubbing on a

benzene-soaked tissue. Polishing is now resumed with a finer grade of abrasive powder on a second piece of plate glass, and the process is carried on as before, until after the finest grade of powder the polishing is completed by rubbing on benzene-soaked tissue. Carborundum powder of 28 μ grain size, followed by alundum powders of 22 μ and 17 μ grain size, is suitable. Benzene has been found to be the most satisfactory solvent for the clearing and final polishing.

This process gives flat smooth surfaces of excellent appearance when viewed in reflected light. The following should, however, be borne in mind when it is employed. Surfaces of anthracene polished in this manner have been found much more susceptible to attack by exposure to air or oxygen than cleaved surfaces or the surfaces of crystals grown from solution or by sublimation (Lipsett, Compton, and Waddington 1957). In particular, the intensity of fluorescence declines after a few hours. The surfaces of naphthalene crystals, on the other hand, deteriorate by sublimation. The surfaces may be preserved by storage in an inert gas (with naphthalene preferably kept in a refrigerator as well) or, if permissible, by coating them with an acryllic cement.

GROWTH OF ANTHRACENE CRYSTALS FROM SOLUTION IN N,N-DIMETHYLFORMAMIDE

The production of crystals in solutions is a common process in chemistry, and many methods have been devised in which large crystals of various materials, rather than purified products, have been obtained (Buckley 1951; Neuhaus 1956). When anthracene is crystallized by cooling of a solution the form of the small crystals usually varies according to the solvent used. A particularly useful solvent for anthracene is N,N-dimethylformamide (abbreviated below as DMF), from which anthracene crystallizes to form approximately hexagonal plates. When crystallization is carried out in the manner described below useful crystals of up to about $1\frac{1}{4}$ in. in the largest dimension may be obtained.

A quantity of anthracene is weighed out and placed in a crystallizing dish about 125 mm. in diameter by 65 mm. high. DMF is then added to make up a mixture of about 15 g./100 ml. of anthracene in DMF. (Since DMF is highly toxic, this and all subsequent operations should be carried out in a fume cabinet.) The dish is placed on a $\frac{1}{2}$ in. thick copper plate, which in turn rests on an electric hot-plate, and a filter paper is placed on top of the crystallizing dish. The mixture is now heated until all the anthracene has gone into solution (about 120° C.), and the heat is turned off. Because of the high heat capacity of the copper plate, the top of the solution tends to be cooler than the bottom, and a "skin" of anthracene crystals forms on the top of the solution. This consists of a mosaic of crystals of various sizes, and the individual crystals range in size up to about $1\frac{1}{4}$ in. across the plate and up to about 0.2 mm. in thickness. These crystals may readily be removed from the solution with a spatula and dried on filter paper. The crystals from the "skin" seldom show the thick steps appearing on crystals which subsequently grow on the bottom and sides of the crystallizing dish. They are of good

optical transparency, and show uniform extinctions when viewed in a polarizing microscope. They are particularly useful in work on fluorescence.

PRODUCTION OF ANTHRACENE SUBLIMATION CRYSTALS

In order to carry out experiments on the absorption spectra of certain organic crystals, in particular naphthalene and anthracene, it is necessary, because of the very high absorption coefficients, to use very thin specimens. This may most easily be done with sublimation crystals, and these crystals may, of course, also be used in other types of experiments. A method of preparing sublimation crystals of naphthalene and anthracene has been given by Obreimov and Prikhotjko (1932) (see also Bree, Carswell, and Lyons 1955) but their procedure was carried out in air and it was desired in the present experiments to avoid this and also to have a technique giving somewhat more reliable results. After a number of trials the method described below was adopted.

The apparatus used for producing anthracene sublimation crystals is shown schematically in Fig. 8. The sublimation vessel consists of a long piece of 5 cm. bore Pyrex tubing, closed at one end and fitted with a large ground cone at the other. When the cone and socket are disassembled the charge of anthracene may be inserted, followed by the collector assembly. In operation

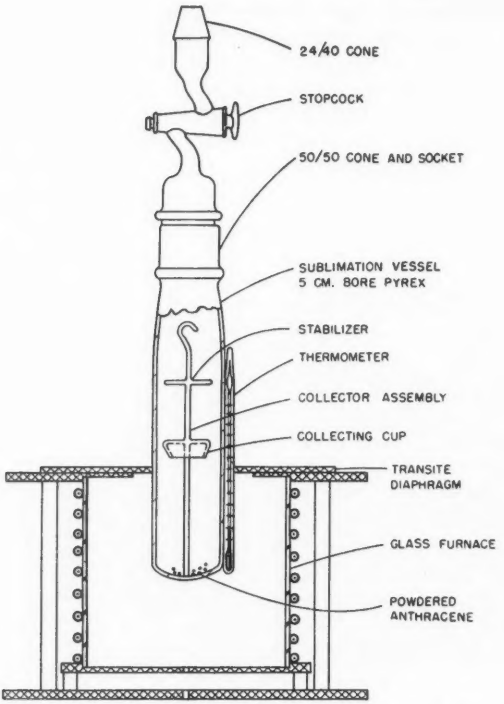

FIG. 8. Diagram of apparatus for the production of anthracene sublimation crystals.

a thermometer is taped to the sublimation vessel and the pair are let through a closely fitting transite diaphragm into a glass furnace of the type described above. The elevation of the vessel is adjusted so that the bottom of the collecting cup is about $\frac{1}{8}$ in. above the diaphragm. Various types of collecting cups were tried, and the one shown in Fig. 8 was found very satisfactory.

The sublimation is carried out in an argon atmosphere, and a pressure of 10 cm. mercury was found to give the best results. If the pressure is lower (1 cm. mercury or less) the product has the appearance of a powder. If the pressure is higher (22 cm. or more) the crystals have an irregular dendritic shape and are of poor optical transparency. The procedure followed in order to sublime the crystals is as follows.

A small amount of anthracene is ground to a powder with a mortar and pestle, and about 0.1 g. is dropped carefully to the bottom of the sublimation vessel. A new charge of anthracene must be used for each run. The collector assembly is then lowered into the vessel and the top assembly fitted. The vessel is now attached, by means of the small cone at the top, to a vacuum system where it is thoroughly outgassed, and argon to a pressure of 10 cm. is admitted through a needle valve. The stopcock above the 50/50 ground glass cone and socket (Fig. 8) is now closed, air is let into the vacuum system, and the sublimation assembly is removed from the vacuum system. The assembly is then placed in the furnace as shown in Fig. 8.

The furnace is now heated. At a temperature of about 160° C. the anthracene starts to sublime. The rate of heating should be adjusted so that 4–8 minutes are required for the temperature to rise from 160° C. to 185° C. During this time small crystals start to grow on the rim of the collecting cup and on the central rod of the collector assembly. The crystals grow in the form of hexagonal plates, and their growth may readily be observed. They show a series of interference colors as their thickness increases. When the crystals are judged to be thick enough or large enough the sublimation vessel is lifted from the furnace and allowed to cool. The sizes of the crystals thus grown range up to about 1 cm. across the flats and about 0.5–2 μ in thickness.

The crystals grow outwards from the collector assembly and are only loosely attached, so great care must be taken during their removal that they do not get detached from the collector and float away in drafts in the room. Air is slowly admitted to the vessel, and the cone and stopcock assembly is carefully detached. The collector assembly is then slowly lifted from the sublimation vessel and transferred to an area free from drafts (including the operator's breath). The crystals may now be gently detached from the collector with a small spatula and tipped into a box or onto a piece of paper. Further handling of the fragile crystals is best carried out by using a piece of Pyrex tubing drawn out to a capillary and connected with a length of rubber tubing. The free end of the rubber tubing is placed in the operator's mouth and the crystals are lifted by placing the open end of the capillary close to the crystal and sucking gently. They may thus be placed on mounts suitable for the experiments on hand.

The thickness of the sublimation flakes may be determined optically by interferometry. Methods for carrying out such measurements have recently been described in detail by Bree and Lyons (1956).

PRODUCTION OF MIXED CRYSTALS

In this section it is desired merely to point out that crystals containing small amounts of certain "impurities" in solid solution, for example anthracene with a few parts per thousand of naphthacene, may be grown by any of the methods described above. In such crystals the fluorescence is characteristic of the impurity rather than of the host compound as a result of the transfer of excitation energy (see for example Northrop and Simpson (1956) and references in their paper). The starting material for these crystals consists of a mixture of host and impurity weighed out in the required proportions, rather than a single material. It should be remembered that the impurity concentration of the finished crystal is not necessarily the same as that of the original materials. The final concentration may readily be determined, however, by preparing a solution in benzene of a portion of the finished crystal and comparing the absorption spectrum of this solution with the spectrum of a similar solution made up from known amounts of the materials.

ACKNOWLEDGMENTS

The author is most grateful to Dr. E. H. Nickel of the Mineral Dressing and Process Metallurgy Division, Department of Mines and Technical Surveys, Ottawa, for his assistance in developing the methods for determining the orientation of large crystals, and to Dr. J. H. Simpson for many helpful discussions. Part of the work described here was carried out in the Physics Department of the University of British Columbia.

The quotation in the Introduction is reprinted with kind permission from the publishers, John Wiley & Sons, Inc.

REFERENCES

Bree, A., Carswell, D. J., and Lyons, L. E. 1955. J. Chem. Soc. 1728.
Bree, A. and Lyons, L. E. 1956. J. Chem. Soc. 2658.
Bridgman, P. W. 1925. Proc. Am. Acad. Arts Sci. **60**, 305.
Buckley, H. E. 1951. Crystal growth (John Wiley & Sons, Inc., New York).
Feazel, C. E. and Smith, C. D. 1948. Rev. Sci. Instr. **19**, 817.
Huber, O., Humble, F., Schneider, H., and Steffen, R. 1949. Helv. Phys. Acta, **22**, 418.
Johnson, P. D. 1951. Ceramic age, **58**, 32 (November).
Leninger, R. F. 1952. Rev. Sci. Instr. **23**, 127.
Lipsett, F. R., Compton, D. M. J., and Waddington, T. C. 1957. J. Chem. Phys. (In press).
Menzies, A. C. and Skinner, J. 1949. Discussions Faraday Soc. **5**, 306.
Mohorčič, G. 1953*a*. Bull sci. conseil acad. R.P.F. Yougoslav. **1**, 43.
——— 1953*b*. Slovenian Acad. Sci. and Arts, "J. Stefan" Inst. Phys. Repts. **1**, 77.
Neuhaus, A. 1956. Chem.-Ing.-Tech. **28**, 155, 350.
Northrop, D. C. and Simpson, O. 1956. Proc. Roy. Soc. A, **234**, 136.
Obreimov, I. W. and Prikhotjko, A. 1932. Phys. Z. Sowjetunion, **1**, 203.
Pimentel, G. C. and McClellan, A. L. 1952. J. Chem. Phys. **20**, 270.
Robertson, J. M. 1953. Organic crystals and molecules (Cornell University Press, Ithaca, New York).
Sangster, R. C. and Irvine, J. W. 1956. J. Chem. Phys. **24**, 670.
Sidman, J. W. 1956. Phys. Rev. **102**, 96.
Stockbarger, D. C. 1936. Rev. Sci. Instr. **7**, 133.
Winchell, A. N. 1947. Elements of optical mineralogy, Part I, Principles and methods, 5th ed. (John Wiley & Sons, Inc., New York).
——— 1954. The optical properties of organic compounds, 2nd ed. (The Academic Press, Inc., New York).
Wolf, H. C. and Deutsch, H. P. 1954. Naturwiss. **41**, 425.

A HIGH-FREQUENCY 500-KILOVOLT COCKCROFT-WALTON ACCELERATOR[1]

PAUL LORRAIN, RENÉ BÉIQUE, PAUL GILMORE,
PAUL-EMILE GIRARD, ALAIN BRETON, AND PIERRE PICHÉ

ABSTRACT

The 500-kilovolt accelerator described is of the Cockcroft–Walton type and is operated at a frequency of 32 kc. It is pressurized for compactness. The circuit comprises 24 stages and is terminated by an inductive load which increases the output voltage by a factor of 1.5. The rectifier filaments are heated by utilizing the current flowing through the stray capacitances of the rectifiers. The circuit calculations are given and the design is described briefly.

1. A MODIFIED GREINACHER VOLTAGE MULTIPLYING CIRCUIT

The Cockcroft–Walton accelerator owes its name to J. D. Cockcroft and E. T. S. Walton (1930) who utilized it to produce the first artificial nuclear disintegrations. It utilizes a voltage multiplying circuit originated by Greinacher (1921) about 10 years earlier. Fig. 1 shows the circuit for the case where the number of stages is equal to 4. R_{DC} is the load resistance.

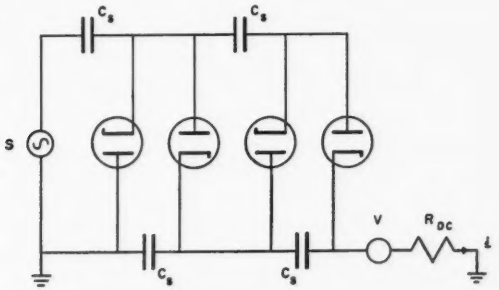

FIG. 1. Conventional four-stage Greinacher voltage multiplying circuit.

If the stray capacitances of the rectifiers are negligible, or if the number of stages N is small, the high voltage V and the ripple voltage ΔV are given by

$$V = N2^{1/2} v_0 - (i/12fC_s)(N^3 + \tfrac{9}{4}N^2 + \tfrac{1}{2}N), \tag{1}$$

$$\Delta V = \pm (i/fC_s)N(N+2) \tag{2}$$

for ideal rectifiers having zero forward resistance and infinite backward resistance (Bouwers and Kuntke 1937). Here, v_0 is the r.m.s. input voltage at S, i is the load current, and f is the operating frequency. The voltages across the capacitors C_s are everywhere $2(2)^{1/2}v_0$, except for the capacitor

[1]Manuscript received September 9, 1956.
Contribution from the Département de Physique, Université de Montréal, Montréal, Canada.

in series with S, across which the voltage is $(2)^{1/2}v_0$. The peak inverse voltages across the rectifiers are $2(2)^{1/2}v_0$.

It appears from equations (1) and (2) that v_0 should be large and that N should be small so that both the internal impedance and the ripple can be low. This was the practice until a few years ago. It turns out, however, that increasing N brings about an over-all decrease in the cost and size of the circuit (Lorrain 1949; Woodyard 1951; Alvarez 1951; Peck 1955; Peck and Eubank 1955).

The stray shunt capacitances C across the rectifiers give rise to alternating currents in the capacitors C_s. It is found (Everhart and Lorrain 1953) that, when the load current i is zero, the voltage V is not really given by equation (1) above, but by

$$V = FN(2)^{1/2}v_0, \tag{3}$$

where the voltage efficiency F is less than 1 and is given by

$$F = (b/N)\tanh(N/b), \tag{4}$$

and

$$b = (C_s/C)^{1/2}. \tag{5}$$

To reduce the effect of the stray shunt capacitances C, one can use an inductor and a blocking capacitor in parallel with the last rectifier as in the modified circuit of Fig. 2, where

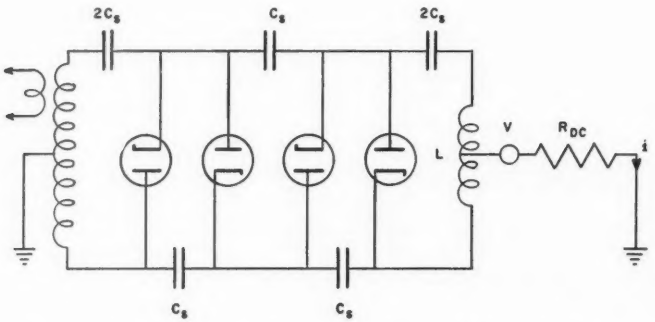

FIG. 2. Modified four-stage Greinacher voltage multiplying circuit.

$$L_{\text{opt}} = (1/\omega^2 bC)\coth(N/2b) \tag{6}$$

and

$$F_{\text{opt}} = (2b/N)\tanh(N/2b). \tag{7}$$

Fig. 3 shows a curve of $V/(2^{1/2}\times 2bv_0)$ as a function of $N/2b$. It shows, effectively, the manner in which the output voltage V varies with the number of stages N for a given value of b. It is interesting to note that, for an infinite number of stages, V tends asymptotically towards $2^{1/2}\times 2bv_0$. Without an

inductor L, the asymptotic value is $2^{1/2}bv_0$. The slope of this curve is plotted in Fig. 3 as

$$d[V/(2^{1/2}\times 2bv_0)]/d(N/2b)$$

as a function of $N/2b$.

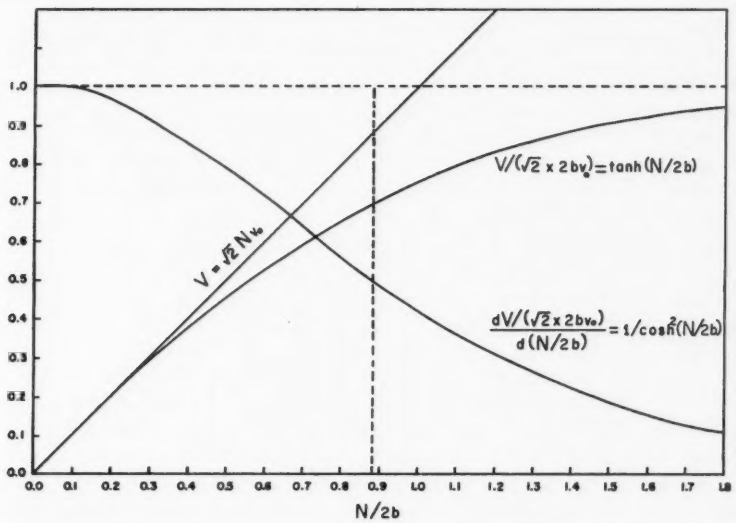

FIG. 3. Graph showing the variation of the output voltage V for a given value of b, as the number of stages N is increased. The optimum value of $N/2b$ is 0.88.

One can define arbitrarily the optimum operating point as that where the output voltage is $1/(2^{1/2}) = 0.707$ of the asymptotic voltage. Then the output voltage V is $2bv_0$. At this point, the slope of the voltage curve is $\frac{1}{2}$, which means that the addition of a further pair of stages would increase the output voltage by only $(1/2)(2\times 2^{1/2}v_0)$. According to this definition, the optimum value of $N/2b$ is 0.88. The actual value of $N/2b$ for the present design is 0.86.

It is interesting to note that, for a given accelerator, i.e. for a given b and a given N, $\omega^2 L_{\text{opt}}$ is a constant, i.e. L_{opt} varies inversely as the square of the operating frequency f. The frequency must therefore be high enough so that L_{opt} can have a reasonable value.

The inductor L can be of considerable help in increasing the voltage efficiency F for a fairly broad range of values of N/b, say between 0.5 and 3. It increases the input impedance somewhat. It is also particularly interesting in the following ways. (*a*) It can supply power to the ion source and to the extraction electrodes, as will be seen below. (*b*) With the high voltage terminal connected to the inductor center tap and the center tap on the input transformer connected to ground as in Fig. 2, the maximum voltage with respect to ground at the input is reduced by a factor of 2. This greatly reduces

corona and insulation difficulties at that point. (*c*) With these connections, the circuit becomes completely symmetrical and there is no ripple at the output due to circulating currents in the capacitors C_s. It is to be noted that with the conventional circuit of Fig. 1, circulating currents in the capacitors C_s cause an alternating voltage to appear at the high voltage electrode (Peck and Eubank 1954). This alternating voltage can be very much larger than the ΔV given by equation (2). Unfortunately, the ripple voltage ΔV given by equation (2) cannot be eliminated by adjusting the position of the tap on the inductor. This is due to the fact that the fundamental component of this ripple is in quadrature with the voltage on the coil.

The optimum value of the inductance, L_{opt}, can be determined as follows. According to equation (6), one requires the values of ω, N, b, and C. The value of ω is determined by the design of the input transformer (see below), while the number of stages N is known. The quantities b and C are related through equation (5), C_s being known through direct measurement, the average value being taken. The only unknown is therefore b, whose value one can find as follows. The input capacitance without inductor L is given by (Everhart and Lorrain 1953)

$$C_0 = (C_s/b)/\coth(N/b). \tag{8}$$

It must be realized, of course, that both the capacitances C_s and C normally vary over, say, $\pm 20\%$ of average. The values of C_s and b shown in equation (8) are thus effective values which are sensitive to the actual values near the input end. C_0 is determined with sufficient accuracy by measuring the resonant frequency of the transformer secondary with and without the voltage multiplying circuit (no inductor) connected in parallel. To determine b, one then draws a curve of C_0 as a function of b according to equation (8), from which the value of b corresponding to the observed value of C_0 can be found.

In the present case, C_s has an average value of 1300 picofarads (micromicrofarads), $N = 24$, and $C_0 = 87$ picofarads (pf.). This gives $b = 14.0$, $C = 6.65$ pf., and $N/b = 1.71$. The operating frequency being 32.1 kc. (see below), $L_{opt} = 380$ mh. and $F_{opt} = 0.810$. This value of F_{opt} compares with $F = 0.547$ which obtains without an inductor. The inductor thus raises the output voltage V by a factor of $0.810/0.547 = 1.5$.

This method of calculating b and L_{opt} is not really accurate, for the individual values of the capacitors C_s vary. The effective value of b in the formula for L_{opt} is sensitive to the actual values of b near the output end, and is different from the effective value of b for C_0. This is shown by the fact that the calculated values for the stray capacitance per stage C, in the case of our accelerator, varied from 6.5 to 8.2 to 6.7 pf. for three different sets of capacitors C_s with average capacitances of 740, 568, and 1300 pf. In all three cases the geometry was the same and hence actual values of C were presumably the same. This variation is of the order of $\pm 15\%$ from average. Such a variation is to be expected, since C varies with the square of b, while b is deduced from C_0.

Another interesting expression for L_{opt} can be obtained by combining equations (6) and (8) to get

$$L_{opt} = (1/\omega^2 C_0)(1+1/\cosh(N/b)). \tag{9}$$

Here again, equation (9) is not quite correct because it does not distinguish between the effective values of b for C_0 and for L_{opt}. Assuming that the above equation is correct, a very rough guess at the value of C/C_s is sufficient to determine L_{opt} with fair accuracy.

Unfortunately, the voltage between the capacitor banks at the output end is very sensitive to the value of the inductance L. It is therefore desirable to first calculate L_{opt} as above and then to adjust the inductance L so that the experimental value of the above-mentioned ratio is equal to unity. If the ratio is greater than unity, the inductance should be increased, and *vice versa*.

It must be remembered that the circuit impedances are high and that the addition of stray capacitance, whether to ground or in parallel with L, can seriously disturb the circuit. A capacitance in parallel with the transformer secondary can either increase or decrease the gain G of the transformer (see below). The voltages between the capacitor plates and ground at both ends of the circuit can be measured with a vacuum tube voltmeter whose probe is extended about two feet with a steel wire. The voltage across the line is the sum of the voltages on either side. These measurements can be made at a-c. input voltages low enough so that the rectifier filaments do not light. Under these conditions, there is of course no d-c. high voltage on the circuit. To reduce ripple on the high voltage electrode, the center tap on L should be adjusted so that there is no a-c. voltage on the high voltage electrode.

The experimental value of L_{opt} thus found was 357 mh. This value is in fair agreement with the above calculated value of 380 mh., if one takes into account the actual values of C_s near both ends of the circuit.

Table I shows calculated and observed values for L_{opt}, $e_{n\,min}/e_1$, F, for the output voltage, and for the input capacitance C_0 for the present case. e_n is

TABLE I

CALCULATED AND OBSERVED VALUES FOR THE VOLTAGE MULTIPLYING CIRCUIT

Quantity	Without inductor L ($L \to \infty$)			With inductor L ($L = L_{opt}$)		
	Formula	Value		Formula	Value	
		Calc.	Obs.		Calc.	Obs.
L_{opt}	—	—	—	$(1/\omega^2 bC)\coth(N/2b)$	380 mh.	357 mh.
$\frac{e_{n\,min}}{e_1}$	$\frac{e^{-\gamma(N-1)} - e^{-\gamma(N+1)}}{1 - e^{-2\gamma N} - e^{-\gamma} + e^{-\gamma(2N-1)}}$	0.380	—	$\frac{e^{-\gamma(\frac{1}{2}N-1)} + e^{-\gamma(\frac{1}{2}N)}}{1 + e^{-\gamma(N-1)}}$	0.736	0.82
F	$(b/N)\tanh(N/b)$	0.547*	—	$(2b/N)\tanh(N/2b)$	0.810*	0.85
Output voltage	$2\frac{1}{2}N v_0 F$	$18.6v_0$	—	$2\frac{1}{2}N v_0 F$	$27.5v_0$	$29v_0$
C_0	$bC/\coth(N/b)$	—	87.0 pf.	$bC/\coth(N/2b)$	64.6 pf.	—

$C_s = 1300$ pf., $C = 6.65$ pf., $b = 14.0$, $N = 24$, $\gamma = 1/b$, $f = 32.1$ kc.

*Not corrected for the voltage drop across the filament transformers or for the voltage drop across the rectifiers.

the voltage across the nth rectifier, counting from the input transformer. The ratio $e_{n\,min}/e_1$ is the ratio e_N/e_1 for the case where there is no inductor L and $e_{N/2}/e_1$ for the case where there is an inductor L.

The operating frequency is determined as follows. With F corrected with an inductor L, the frequency must be rather high, as was noted above. This consideration fixes an approximate lower limit for the operating frequency f, while dielectric losses in the glass of the rectifier tubes fix an upper limit for f which is specified by the manufacturer. This upper limit is about 250 kc. for presently available tubes. Within these limits, f must be chosen with regard to Joule losses in the inductor L. The capacitors C_s are assumed to have proper high-frequency characteristics. If the voltage multiplying circuit is fed through a high frequency air core transformer, due regard must be given to its Joule losses, its voltage gain, and its regulation. The relevant theory is given below.

Ripple in the high voltage is not a serious problem. When an inductor L is used, ripple due to alternating currents in the capacitors C_s is reduced to negligible proportions by adjusting the tap on the input transformer or that on the inductor. An alternating voltage of the proper magnitude, phase, and waveform can also be injected between the voltage multiplying circuit and ground to eliminate ripple.

2. THE INPUT TRANSFORMER WITHOUT LINK

The design of the input transformer is not simple and at high frequencies the voltage multiplying circuit should be fed, if possible, directly from the plates of the power amplifier without the intermediary of a transformer. In the case of the accelerator described below, a transformer was required so as to step up the voltage supplied by the power amplifier to the required level and also to permit placing the power amplifier a few feet away from the voltage multiplying circuit, the primary and the secondary of the transformer being connected through a low-voltage high-current link.

We shall first discuss the input transformer where primary and secondary are coupled directly without the intermediary of a link (Béique 1952; Gilmore 1953; Mathers 1948, 1949; Mautner and Schade 1947). The circuit is shown in Fig. 4. C_2 stands for the input capacitance of the voltage multiplier plus the stray capacitance of L_2 and its leads. R_{DC} is the load resistance at the output of the voltage multiplying circuit. It is transformed into the resistance R_L at the input by choosing R_L so that it dissipates the same amount of power as R_{DC}. The approximation is very crude in that it assumes a voltage efficiency F of 1, it neglects the drop in voltage which occurs when a load current is drawn, and it neglects the fact that direct current is drawn in bursts from

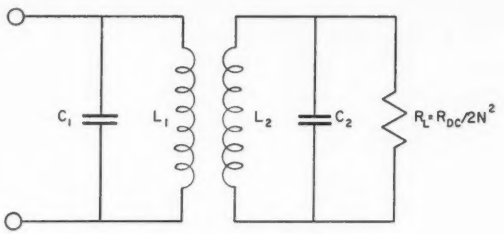

FIG. 4. Input transformer.

the secondary, so that the resistance presented to it is non-linear. The approximation is satisfactory for the present purposes. The parallel elements C_2 and R_L can be transformed into a capacitor C_2 and a series resistor whose value is $1/\omega^2C_2^2R_L$ or $2N^2/\omega^2C_2^2R_{DC}$, for the usual case where

$$R_L \gg 1/\omega C_2. \tag{10}$$

The voltage gain $|G|$ of the transformer is given by

$$|G| = M/[(R_1R_2C_2)\{(1-Q_1Q_2\theta_2+K^2/K_c^2)^2+(Q_2\theta_2+Q_1)^2\}^{1/2}], \tag{11}$$

where

$$Q_1 = \omega L_1/R_1, \qquad Q_2 = \omega L_2/R_2, \tag{12}$$

$$\theta_2 = 1-(\omega_2^2/\omega^2), \tag{13}$$

$$K^2 = M^2/L_1L_2, \text{ and } K_c^2 = 1/Q_1Q_2. \tag{14}$$

K is the coefficient of coupling and K_c the critical coefficient of coupling between primary and secondary. The gain $|G|$ is greatest near the resonant frequency of the secondary.

The conditions required for good regulation can be found from equation (11), by rewriting it as follows:

$$M^2/|G|^2C_2^2R_1^2 = (R_2^2+X_2^2)(1+Q_1^2)+Q_1\omega L_2K^2\{2R_2+\omega L_2(K^2Q_1-2\theta_2)\}. \tag{15}$$

For proper regulation, $|G|$ should be quite independent of R_2. Then we must have first

$$X_2^2 \gg R_2^2. \tag{16}$$

This means that X_2 should not be zero and that the resonant frequency of the secondary should be different from the operating frequency.

Since θ_2 is of the order of 1, the term $2\theta_2$ in the last parenthesis of equation (15) can be expected to be negligible with respect to K^2Q_1. In the present case, $\theta_2 = -0.41$ and $Q_1 = 171$. There is no value for K because, actually, a link was used between primary and secondary, but one could expect it to have a value of about 0.5. With these values,

$$K^2Q_1 = 43 \text{ and } 2\theta_2 = -0.82.$$

For proper regulation, we must also have

$$\omega L_2K^2Q_1 \gg 2R_2. \tag{17}$$

Here we have $\omega L_2K^2Q_1 = 1.98\times10^6$. This is much larger than $2R_2$, which ranges from 500 ohms for zero current to 2×10^4 ohms at 1 ma. beam current. However, condition (16) is satisfied only for currents up to about 500 μa. because $X_2 = -1.90\times10^4$ ohms. As will be seen below, the loss in gain with load current is compensated to a certain extent.

The efficiency E of the transformer can be defined as the ratio of the power spent in R_L to the power input to the primary. It is given by

$$E = \frac{K^2/K_c^2}{(K^2/K_c^2+1+Q_2^2\theta_2^2)(1+\omega^2C_2^2R_LR_S)}, \tag{18}$$

where R_S is the internal resistance of L_2.

3. THE INPUT TRANSFORMER WITH LINK

Fig. 5 shows the circuit in which primary and secondary are coupled through a link. This is the arrangement actually used (Gilmore 1953; Girard 1955).

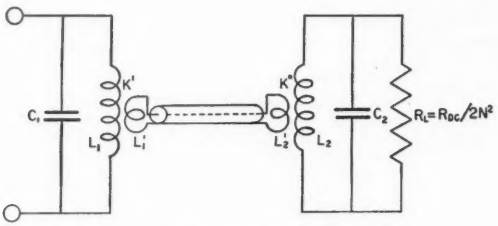

FIG. 5. Input transformer with link.

As is the usual practice, we use $L_1' = L_2' = L'$ and $R_1' = R_2' = R'$, where R_1' and R_2' are the internal resistances of L_1' and L_2'. The current in the secondary is given by

$$(19) \qquad |i_{2_L}|^2 = \frac{K'^2K''^2L_2e_1^2}{L_1Z_2^2[\{(2/Q')+AR_2+(K'^2/Q_1)\}^2+(2-AX_2-K'^2)^2]},$$

where K' and K'' are the coupling coefficients between the primary and its link and between the secondary and its link, respectively, Q' is the Q-factor of the link,

$$(20) \qquad Z_2^2 = R_2^2+X_2^2,$$

and

$$(21) \qquad A = \omega K''^2L_2/Z_2^2.$$

Equation (19) is approximate in that it is assumed that $Q_1^2 \gg 1$. This approximation is excellent, Q_1 being equal to 171 in the present case.

The gain $|G_L|$ is given by

$$(22) \qquad |G_L| = |i_{2_L}|/e_1\,\omega C_2$$

and is again greatest in the neighborhood of the resonance frequency of the secondary.

We find the conditions for good regulation as above by writing

$$(23) \qquad \frac{K'^2K''^2L_2}{|G_L|^2\omega^2C_2^2L_1} = \left[\left(\frac{2}{Q'}+AR_2+\frac{K'^2}{Q_1}\right)^2+(2-AX_2-K'^2)^2\right]Z_2^2.$$

Again, good regulation requires that condition (16) be satisfied. Then

$$(24) \qquad A = K''^2/\omega L_2\theta_2^2,$$

approximately, and the bracket on the right-hand side of equation (23) can be rewritten

$$\left(\frac{2}{Q'}+\frac{K'^2}{Q_1}+\frac{K''^2R_2}{\omega L_2\theta_2^2}\right)^2+\left(2-\frac{K''^2}{\theta_2}-K'^2\right)^2.$$

This expression is quite independent of R_2 as long as $Q_2 = \omega L_2/R_2$ is at least of the order of about 5, as can be seen by neglecting the first two terms of the first parenthesis and remembering that θ_2 is of the order of unity. Here Q_2 varies from about 5 for a 1 ma. load current to 200 for zero load current, so that this condition is satisfied.

The efficiency of the transformer is now given by

$$E_L = \frac{1}{(1+[R_1/R_r])} \cdot \frac{1}{(1+[\omega^3 L_2 C_2^2 R_L/Q_2'])}, \tag{25}$$

where Q_2' is the value of Q_2 under no load, i.e. for R_{DC} infinite, and where R_r is the resistance reflected into the primary:

$$\begin{aligned} z_r &= R_r + jX_r \\ &= \frac{\omega L_1 K'^2([2/Q']+AR_2) - j\omega L_1 K'^2(2-AX_2)}{([2/Q']+AR_2)^2+(2-AX_2)^2}. \end{aligned} \tag{26}$$

The term $C_2^2 R_L/Q_2'$ is quite independent of the frequency. For a given value of L_2, the efficiency of the secondary therefore varies rapidly with frequency and it is important that ω be not too high if this efficiency is to be high. The efficiency of the primary, on the other hand, depends on R_r, which is given by the real part of equation (26) in which equation (24) can be used. Then

$$R_r = \frac{\omega L_1 K'^2\left(\frac{2}{Q'}+\frac{K''^2}{Q_2\theta_2^2}\right)}{\left(\frac{2}{Q'}+\frac{K''^2}{Q_2\theta_2^2}\right)^2+\left(2-\frac{K''^2}{\theta_2}\right)^2}. \tag{27}$$

The Q's can be taken to be independent of the frequency. The term θ_2 is necessarily of the order of 1 for operation in the neighborhood of resonance. For a given value of L_1, R_r is thus approximately proportional to ω. The efficiency of the primary therefore varies much more slowly with frequency than that of the secondary and it need not be taken into account in the determination of the operating frequency.

The L_2 coil follows a design by Mautner and Schade (1947) and has an inductance of 230 mh. It has a stray capacitance of 11 pf., submerged in oil. The input capacitance of the voltage multiplier with the inductor L is 65 pf., which gives $C_2 = 76$ pf. and a resonant frequency of 38.2 kc. for the secondary with the inductor L connected.

The operating frequency f must be fairly close to 38.2 kc., so that the gain G can be sufficiently high, but not too close so that condition (16) can be satisfied. The operating frequency can be either above or below 38.2 kc., the latter choice being preferable from the standpoint of the efficiency of the secondary.

The primary inductance L_1 is 2.57 mh., its resistance R_1 is 3.22 ohms, $K' = 0.585$ and $K'' = 0.484$, $Q_1 = 171$ and Q' is of the order of 60.

Table II shows calculated data for $N = 24$, $f = 32.1$ kc., $F = 0.810$, and an output voltage of 500 kv.

TABLE II

CALCULATED DATA FOR $V = 500$ KV.

Beam current	Nil	500 μa.
R_r	1.08 ohms	4.98 ohms
X_r	68.4 ohms	68.0 ohms
G	4.04	3.90
E_L	Nil	0.608
e_2	18.2 kv.	18.2 kv.
e_1	4.50 kv.	4.66 kv.
i_{1_L}	7.70 amp.	7.98 amp.
i_{2_L}	0.278 amp.	0.278 amp.
W_1	192 w.	205 w.
W_2	19.4 w.	19.4 w.

The gain G of the transformer can be adjusted by changing the resonant frequency of the secondary with an oil-immersed variable capacitor in parallel with L_2. Since the operating frequency is lower than the resonant frequency of the secondary, an increase in this capacitance moves the resonant frequency closer to the operating frequency and increases the gain.

4. THE FILAMENT TRANSFORMERS

Three types of rectifiers are available for voltage multiplier circuits: thermionic rectifiers (vacuum or gas), cold-cathode rectifiers, and barrier-layer rectifiers (selenium, copper oxide, germanium, silicon). They must operate at high peak inverse voltages so that the number of stages N and the voltage efficiency F can have reasonable values. (It must be remembered that the maximum obtainable voltage, for F equal to unity, is one half the sum of the peak inverse voltages of all the rectifiers.) If a loading inductor L is used, the rectifiers must be able to operate at high frequencies. Then, vacuum thermionic rectifiers seem to be the best choice at present.

If thermionic rectifiers are used, the filaments can be heated in various ways. One good method at high frequencies is to use auto transformers in *series* with the rectifiers as in Fig. 7. The primaries then pass an alternating current which is due to the stray capacitances of the rectifiers. Since this current is rather weak, a factor of two is gained by arranging the circuit so that each primary passes the current of two rectifiers. Then another factor of the order of 20 is gained by establishing parallel resonance on the primary with a capacitor of the proper value.

The presence of the primaries reduces the voltages across the rectifiers and the high voltage is decreased accordingly. A loss of voltage of the order of 10% is calculated with the present design.

Approximate values for the primary and secondary inductances, and for the tuning capacitor, are found from the expressions for the secondary current and for the input impedance of the transformer (Lorrain *et al.* 1956). Final adjustment is made at low voltage by varying a rheostat in series with the primary. The transfomers must be individually adjusted because the voltage between the capacitor banks is not constant, being maximum at the input and at the output. Some variation in the stray capacitances of the rectifiers and

associated conductors must also be expected. The primary inductance is 10.5 mh. and the secondary, a few microhenrys. A 0.002 μf. mica capacitor is used to tune the primary.

5. DESIGN

Figs. 6 and 7 show respectively a view of the accelerator with its tank removed and a schematic diagram of the voltage multiplying circuit. The capaci-

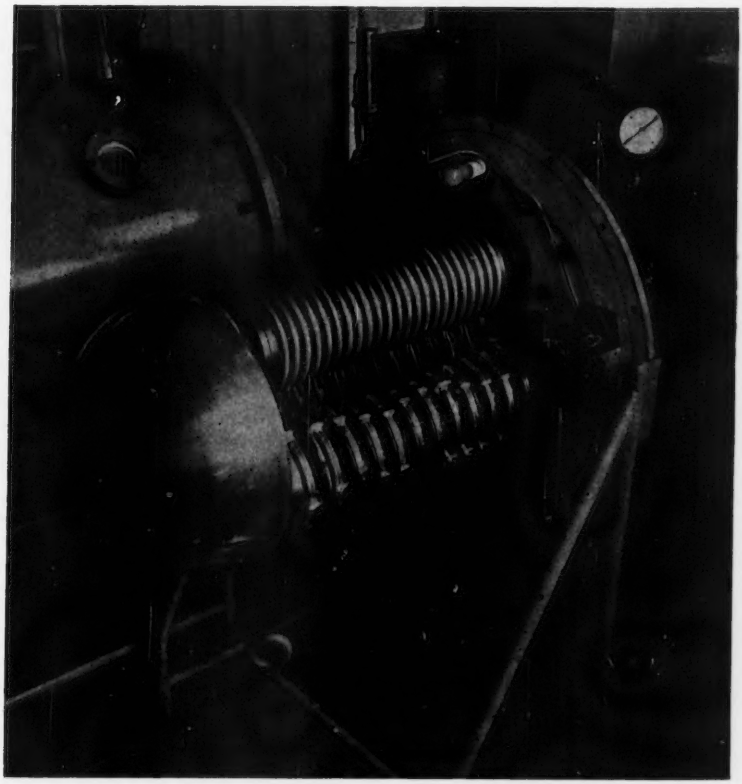

FIG. 6. View of accelerator with tank removed, showing the high voltage electrode, the accelerating tube (top), and a capacitor bank.

tors C_s are made from aluminum plates sheathed in Mylar. The high frequency is produced by a tuned plate oscillator which feeds a push–pull Class-C power amplifier (Lorrain *et al.* 1956).

The ripple voltage due to the periodic charging and discharging of the capacitors is given by equation (2). It amounts to 15 v./μa. If necessary, this ripple could be eliminated by applying a derippling voltage between the center-tap of the transformer secondary and ground (Cock 1955).

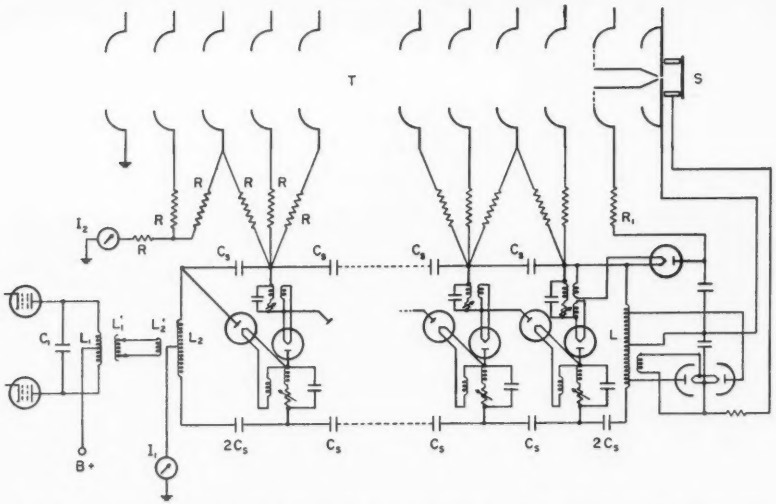

FIG. 7. Schematic diagram of voltage multiplying circuit, accelerating tube (T), extraction electrode (E), and ion source (S).

That part of the output impedance which is due to the charging currents in the capacitors is found from equation (1), which gives 30 megohms. The voltage drop from this cause is thus 30 v./μa. (see below). The regulation also depends on the design of the input transformer to the voltage multiplying circuit (see Table II) and on the voltage drop across the rectifiers. If currents greater than about 1 ma. were required, the inductance L would have to be decreased.

The output voltage is best measured by observing (p, γ) resonances in lithium fluoride. Fluorine has a resonance at 340 kev. which gives 6.0 Mev. gamma rays, while lithium has a resonance at 440 kev. giving 17.5 Mev. gamma rays. These two resonances are used to calibrate the voltmeter and also to determine the voltage efficiency F.

For prolonged operation, the high voltage must be kept close to the rated value for the following reason. The filaments must be operated in the proper voltage range, say between 1.4 and 1.6 v. The high voltage must, however, be kept within even closer limits because the filament voltage varies approximately with the 1.6th power of the output voltage.

The ion source is of the PIG type (Lorrain 1947, 1948; Gow and Foster 1953; Saint-Pierre 1955). It can be dismantled for cleaning, the glass-to-metal seals being made with indium foil. The electrodes are machined from 2S aluminum. Alnico magnets provide a magnetic field of about 500 gauss in the region of the discharge. The ion beam is extracted through a hole 1/32 inch in diameter in the lower cathode.

The ion source power supply utilizes the inductor L as in Fig. 7. This circuit shunts the inductor to a certain extent, but this is fortunate for the following reason. When the ion source is turned on, the shunting effect of its

power supply reduces the effective inductance, which tends to increase the voltage across the rectifiers near the high voltage end of the multiplier circuit. Now when a beam current is drawn, the voltage wave on these same rectifiers is clipped to a certain extent. These two effects tend to compensate to improve the regulation.

A d-c. voltage is required between the ion source and the extraction electrode so that both the ion beam intensity and focusing should be constant. The required voltage is obtained by rectifying one half of the alternating voltage across the inductor L as in Fig. 7. The half-wave rectifier shunts half of the inductor, but the effect is negligible in the present case.

The accelerating tube was built in our laboratory according to the M.I.T. techniques with glass rings* and dished aluminum electrodes.† The electrodes have an inner diameter of 4.5 in.

The pressure tank which contains the voltage multiplying circuit, the accelerating tube, and the high voltage electrode is 38 in. in diameter and 53 in. long. All components are fixed to the front cover plate which is itself fixed to the floor. The tank proper is on casters and is rolled away for servicing the accelerator. The gas used is a 50/50 mixture of CO_2 and Freon-12 at a total pressure of 30 lb. absolute.

The unanalyzed beam current is presently about 25 to 30 μa.,‡ which is quite sufficient for our present purposes. It is limited by the ion source. If this limitation were removed, the beam current would then be limited by the rectifier tubes which have an average current rating of 2 ma.

The focusing is excellent. The ion beam pierces a hole 1.0 mm. in diameter in steel shim at the position of the target 9 ft. away from the ion source.

Stray X-radiation is produced at the ion source base plate. This is due to the backwards electron beam which misses the ion source hole. The intensity of the radiation is negligible, however, except close to the tank where it reaches tolerance level.

The many safety devices used permit unattended operation.

SOMMAIRE

L'accélérateur décrit est du type Cockcroft–Walton. Il est alimenté à 32 kc., et comporte 24 étages. Il est maintenu sous pression dans un réservoir afin de réduire l'encombrement. Le circuit est terminé par une charge inductive qui augmente la tension de sortie par un facteur de 1.5. Le chauffage des filaments utilise le courant dans les capacités parasites des valves. La première partie comporte le calcul des circuits et la seconde partie donne quelques détails de construction.

ACKNOWLEDGMENTS

The work described above was financed jointly by the Université de Montréal and the Atomic Energy Control Board of Canada. The *Office de Recherches de la Province de Québec* also awarded bursaries to two of us (René

*Research Machine Company, Whitman, Massachusetts.
†High Voltage Engineering Corporation, Cambridge, Massachusetts.
‡ *Note added in proof:* The present beam current is about 100 to 125 μa. with magnesium cathodes and a hole 1/32 in. in diameter in the ion source.

Béique and Paul Emile Girard). We are particularly grateful to Drs. R. W. Cloud, H. Weiss, M. Elkind, and G. Y. Chu of the M.I.T. High Voltage Research Laboratory for information on the fabrication of accelerating tubes and on various aspects of high voltage technique. Mr. C. Saint-Pierre contributed much valuable information on the ion source. It is a pleasure to acknowledge the very able assistance of Mr. André Brunel, of Mr. J. Déziel, the laboratory technician, and of Mr. E. Gosselin, the Physics Department machinist.

REFERENCES

ALVAREZ, L. 1951. Rev. Sci. Instr. **22**, 705.
BÉIQUE, R. 1952. M.Sc. Thesis, Département de Physique, Université de Montréal.
BOUWERS, VON A. and KUNTKE, A. 1937. Z. tech. Phys. **18**, 209.
COCKCROFT, J. D. and WALTON, E. T. S. 1930. Proc. Roy. Soc. **129**, 477.
COCK, B. 1955. Rev. Sci. Instr. **26**, 210.
EVERHART, E. and LORRAIN, P. 1953. Rev. Sci. Instr. **24**, 221.
GILMORE, P. 1953. M.Sc. Thesis, Département de Physique, Université de Montréal.
GIRARD, P. E. 1955. M.Sc. Thesis, Département de Physique, Université de Montréal.
GOW, J. D. and FOSTER, J. S. 1953. Rev. Sci. Instr. **24**, 606.
GREINACHER, H. 1921. Z. Physik, **4**, 195.
LORRAIN, P. 1947. Can. J. Research, A, **25**, 338.
——— 1948. Helv. Phys. Acta, **12**, 497.
——— 1949. Rev. Sci. Instr. **20**, 216.
LORRAIN, P., BÉIQUE, R., GILMORE, P., GIRARD, P. E., BRETON, A., and PICHÉ, P. February 1956. A high-frequency 500 kilovolt Cockcroft–Walton accelerator (unpublished report).
MATHERS, G. W. C. 1948. National Research Council of Canada, Departmental Report N.R.C. No. 1725, Report No. ERA–147.
——— 1949. Proc. I.R.E. **37**, 199.
MAUTNER, R. S. and SCHADE, O. H. 1947. RCA Review, **8**, 43.
PECK, R. A., JR. 1955. Rev. Sci. Instr. **26**, 441.
PECK, R. A., JR. and EUBANK, H. P. 1954. High current Cockcroft–Walton accelerator for neutron production, Department of Physics, Brown University, Providence, Rhode Island (unpublished).
——— 1955. Rev. Sci. Instr. **26**, 444.
SAINT-PIERRE, C. 1955. Thesis, Département de Physique, Université de Montréal.
WOODYARD, J. R. 1951. R.f. power supply for a 500 kv. ion source, Radiation Laboratory, Department of Physics, University of California, Berkeley, California (unpublished).

NEW TYPE OF MAGNETIC TRANSITION IN Mn_3ZnC[1]

B. N. Brockhouse[2] and H. P. Myers[3]

ABSTRACT

Alloys with the approximate composition Mn_3ZnC are known to be ferromagnetic but the saturation magnetization shows a maximum in the region of 231° K. X-Ray and neutron diffraction measurements are reported which demonstrate that at 231° K. there is a second order transition below which ordering of the manganese ions occurs, resulting in a tetragonal distortion of the normally cubic lattice and a complex magnetic structure. One possible magnetic structure is discussed. Above the transition the alloy is apparently a normal ferromagnetic substance.

INTRODUCTION

Alloys with the approximate composition Mn_3ZnC, like other similar alloys with aluminum, gallium, tin, etc., replacing the zinc, are ferromagnetic with Curie temperatures somewhat above room temperature and saturation magnetizations of 1 to 2 Bohr magnetons per Mn atom. The structure of the alloys is cubic (space group O_h^1, one formula weight per unit cell) with the carbon going into body center positions, the manganese into face centers, and the zinc into cube corners. Manganese can replace zinc on the cube corners, but the zinc cannot take face center positions, the range of composition of the phase being approximately Mn_3ZnC to $Mn_{3.5}Zn_{0.5}C$ (Butters and Myers 1955 *a*, *b*; Morgan 1954). For compositions close to the ideal Mn_3ZnC the saturation magnetization has a maximum near 230° K. As the alloy composition departs from the ideal, the anomaly becomes less marked and finally disappears at a composition of about $Mn_{3.25}Zn_{0.75}C$, alloys with less zinc exhibiting a conventional magnetization vs. temperature curve (Butters and Myers 1955*a*). X-Ray measurements (Pearson 1954) showed that at liquid nitrogen temperature an alloy with 19.1% zinc had a tetragonal structure closely related to the cubic high temperature structure, with a c/a ratio of 0.9947. Butters and Myers attempted to interpret this behavior in terms of Néel ferrimagnetism of the alloys. Independently Dr. E. R. Morgan suggested to one of us (B.N.B.) the possibility of ferrimagnetism in the general system of alloys and proposed neutron diffraction measurements on Mn_3AlC, the results of which indicated that this alloy is probably a normal ferromagnetic (Brockhouse and Morgan 1954). Magnetic measurements also show that the anomalous behavior does not occur in Mn_3AlC although it has the same structure as Mn_3ZnC and otherwise similar magnetic properties (Butters and Myers 1955*b*). The X-ray and neutron diffraction

[1]Manuscript received November 16, 1956.
Contribution from the General Physics Branch, Atomic Energy of Canada Ltd., Chalk River, Ontario, and the Department of Mining and Metallurgy, University of British Columbia, Vancouver, British Columbia.
Issued as A.E.C.L. No. 409.
This paper was presented at the Chicago meeting of the American Physical Society, Nov. 25–26, 1955 (Phys. Rev. **100**, 1242 (1955)).
[2]Atomic Energy of Canada Ltd.
[3]University of British Columbia. Now at A. B. Atomenergi, Stockholm, Sweden.

experiments described herein were undertaken to elucidate the nature of the anomalous changes and to determine the magnetic structure of the alloys.

EXPERIMENTAL RESULTS

Specimen Materials

The alloys used in these experiments were prepared by sintering a mixture of zinc, manganese, and graphite powders in a sealed quartz tube as described by Butters and Myers (1955*a*). Powder X-ray measurements on the specimen used in the measurements described in the paper gave a lattice parameter of 3.923 Å at room temperature which, following Butters and Myers, indicates a composition $Mn_{3.07}Zn_{0.93}C$. Magnetic measurements were made of the saturation magnetization as a function of temperature and are shown in Fig. 1. The Curie temperature of 392° K. is in agreement with the measure-

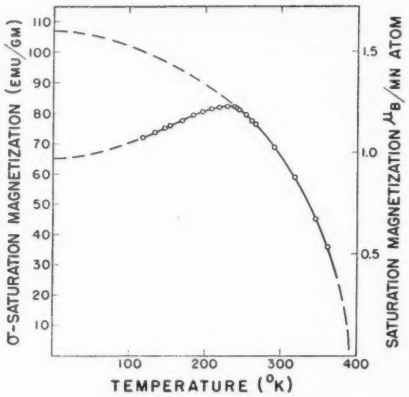

FIG. 1. Saturation magnetization of specimen as a function of the temperature, in units of e.m.u./gram of alloy, and in Bohr magnetons per atom of contained manganese.

ments of Butters and Myers for a composition $Mn_{3.07}Zn_{0.93}C$ but the saturation magnetization at the peak is about 5% lower than they obtained for this composition.

Chemical analysis showed that the specimen contained 65.6% Mn, 27.7% Zn, 0.1% spectroscopic impurities, the remaining 6.6% being presumably carbon. This would be consistent with the composition $Mn_{3.07}Zn_{0.93}$ if in addition the specimen contained about 5% by weight dispersed zinc and graphite thus accounting for the lower saturation magnetization. Such excess constituents have been previously observed in this system. No extra lines were observed in the diffraction patterns however.

The magnetic measurements were made with a field of 16,000 oersteds. Some measurements at lower field strengths, down to 8000 oersteds, were not appreciably different, indicating that saturation was achieved unless the crystalline anisotropy is improbably high.

X-Ray Measurements at Low Temperatures

The change from a cubic structure at room temperature to a tetragonal structure at liquid nitrogen temperature was studied in detail using a photographic method to determine the lattice parameters and a Norelco Geiger counter spectrometer to measure relative intensities of the components.

Geiger counter studies were carried out with FeK_α and CrK_α radiation on the 200, 220, and 311 lines at room temperature and at liquid nitrogen temperature using a low temperature attachment described elsewhere (Butters and Myers 1955*c*). In addition the 311 line was studied in detail at temperatures in the region of the anomaly in the magnetization from −33° C. to −76° C. These results are shown in Fig. 2. It will be seen that broadening commences near −40° C. as the temperature is lowered and progressively increases with decreasing temperatures.

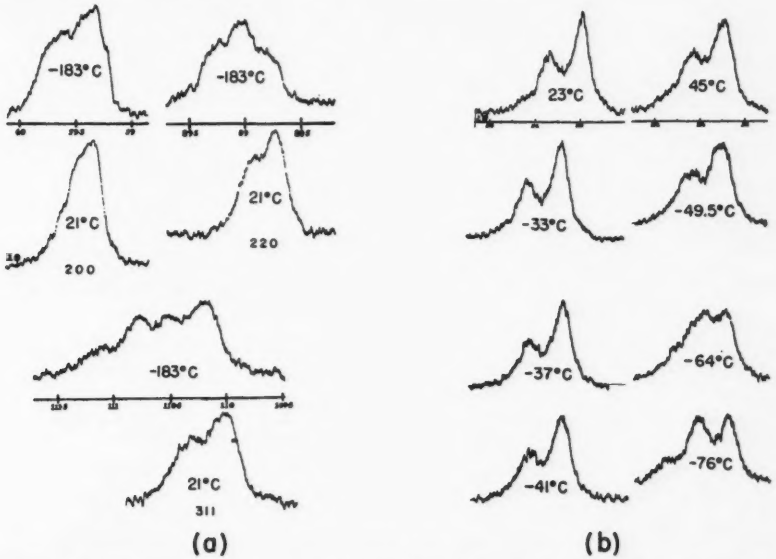

FIG. 2. (*a*) Geiger counter intensity profiles of 200, 220, and 311 lines at 23° C. and −183° C. using FeK_α radiation. (*b*) Intensity profiles of line 311 for temperatures between 23° C. and −74° C. using CrK_α radiation.

The 400 line was studied using FeK_α radiation and a low-temperature back-reflection camera. The specimen was held at different temperatures, back-reflection photographs taken, and the lattice parameters determined from the two components of the 400 line observed. The lattice parameters obtained are plotted against the temperature in Fig. 3.

The results are collected in Table I. They indicate that a tetragonal distortion of the unit cell occurs at low temperatures. From Fig. 3 this distortion is seen to take place gradually in a way characteristic of a second order transition, the transition temperature being about −42° C. or 231° K.

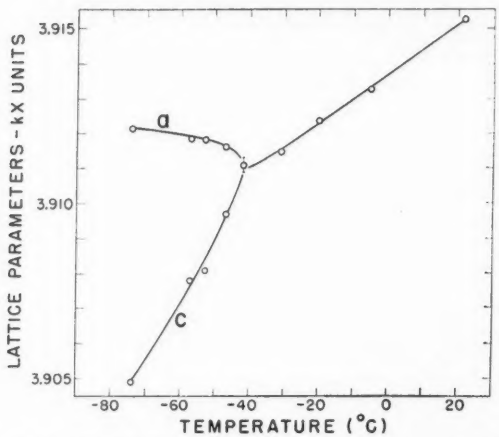

FIG. 3. Lattice parameters as functions of the temperature, obtained from back-reflection photographs on the 400 line with FeK_α radiation. Above the transition the structure is cubic, below tetragonal with lattice spacings along the tetragonal axis (c) and normal to it (a) as shown.

TABLE I

Cubic *hkl*	Form of splitting observed at −183° C.	Expected result for tetragonal distortion
111	No splitting or broadening	No splitting
200	Two components, the inner (lower θ value) stronger than the outer. Measured intensity ratio 2.05:1	Two components, multiplicity factors 2:1
220	Two components, the inner weaker than the outer. Measured intensity 1:2.3	Two components, multiplicity factors 1:2
311	Two components, the inner stronger than the outer. Measured intensity ratio 1.7:1	Two components, multiplicity factors 2:1
222	No splitting or broadening	No splitting
400	Two components, the inner stronger than the outer. Visual estimate of intensity ratio *ca.* 2:1	Two components, multiplicity factors 2:1

Neutron Diffraction Measurements

Neutron diffraction measurements were made on a large powder specimen at a temperature above the Curie temperature of about 392° K., at room temperature (295° K.) between the low temperature anomaly and the Curie temperature, at 100° K. well below the low temperature anomaly, and at liquid helium temperature. The intensities of the peaks were placed on an absolute basis by means of a vanadium standard.

Above the Curie Temperature

The structure factors of the lines observed at 433° K. are listed in Table II. Since this temperature is higher than the Curie temperature, no magnetic contributions are expected and structure factors were computed for the

TABLE II

EXPERIMENTAL AND CALCULATED STRUCTURE FACTORS AT 433° K.

hkl	Experimental		Calculated jF^2	
	$jF^2\,e^{-2W}$	jF^2	$Mn_{3.07}Zn_{0.93}C$	Mn_3ZnC
100	0.34×10^{-24}	0.34×10^{-24}	0.32×10^{-24}	0.54×10^{-24}
110	28.4	28.9	28.8	31.1
111	12.8	13.1	12.5	11.1
200	<0.4	<0.4	0.035	0.12
210	1.0	1.1	1.30	2.16
211	52.8	55.9	57.6	62.2

NOTE: In this and the following table j represents the multiplicity and

$$F = \sum_k b_k \exp\{2\pi i(hx_k+ky_k+lz_k)\},$$

where b_k is the neutron scattering amplitude of the kth nucleus in the unit cell.

perovskite structure which Butters and Myers (1955*a*) had found consistent with their X-ray measurements. The carbon atoms were taken to lie at the body center position, three manganese atoms at the three face centers, and 0.93 zinc and 0.07 manganese atoms at the cube corner. Scattering amplitudes used were those given by Hughes and Harvey (1955). Because of the negative amplitude of manganese the structure factors are very sensitive to the position of the manganese atoms vs. the zinc and carbon atoms. For comparison the calculated structure factors for ideal Mn_3ZnC are also shown. Very good agreement between the observed and calculated structure factors for $Mn_{3.07}Zn_{0.93}C$ was obtained when the constant $2B$ in the temperature factor $e^{-2W} = e^{-2B(\sin\theta/\lambda)^2}$ was chosen as 0.7×10^{-16}.

Below the Curie Temperature

The patterns obtained at 295° K., above the anomalous region, and at 100° K., below it, are shown in Fig. 4. An extra set of reflections is observed at the lower temperature which can be indexed as the 111, 311, and 331 lines

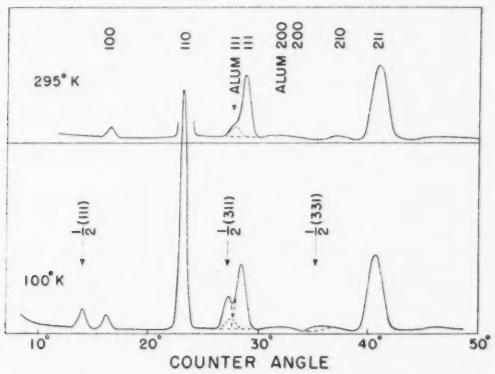

FIG. 4. Neutron diffraction patterns at temperatures of 295° K. and 100° K. for neutrons of wavelength 1.12 Å.

of a unit cell of double the normal size. If the peaks are ascribed a magnetic origin they imply differences in the magnetic population of alternate 111 planes. The other lines are little changed in intensity except for the weak 100 and 200 lines. The structure factors for the observed peaks are listed in Table III. The splittings observed with X-rays could not be seen because of poor resolution.

TABLE III

EXPERIMENTAL STRUCTURE FACTORS FOR $Mn_{3.07}Zn_{0.93}C$ AT 100° K. AND 296° K.

hkl	jF^2e^{-2W} or $\sum q^2F^2e^{-2W}$ *	
	100° K.	296° K.
111/2	0.97×10^{-24}	Not obs.
100	0.88	0.53×10^{-24}
110	29.2	28.4
311/2	4.0	Not obs.
111	13.6	13.2
200	1.8	1.1
331/2	1.3	Not obs.
210	1.3	1.5
211	54.5	52.5

*The equivalent for magnetic reflections (see, for example, Bacon 1955).

The 100 and 111/2 peaks were studied in detail as a function of temperature and the measured structure factors are shown in Fig. 5. The 100 line is

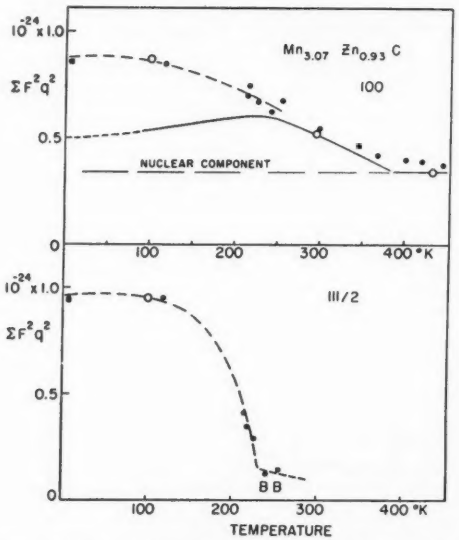

FIG. 5. Structure factors for the 100 and 111/2 lines as functions of the temperature. The dashed straight line represents the nuclear component of the 100 line, the solid curve includes the magnetic component calculated for all the manganese atoms equivalent, i.e. normal ferromagnetism. The points marked "B" were substantially broadened over the usual resolution width.

apparently continuous or nearly so through the anomalous region, the 111/2 line gradually decreases in intensity as the temperature is raised, vanishing at about 231° K. except for a broad component which is also apparent just below 231° K. and is ascribed to short range order or fluctuation scattering.

Diffuse Scattering Measurements

The diffuse scattering of a flat specimen near the forward direction was studied at room temperature (295° K.) and at 425° K. just above the Curie temperature and is shown in Fig. 6. The multiple scattering was computed

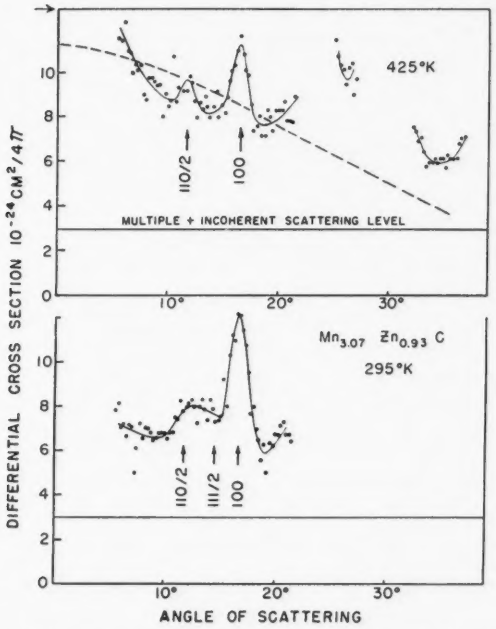

FIG. 6. Diffuse scattering cross section per unit cell for temperatures of 425° K. and 295° K. The horizontal arrow indicates the expected diffuse scattering in the forward direction for uncoupled moments of 1.5 μ_B/Mn atom. The dashed curve indicates the expected scattering in the absence of short range order but including effects of neutron change of energy. The lower curve illustrates short range order contribution at 111/2 position at room temperature.

following Brockhouse, Corliss, and Hastings (1955), the incoherent scattering computed using the compiled cross sections of Hughes and Harvey (1955), and the remainder ascribed to magnetic scattering and, at the larger angles, thermal diffuse scattering. Diffuse scattering is observed which falls off in intensity with increasing angle of scattering as expected for paramagnetic diffuse scattering. Some indication of short range order is observed, anomalous peaking being seen near the forward direction, indicating short range ordering of a ferromagnetic kind (Slotnick 1951; Brockhouse, Corliss, and Hastings 1955).

DISCUSSION

Above the Curie Temperature

The inverse susceptibility vs. temperature curve of Mn_3ZnC shows a small curvature indicating that the Curie–Weiss law is not accurately obeyed (Butters and Myers 1955*a*), but if this is ignored and the number of Bohr magnetons per atom computed in the usual way from the Curie constant it is found that $n_{\mu_B} \simeq 1.6\ \mu_B$. The diffuse scattering expected in the forward direction for uncoupled Mn ions with $n_{\mu_B} = 1.5$ is indicated by the horizontal arrow in Fig. 6. The elastic form factor of Shull and Wollan (1956) was corrected for the effect of the estimated change of neutron energy on scattering (Van Vleck 1939; Brockhouse 1955), and the expected scattering for equivalent Mn ions with $n_{\mu_B} = 1.5$ is shown as the dashed line. Short range order effects of a ferromagnetic kind are observed and at larger angles thermal diffuse scattering is important, but the general agreement is satisfactory. The results therefore indicate simple ferromagnetic coupling of equivalent manganese ions above the Curie temperature, the moment being about 1.5 μ_B per Mn atom.

Between 231° K. and the Curie Temperature

The neutron and X-ray diffraction results establish that a second order transition occurs at about 231° K. Above this temperature the structure is apparently cubic, though the occurrence of ferromagnetism ensures that some small distortion occurs. Because it has not been possible to make single crystals of the material no information on the anisotropy of magnetization is available.

At 295° K. the intensities of the 100 and 200 peaks were significantly higher than at 433° K., above the Curie temperature, as seen by comparing Tables III and II. All Mn atoms contribute equally in the 200 reflection and hence any magnetic intensity arises from the ferromagnetic saturation moment. Because of symmetry the intensity is independent of the orientation of the moments, but because of the large angle of scattering the form factor of the electrons has a very important effect. Calculation of the intensity using the form factor for Mn^{2+} given by Shull and Wollan (1956) gives a result too low by a factor of two. Roberts (1956) has found that the form factor for the Mn ions in MnBi is considerably higher than that for Mn^{2+} ions and since the intensity of this very weak line is known only within 50% it is likely that the extra intensity of the 200 reflection can in fact be accounted for by magnetic scattering.

The structure factor for the 100 line is shown as a function of temperature in Fig. 5. The manganese ions do not contribute equally to this reflection and hence it is sensitive to the magnetic structure. The dashed horizontal line represents the contribution of the ordinary nuclear scattering. Assuming the saturation magnetization to be distributed equally on the manganese atoms the magnetic scattering increases the structure factor below the Curie temperature as shown by the solid line. The intensity of the reflection is independent of the orientations of the moments and because of the small angle of scattering is relatively insensitive to the choice of form factor. The Mn^{2+}

form factor of Shull and Wollan was again used. Agreement with the experimental points is good, indicating that in the region between the transition temperature of 231° K. and the Curie temperature Mn_3ZnC is a normal ferromagnetic substance in which the manganese atoms are magnetically equivalent.

Below the Transition at 231° K.

It has been established that the seemingly normal ferromagnetic alloy Mn_3ZnC undergoes at 231° K. a second order transition resulting in a tetragonally distorted crystal structure and anomalous magnetic properties. The appearance of the 111/2 system of lines in the neutron patterns would seem to imply an additional rhombohedral distortion possibly beyond the resolution of the X-ray measurements, and therefore the low temperature structure is probably triclinic.

It seems certain that the extra system of lines must be assigned a magnetic origin because of the good agreement of the main lines with the calculated intensities (compare Tables II and III). This implies differences in the magnetic population of adjacent 111 planes. The fact that the structure factor of the 100 line is higher than that calculated on the basis of equivalent Mn atoms implies differences between the Mn atoms in adjacent 200 planes. A magnetic structure was looked for which had these properties and in addition satisfied the following requirements:

(*a*) An algebraic mean moment of about 1 μ_B/Mn atom at 0° K. in order to satisfy the magnetization vs. temperature curve (Fig. 1).

(*b*) Possibilities for a tetragonal distortion of the lattice.

(*c*) An arithmetic mean moment of about 1.5 μ_B/Mn atom at 0° K., based on the assumption that this quantity will not change much through the transition.

(*d*) Integral moments per atom as suggested by (*a*).

A structure which satisfies all these requirements is shown in Fig. 7. Manganese atoms of three kinds are arranged as indicated in the one half of the large unit cell shown. The other half is similar but displaced one-half unit along the *X*-axis. The moments lie along a 111 axis as indicated. The algebraic

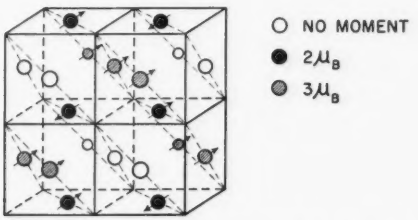

FIG. 7. Possible magnetic structure of Mn_3ZnC at 0° K. Only the manganese ions are shown, the moments being as indicated. The moments are oriented along a 111 body diagonal.

mean moment of the Mn atoms is 1 μ_B, the arithmetic mean is 1.66 μ_B, and there are obvious possibilities of tetragonal distortion. Table IV gives the

TABLE IV

COMPARISON BETWEEN OBSERVED STRUCTURE FACTORS AND THE CALCULATED STRUCTURE FACTORS FOR THE MODEL OF FIG. 7

hkl	$\sum q^2F^2$	
	Experimental	Calculated
111/2	0.97×10^{-24}	0.88×10^{-24}
311/2	4.0 (100° K.)	4.7
331/2	1.3	1.6
100	0.54	0.58
	Diff. (0° K.–433° K.)	

measured structure factors of the various magnetic lines, together with calculated structure factors for the structure of Fig. 7. In the calculated structure factors the form factor for Mn^{2+} of Shull and Wollan was used as before.

The structure of Fig. 7 is a possible structure, and if it is not the real structure the latter must be about as complicated. In particular no model with equal spins on each atom arranged parallel or antiparallel will satisfy the data. It is of interest to note that Kasper and Roberts (1956) have found it necessary to postulate three different kinds of manganese atoms, one with zero moment, in the antiferromagnetic structure of α-manganese.

REMARKS

To determine the structure with certainty a study of specimens of several different compositions would be required in order to determine the orientation and moments of the manganese ions on the cube corners, which become important when small variations in intensity are considered. Analysis of the saturation magnetizations of alloys of varying composition as determined by Butters and Myers (1955 *a* and *b*) suggests that below the transition each corner manganese atom contributes about 4 μ_B parallel to the over-all magnetization and that above the transition each corner atom contributes 4 μ_B antiparallel to the over-all magnetization, as also occurs in Mn_3AlC. But it is uncertain whether the moments on the other atoms remain unchanged upon the addition of corner manganese ions and this could only be determined by the neutron diffraction study.

It is remarkable that this ordering transition does not occur in Mn_3AlC although the two alloys are isomorphous, their lattice constants differing by less than 1½%. By extrapolating the data of Butters and Myers to 0° K. the saturation magnetization of Mn_3AlC is found to be 1.25 μ_B per Mn atom or 3.75 μ_B per unit cell. By extrapolating the data of Mn_3ZnC above the transition at 231° K. in the same way, as in Fig. 1, the saturation magnetization in the high temperature region is found to be 1.57 μ_B per Mn atom or 4.71 μ_B per unit cell. The difference of about 1 μ_B suggests that the zinc and aluminum have their usual valences of 2 and 3 respectively, the manganese ions being

on the average more highly charged in the zinc than in the aluminum compound. This higher average charge for the manganese in the zinc alloy may result in a tendency for different charge states to segregate and order.*

ACKNOWLEDGMENTS

The authors wish to thank Mr. R. G. Butters of the University of British Columbia for preparing the alloy specimen and the Analytical Development Chemistry group at Chalk River for the chemical analyses. We are also indebted to Dr. D. G. Henshaw for the neutron diffraction measurements at liquid helium temperature.

REFERENCES

BACON, G. E. 1955. Neutron diffraction (Oxford University Press).
BROCKHOUSE, B. N. 1955. Phys. Rev. **99**, 601.
BROCKHOUSE, B. N., CORLISS, L. M., and HASTINGS, J. M. 1955. Phys. Rev. **98**, 1721.
BROCKHOUSE, B. N. and MORGAN, E. R. 1954. Unpublished.
BUTTERS, R. G. and MYERS, H. P. 1955*a*. Phil. Mag. (7), **46**, 132.
——— 1955*b*. Phil. Mag. **46**, 895.
——— 1955*c*. Can. J. Technol. **33**, 356.
HOWE, L. M. and MYERS, H. P. 1956. Unpublished.
HUGHES, D. G. and HARVEY, J. A. 1955. Neutron Cross Sections BNL-325 (Supt. of Documents, U.S. Govt. Printing Office, Washington).
KASPER, J. S. and ROBERTS, B. W. 1956. Phys. Rev. **101**, 537.
MORGAN, E. R. 1954. J. Metals, **6**, 983.
PEARSON, W. B. 1954. Unpublished.
ROBERTS, B. W. 1956. Phys. Rev. **104**, 607.
SHULL, C. G. and WOLLAN, E. O. 1956. Advances in solid state physics, Vol. II (Academic Press, Inc., New York), p. 211.
SLOTNICK, M. 1951. Phys. Rev. **83**, 1226.
VAN VLECK, J. H. 1939. Phys. Rev. **55**, 924.

*Since this work was carried out the mixed alloy system $Mn_3Zn_xAl_{1-x}C$ as well as the system $Mn_3Zn_xGa_{1-x}C$ have been studied by Howe and Myers (unpublished). The systems show a complex behavior which could not be interpreted on this simple valence hypothesis and it seems likely that other factors must be considered as well.

THE EMISSION OF IONIZING RADIATION DURING A SPARK DISCHARGE[1]

W. A. Prowse and G. R. Bainbridge[2]

ABSTRACT

A high voltage pulse lasting 0.35 microsecond is applied to a pair of delay lines, so that two pulses can be picked up from adjustable points of connection on the lines. One is applied to an irradiating gap and the other to a longer test gap, the gaps being so arranged that only mid-gap irradiation occurs. The sparking probability, P, of the test gap is used to indicate the presence of ionizing radiation. Variations of P with the time interval between the two pulses are recorded. They indicate that ionizing radiation is emitted in repeated short flashes. Photographic observations support this view.

I. INTRODUCTION

In order to account for the rapidity with which breakdown develops in certain types of sparking, in particular in long gaps at high pressures and high overvoltages, it is usually assumed that photons from the developing electron avalanche produce new electrons in the gas which in turn start new avalanches. If this occurs, penetrating photons generated in one spark gap ought to be capable of triggering breakdown in an adjacent gap by action in the gas alone. This has been observed in various gases (Prowse and Jasinski, 1951), when the adjacent gap was stressed at ultra-high frequencies, and some exploratory experiments with unidirectional pulses have been recorded. The origin of the photons has been discussed by Hopwood (1949), who regards recombination between positive ions and electrons as the most probable source. Whatever the nature of the actual mechanism, it has appeared desirable to examine the action of the radiation liberated in the early stages of breakdown, in particular to look for any time lag in emission and any persistence of the triggering effect after the initial breakdown of the irradiating gap. The experiments to be described constitute an attempt to achieve this objective.

II. EXPERIMENTAL

From a d-c. generator giving up to 30 kilovolts, at intervals arranged to be between 2 and 4 seconds, short pulses were applied to the junction of two similar, properly terminated delay lines. These were arranged in circular form as shown in Fig. 1, each being sectional, consisting of 109 units of inductance and capacitance. The maximum delay possible on each line was 8×10^{-8} sec. Radial connections with a much smaller delay could be taken from any point on either line. One pair of connections was applied to a spark gap with tungsten wire electrodes, set short so that it fired vigorously for every pulse; the other pair was applied to a test gap with plane-ended brass electrodes separated by 0.21 cm. so that in the absence of a triggering process it very rarely broke down. These gaps and their mountings were placed in an evacuable Pyrex

[1]Manuscript received November 5, 1956.
Contribution from the Department of Physics, Durham University, Durham City, England.
[2]Now with the United Kingdom Atomic Energy Authority.

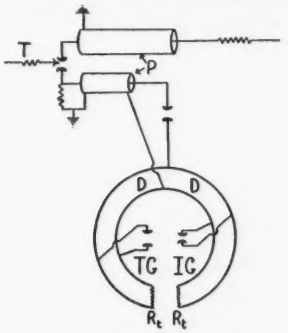

FIG. 1. Circuit diagram showing the method of applying pulses to the circular delay lines (*D*) and the connections to the irradiator (*IG*) and test gap (*TG*). *P* are the pulse-forming condensers, *T* is the trigger lead, and R_t are the proper resistor terminations for the lines.

glass chamber. They were arranged as shown in Fig. 2 so that a narrow collimated beam of radiation from the shorter gap (the irradiator) entered the gas between the electrodes of the larger gap (the test gap) 9.5 cm. away without touching the electrodes. By adjusting the connections it was possible to cause the irradiator pulse to occur earlier than, coincident with, or later than the test pulse.

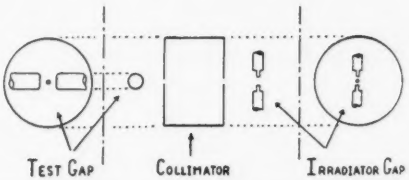

FIG. 2. Arrangement of the spark gaps and collimator in the test chamber. Center shows side elevation. At the ends are the elevations showing the electrodes looking towards the collimator.

Measurements of the effectiveness of the ionizing radiation were made by observing the sparking probability, *P*, of the test gap, where *P* is the fraction of the applied pulses which produce breakdown. In order to make a faithful count of the sparks in the two gaps it was essential that the conduction current only, as distinct from the charging current to the electrodes, should operate the counters. For the strong irradiator spark an inductive connection with electrostatic shield transferred energy sufficient to operate a gas relay tube, so driving an electromechanical counter. Sparks were generally much weaker in the less heavily overvolted test gap and more sensitive discrimination between conduction and displacement currents was required. This was achieved by balancing out the charging current, using a differential transformer with the gap in one branch and an equivalent condenser in the other. A stage of amplification was found necessary to obtain reliable operation of

the gas relay tube and counter in this case. Even with this arrangement, when the irradiator pulse was applied later than the test pulse, incipient weak sparks sometimes occurred; these were visible only in a darkened room, and the current flow was so slight that no automatic count could be made. Their significance is discussed later.

Sparking probabilities were measured for air, nitrogen, oxygen, and hydrogen at several pressures, and for a number of selected voltages applied to the pulse-forming condenser. High gas purity was not attempted in these exploratory experiments, dry commercial cylinder gases with up to 0.25% impurity being used, but mercury vapor was completely excluded by using differential gauges for pressure measurements.

The procedure adopted with each gas was to adjust the irradiator gap so that each applied pulse, at the lowest working voltage, produced a spark without any irradiation. Next the test gap was set so that, in the absence of irradiation, no breakdown occurred there when pulses were applied at the working voltage to be used, but so that the sparking probability exceeded 5/10 when a source equivalent to 1 mg. of radium was placed just outside the test chamber. The test gap was now connected to a place 20 sections down one of the delay lines from the input; the irradiator was connected to a place 20 sections down its own line and a measurement of P was made, with several hundred trials mechanically counted. The process was repeated for various settings of the irradiator connections, after which the test gap connections were altered and a new series of values of P was obtained. Typical examples of the resulting data are shown in Table I for hydrogen, arranged so that the center column gives the value of P (in tenths) for coincident irradiator and test

TABLE I

SPARKING PROBABILITY, P, (IN TENTHS) FOR VARIOUS TIME INTERVALS, Δt, BETWEEN IRRADIATOR AND TEST PULSES; A DOT SIGNIFIES AN OBSERVED ZERO VALUE FOR P

	Irradiator early									Irradiator late							
t	59	51	44	37	29	22	15	7	0	7	15	22	29	37	44	51	$\times 10^{-9}$ sec.
A. Hydrogen, 24 kv., 739 mm. Hg																	
									10	10	10	10	10	10	10	10	
								10	10	10	10	10	10	10	10		
							10	10	10	10	10	10	10	10			
						.	10	10	10	10	10	10	10				
					8	5	10	10	10	10	10	10					
				10	10	5	.	9	10	10	10						
			10	10	8	2	5	10	10	10							
		10	10	10	5	.	10	10	10								
	10	10	10	10	7	.	.	3									
Mean																	
	10	10	10	10	8	2	6	9	10	10	10	10	10	10	10	10	
B. Hydrogen, 16 kv., 550 mm. Hg																	
								10	10	10	10	.	.	.	.		
						10	10	10	10	10	.	.	.	.	.		
				.	3	10	10	10	10	10	6	.					
		10	6	.	.	10	10	10	10								
Mean		10	6	.	2	10	10	10	10	10	5	.	.	.	.		

pulses and each horizontal row corresponds with one setting of the test gap on the delay line. At the head of the table is the value of the interval Δt by which the irradiator pulse differed from the test pulse.

In the first measurements with air it was established that P was quite insensitive to changes in the terminating resistors of the 170 ohm delay lines over the range 100 to 500 ohms. It had earlier been established by oscillographic inspection of the pulse shape that reflections at the terminations were negligible with the lines properly terminated. Further, the attenuation constant for the lines was measured to be 2.6×10^{-3} per section and it will be seen from the P–Δt tables that the attenuation of the pulse on the line has only a minor effect on P. It is accordingly considered legitimate to take the mean values of P in the vertical columns to give a final account of the variation of P with the time interval between irradiator and test pulse.

Some of the results were repeated with the irradiator and test gap connections interchanged, but they showed no measurable electrical asymmetry of the delay lines. Measurements made with various resistors in the leads from the delay lines to the gaps showed that the effect of increasing resistance was to delay the appropriate pulse by an interval consistent with the change in RC value, where C refers to the capacitance of the gap. All reported measurements were made with resistors placed in the leads close to the gaps both to avoid reflections and to give both gap circuits a similar small time constant.

Further tests made with the gap system in open air showed that a thin polythene or paper strip between the irradiator and test gap always brought P to zero, even when the gaps were only 1 cm. apart, confirming that electrostatic coupling was not the agent triggering the test gap. When the gaps were far apart, up to 50 cm., a magnetic field of about 4000 oersteds applied across the line joining the gaps had no effect on P, so excluding the possible action of charged particles. Changes in the material of the electrodes and changes in the waiting interval between successive tests had also no measurable effect on P.

The principal dimensions of the test gap system finally used are shown in Table II together with particulars of the pulse shape.

TABLE II

DETAILS OF TEST SYSTEM AND PULSE SHAPE

Test gap width	0.21 cm.
Irradiator gap width	0.10 cm.
Diameter of collimator aperture, test gap side	0.035 cm.
Diameter of collimator aperture, other side	0.040 cm.
Test gap to near side of collimator	2.20 cm.
Test gap to irradiator	9.50 cm.
Capacitance of test gap	97 $\mu\mu$f.
Capacitance of irradiator gap	195 $\mu\mu$f.
Resistance in series with test gap	150 ohms
Resistance in series with irradiator gap	100 ohms
Rise time of pulse	5×10^{-8} sec.
Duration of flat top of pulse	8×10^{-8} sec.
Duration of tail of pulse	22×10^{-8} sec.

III. RESULTS

i. From Mechanical Counts

The whole range of observations, of which a sample is given in Table I, is summarized in Figs. 3 and 4, where P is plotted as a function of the delay time Δt between the irradiator pulse and the test pulse. Experimental points

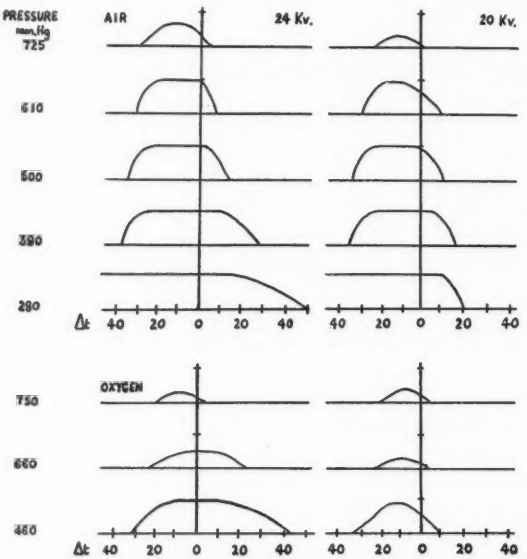

FIG. 3. Probability–time (P–Δt) curves for air and oxygen. P is plotted vertically, with marks at $P = 10/10$. Δt in 10^{-9} seconds. Center lines indicate $\Delta t = 0$.

are omitted for clearness, as only the values of Δt shown in the tables were used. At the lower pressures where no curve is given each pulse produced a spark in the test gap, at first still dependent on irradiation but at still lower pressures the sparks were not dependent on irradiation.

The most remarkable feature of the results is the very small range of time intervals for which the irradiator is effective in triggering the test gap, particularly at low voltages (see Fig. 4), e.g. in nitrogen at 610 mm. Hg pressure with a nominal 20 kilovolt pulse, P exceeds 5/10 for approximately 3×10^{-8} sec., which is less than the rise time of 5×10^{-8} sec. of the applied pulse. It cannot be accepted that the applied voltage exceeds an onset value for such a short time only. The oscillographic measurements showed the pulse to be flat-topped for 8×10^{-8} sec.

The conditions can be envisaged by considering a hypothetical irradiator which would emit a single very short flash of ionizing radiation. If the flash preceded the test pulse by an interval much less than the free life of an electron in the stressed gas, the electrons would be cleared in about 10^{-8} sec., which is small compared with the rise time of the pulse. Thus the sharp fall in P when

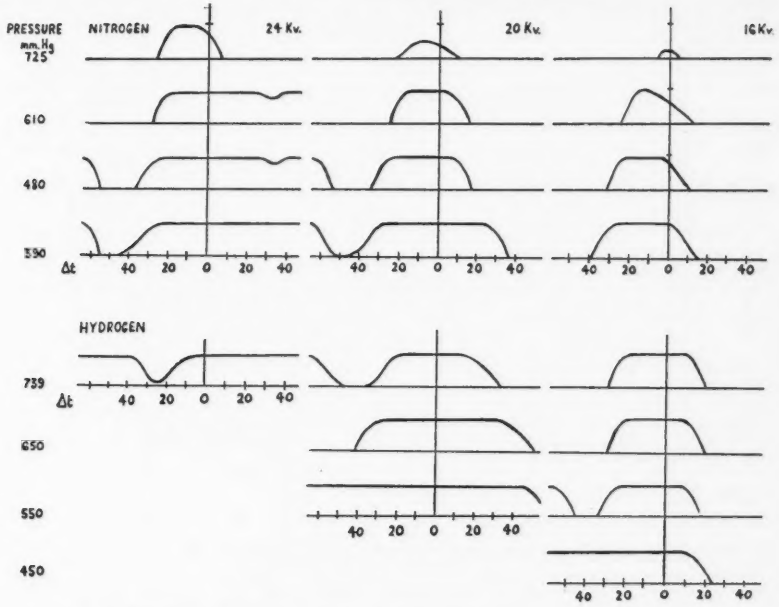

FIG. 4. P–Δt curves for nitrogen and hydrogen. Display as for Fig. 3.

the irradiator is just too early can be accounted for by assuming that the irradiator emits a very brief flash of ionizing radiation which comes to an abrupt end in its effects.

It is possible in Fig. 4 to follow the effect on P of changes in gas pressure for constant pulse amplitude and of changes in pulse amplitude at constant gas pressure. Several of the curves for nitrogen and hydrogen show the separate appearance of an appreciable value of P when the irradiator is some 5×10^{-8} sec. earlier than the test pulse. This clearly indicates a second flash of ionizing radiation. Unfortunately the total length of the delay line was too small to display the effective duration of this second emission.

ii. From Photographic Observations

When the discharges were watched in a darkened room it was seen that in conditions of low sparking probability, particularly when the irradiator was late, occasional very weak sparks occurred. Photographs of the sparks in the test gap were taken with a systematic distribution on the film so that the values of P could be obtained as well as records of brightness and form of the sparks. In no case were faint, non-recording sparks observed in sufficient number to cause a significant correction to the mechanically determined value of P.

In all cases the sparks were brightest for large values of P and then multiple channels were observed in air and nitrogen, but not in oxygen and hydrogen. When multiple channels developed, the brightest of them was usually on the

side of the gap near the irradiator, showing quicker development there. In nitrogen the brightest sparks showed luminous wings in the mid-gap, irradiated part of the spark channel.

In hydrogen, photographs were taken for such overvoltage of the test gap spark that sparking occurred at every trial, whether or not the irradiator was used. The irradiator, when applied, caused the brightness of the sparks to increase as the timing passed through coincidence of the irradiator and test pulses.

Absorption coefficients of the effective radiation have been reported earlier (Bainbridge and Prowse 1956), and the results were shown to be in fair accord with those of other workers in the same pressure range. They confirm that short ultraviolet radiation was the triggering agent in the probability experiments. It will be noticed that in oxygen the values of P are lower than in the other gases and this may be associated with the heavier absorption in this gas.

IV. DISCUSSION

The probability observations described above indicate that the emission of ionizing radiation during the breakdown of a short gap occurs in a very brief flash. In two of the gases, nitrogen and hydrogen, more than a single stage seems to occur in breakdown, in each part of which ionizing radiation is emitted. A similar two-phase breakdown has recently been reported by Saxe (1956), who describes an early diffuse glow in the gap, succeeded by a filamentary channel progressively developing with the glow from cathode to anode.

The photographic observations show that irradiation at a suitable time can still affect the completeness of breakdown, even in conditions where some form of breakdown is certain; also the observation of multiple spark channels with good conditions of irradiation shows that the development of the discharge is associated with the direction of the ultraviolet light source.

If, as appears to be the case from our experiments, ionizing radiation comes from the irradiating gap in a succession of short flashes the first of these may initiate a pilot discharge, the non-recording weak discharge, and later emissions help the conversion of this into a complete spark channel. On this interpretation P is to be regarded as the product of two probabilities, one (P_1) the probability that a pilot discharge will occur, the other (P_2) the probability of conversion of the pilot discharge into a complete spark. Over the range of delay times examined, when the irradiator is too early P_1 is zero and when it is too late P_2 is zero. Repeated emissions of radiation of longer wavelength have been observed by other workers in point discharges (Armin 1954; Gaunt and Craggs 1948; Murphy, Craggs, and Meek 1955; Prime and Saxe 1949; Saxe and Meek 1948, 1955).

The authors gratefully acknowledge the interest taken in this problem by the British Electrical and Allied Industries Research Association.

REFERENCES

ARMIN, M. R. 1954. J. Appl. Phys. **25**, 210, 358.
BAINBRIDGE, G. R. and PROWSE, W. A. 1956. Can. J. Phys. **34**, 1038.
GAUNT, H. M. and CRAGGS, J. D. 1948. Rept. Brit. Elec. Assoc. L/T 294.
HOPWOOD, W. 1949. Proc. Phys. Soc. **62**, 657.
MURPHY, B., CRAGGS, J. D., and MEEK, J. M. 1955. Nature, **176**, 397.
PRIME, H. A. and SAXE, R. F. 1949. Proc. Inst. Elec. Engrs. Part II, **96**, 662.
PROWSE, W. A. and JASINSKI, W. 1951. Inst. Elec. Engrs. Monograph No. 10.
SAXE, R. F. 1956. J. Appl. Phys. **7**, 336.
SAXE, R. F. and MEEK, J. M. 1948. Nature, **162**, 263.
——— 1955. Inst. Elec. Engrs. Monograph No. 124M.

THE NEAR ULTRAVIOLET ABSORPTION SPECTRUM OF 1,2,4-TRIFLUOROBENZENE VAPOR[1]

K. Narahari Rao[2] and H. Sponer

ABSTRACT

The vapor spectrum of 1,2,4-trifluorobenzene at 2810–2460 Å was obtained with a 3 meter grating in an Eagle mounting. The band at 37126 cm^{-1} was taken as the 0–0 band of the $A'—A'$ transition. The excited state vibrations 698, 746, 1274, and 1369 cm^{-1}, which are totally symmetric, appear in progressions and combinations. Their correlation to vibrational modes is discussed. The 1274 belongs to a C—F bond stretching mode. Possibilities are discussed to explain the structure of the first group upon which the spectrum is built.

INTRODUCTION

It was pointed out (Sponer 1954) that the electronic transitions of simple aromatics containing fluorine atoms reveal certain peculiarities not noticed in other substituted benzenes. It is known that the electronic transition which occurs in benzene in the region λ 2700–2200 appears at longer wave lengths upon substitution. This shift increases more or less regularly in the series chlorobenzene, dichlorobenzene, and trichlorobenzene. However, in the series fluorobenzene (Wollman 1946), metafluorobenzene (Rao and Sponer 1952), and 1,3,5-trifluorobenzene (Sastri 1951) the shift becomes smaller when we go from the monoderivative to the diderivative and, in fact, the electronic transition of the symmetric trisubstituted compound shifts to shorter wave lengths.* It was considered useful to study the absorption spectra of 1,2,4-trifluorobenzene and 1,2,4,5-tetrafluorobenzene vapors in the λ 2600 region, as they have not been studied before in this part of the spectrum. The corresponding spectrum of liquid 1,2,4-trifluorobenzene has been obtained by H. D. Stephenson in this laboratory (API Catalog of Ultraviolet Spectral Data, Serial No. 494). This paper deals with the results on the 1,2,4-trifluoro compound.

EXPERIMENTAL

The procedure followed in obtaining the present spectra is the same as in previous similar studies from this laboratory. A 25 cm. quartz absorption cell was used and the spectra were photographed on Eastman Kodak II-0 plates in the first order of a 3 meter grating in a modified Eagle mounting (dispersion 5.535 Å/mm.). A high voltage hydrogen discharge lamp of conventional design was used as the source of light. The measurements have been made

[1]Manuscript received October 23, 1956.

Contribution from the Department of Physics, Duke University, Durham, North Carolina, U.S.A. This work was supported by the Office of Naval Research under Contract N6ori-107, T.O.I with Duke University during 1952–1953.

[2]Present address: Department of Physics, The Ohio State University, Columbus, Ohio, U.S.A.

*An interesting treatment of these shifts based on approximate molecular orbital theory was presented by John A. Petruska at the Symposium on Molecular Structure and Spectroscopy, Columbus, Ohio, June 11–15, 1956.

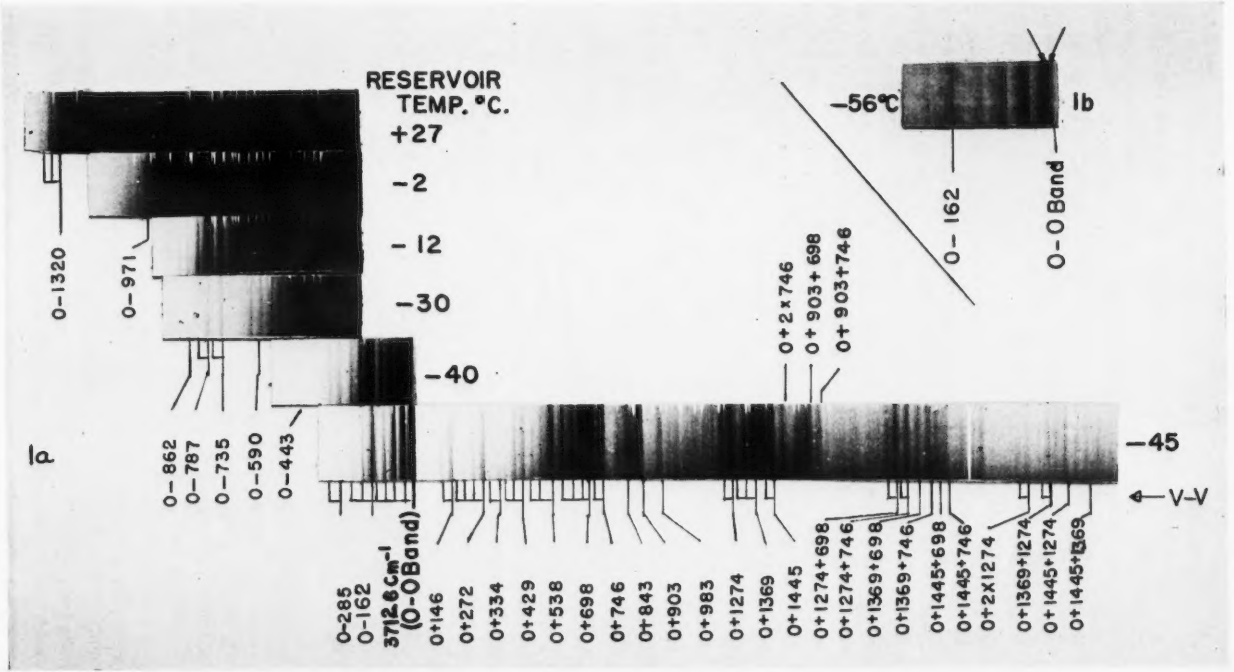

FIG. 1. Near ultraviolet absorption spectrum of 1,2,4-trifluorobenzene.

against an Fe comparison spectrum, and it is believed that the positions of sharp bands were obtained with an accuracy of about 2 cm^{-1}. The sample of 1,2,4-trifluorobenzene was obtained through the courtesy of Mrs. N. B. Moran of the Naval Research Laboratory. It had been prepared by Dr. G. C. Finger and his group of the Illinois State Geological Survey. No information was available as to its purity. Freezing and boiling points of 1,2,4-trifluorobenzene are at −35° C. and 88° C., respectively.*

RESULTS

Figure 1*a* shows how the absorption spectrum of 1,2,4-trifluorobenzene develops with increasing pressure in the absorption cell corresponding to the various temperatures of the side arm containing the substance. At first glance, it appears that the spectrum resembles the spectrum of 1,2,4-trichlorobenzene, which has been analyzed by Kohn and Sponer (1949). This is to be expected, as the two molecules, 1,2,4-$C_6H_3Cl_3$ and 1,2,4-$C_6H_3F_3$, have similar structures.

The characteristic features of the well-developed spectrum of the 1,2,4-trifluorobenzene molecule are five main groups of bands nearly equally spaced from one another. However, at a temperature of −82° C. of the side arm one may distinguish only the bands at 37126 (0–0 band), 37824, and 37872 cm^{-1}.

As can be seen from the reproductions, the bands are degraded to the red and many of them show sharp heads. This discreteness of the spectrum appears to be more pronounced in the fluorobenzenes than in the corresponding chloro-substituted compounds. The doublet appearance of quite a few bands, which was also observed in other cases as, for instance, in the spectrum of 1,2,4-trichlorobenzene, is clearly noticed in the spectrogram taken in the second order of a 6 meter grating in a Wadsworth mounting (illustration given in Fig. 1*b*; this plate was obtained with a Nestor hydrogen lamp providing the continuous radiation). The wave numbers of the bands are listed in Table I. Many of them represent average values calculated from plates taken under different conditions. The intensity classification is indicated at the end of the table.

DISCUSSION

The 1,2,4-trifluorobenzene molecule has the lowest symmetry of the halogenated benzenes and belongs probably to the symmetry class C_s, the only symmetry element being the molecular plane containing all the atoms. Hence there are only two types of electronic and vibrational levels, those symmetrical and those antisymmetrical to the molecular plane. The electronic transition involved in the spectrum is of the allowed type $A'—A'$. The transition moment lies in the molecular plane. It is to be expected that the 0–0 band (the pure electronic transition) should be present in the first group of bands towards longer wave lengths, and the band at 37126 cm^{-1} (2692.7 Å) is assigned as the 0–0 band. As can be clearly seen from Figure 1*a*, towards longer wave

*Taken from a table in Finger *et al.* (1951).

TABLE I

ABSORPTION BANDS OF 1,2,4-TRIFLUOROBENZENE AT 2810–2460 Å

Wave number, cm^{-1}	Intensity[a]			Separation from 0–0 band	Assignments
	27° C.	5° C.	−12° C.		
35572	ew			−1554	0–1514–38
612	vw			−1514	0–1514
659	vw			−1467	0–2×735; 0–1467?
727	vw			−1399	0–1320–2×38
770	w			−1356	0–1320–38
806	s	vw	ew	−1320	0–1320
886		ewd	ew	−1240	0–1240
929		ew		−1197	0–1197
957		ew		−1169	0–2×588
36045	−6.5° C.	ew		−1081	0–1081?
053		ew	ewd	−1073	0–735–344
076	ew		ewd	−1047	0–971–2×38; 0–971–78
106	ewd			−1020	(0–787–238)
117	ewd		ewd	−1009	0–971–38
139	ew		ew	− 987	
155	vw		ew	− 971	0–971
178	vw		vw	− 948	0–503–443
193	ew	−30° C.	ewd	− 933	(0–932)
232	vw	ew	vw	− 894	
243	ew		ew	− 883	0–2×443
264	vw	ew	vw	− 862	0–787–2×38; 0–787–75
278	ew		ew	− 848	0–848
303		vw	mw	− 823	0–787–38
339	m	mw	m	− 787	0–787
355	m	vw	mw	− 771	0–735–38
380	ew	ew		− 746	
391	s	m	s	− 735	0–735
461	ew	ew	−40° C.	− 665	0–588–2×38; 0–588–77
500	−45° C.	vw	ew	− 626	0–588–38
538	ew	vw	ew	− 588	0–588
581		vw	ew	− 545	0–503–38
623	ew	vw	ew	− 503	0–503
660	vw	w	vw	− 466	
683	ew	w	vw	− 443	0–443
766	ew			− 360	0–285–2×38; 0–285–75
782	ew			− 344	0–344

Wave number, cm^{-1}	Intensity[a]			Separation from 0–0 band	Assignments
807	w	−54.5° C.	w	− 319	0–285–38; 0–2×162
841	w	ew	vw	− 285	0–285
888	w	ew	w	− 238	0–238; 0–162–2×38; 0–162–76
924	m	w	m	− 202	0–162–38
934	ew			− 192	
946	vw			− 180	
954	w	ew		− 172	0–162–10
964	m	w	m	− 162	0–162
972	vw			− 154	
979	vw	ew	m	− 147	
37012	mwdb	vw	m	− 114	0–3×39; 0–75–39
027	vw			− 99	
043	ms	mw		− 83	0–75–8
051	sb	m	sb	− 75	0–75; 0–2×39
078	s	ms		− 48	0–39–10
087	sb	ms	sb	− 39	0–39
116	vs	s		− 10	0–10
126	vsb	s	vsb	0	0–0
190*	ew			64	
204	ew	ew		78	
223*	ew			97	0+146–8–39
232	vw	ew		106	0+146–39
263	w			137	0+146–9
272	mw	vw		146	0+146
283	ew			157	0+166–9
292	ew			166	0+166
320	ewd			194	0+273–2×38; 0+273–78
350	vw			224	
360	w	ew		234	0+273–38
384	ewd			258	
391	w	ew		265	0+273–8
399	mw	w		273	0+273
413	ew			287	0+334–38–10
423	vw			297	0+334–38
450	ew			324	0+334–10
460	vw	ew		334	0+334; 0+2×166
483	ewd			357	0+394–38
520	w	ewd		394	0+394
547	vw	ew		421	0+429–8
555	w	vw		429	0+429

TABLE I (*concluded*)

ABSORPTION BANDS OF 1,2,4-TRIFLUOROBENZENE AT 2810–2460 Å

Wave number, cm^{-1}	Intensity[a]		Separation from 0–0 band	Assignments
585	vwd		459	0–285+746; 0+538–2×38
622	vw		496	0+538–38?
628*	ew		502	0–238+746?
664	mw	vw	538	0+538
669	ew		543	0–162–38+746; 0+2×273?
681	ewb		555	0–sep.192+746
711	mw		585	0+746–162; 0+698–3×38
742*	w		616	0+698–2×38–7
749	mw	vw	623	0+698–2×38; 0+698–75
787	msb	mw	661	0+698–38; 0+2×334
817	ms		691	0+698–7
824	s	s	698	0+698
834	m		708	0+746–38
863	ms	mw	737	0+746–9
872	s	s	746	0+746; 0+903–162
922*			796	0+146+698–10–38
932	ew		806	0+146+698–38
942*			816	0+146+746–2×38; 0+2×429–38?
955	ew		829	0+903–2×38
969	vw	ew	843	0+698+146; 0+843?
980	vw	ew	854	0+146+746–38; 0+2×429?
992	ew	ew	866	0+903–38
38020	mwd	w	894	0+146+746; 0+894?
029	w	w	903	0+903
098	vw	ew	972	0+983–10; 0+238+746–10
109	vw	ew	983	0+983; 0+238+746
136*	ew		1010	0+273+746–8
144	vw		1018	0+273+746
180	ew		1054	
217	ew		1091	0–sep.180+1274
237	vw		1111	0+1274–162; 0+273+843?
253	ew		1127	0–sep.147+1274; 0+429+698
284	ew		1158	0+1274–8–3×39
292*	ew		1166	0+1274–3×39
302	ew		1176	0–sep.99+1274; 0+429+746
322	vw	ew	1196	0+1274–2×39; 0+1274–78
361	mw	w	1235	0+1274–39
392	mw	w	1266	0+1274–8
400	m	mw	1274	0+1274; 0+2×146+983; 0+429+843?
415	vwd		1289	0+538+746
458	mw	vw	1332	0+1369–38; 0+2×746–162
488	mw	w	1362	0+1369–7
495	m	w	1369	0+1369; 0+698+746–2×38
523	m	w	1397	0+2×698; 0+746+698–9–38
533	m	w	1407	0+746+698–38
563		w	1437	0+746+698–8
571	m	w	1445	0+746+698; 0+1445?
608	vw		1482	0+2×746–10
618	w	vw	1492	0+2×746; 0+903+586
687	ewd		1561	
716	ewd	ewd	1593	0+698+903–8
727	w		1601	0+698+903; 0+2×429+746; 0+sep.1640–38
736	w		1610	0+746–38+903
766	vw	ewd	1640	0+746+903–8; 0+146+2×746; 0+273+1369
773	vw		1647	0+746+903
794*	ew		1668	0+698+sep.972
801*	ew		1675	0+698+983; 0+273+746+2×334?
986	ewd		1860	0+2×698+538–2×38
39022	ewd		1896	0+698+1274–2×38; 0+2×698+538–38
059	vwd	ew	1933	0+698+1274–38; 0+2×698+538
097	w	vw	1971	0+698+1274
106	vwsh		1980	0+538+sep.1445
147	w	vw	2021	0+746+1274
156*	ewsh		2030	0+538+2×746
191	vw	vw	2065	0+698+1369
220*			2103	0+746+1369–10
239	vw	ew	2113	0+746+1369; 0+146+698+1274
269	vw		2143	0+746+2×698
303	ew		2177	0+903+1274; 0+698+2×746–10
314	ew		2188	0+698+2×746
471	ewd		2345	0+698+746+903
		−40° C.		
626	ew	ew	2500	0+538+698+1274; 0+429+698+1369
672	ew	ew	2546	0+2×1274; 0+429+746+1369
728	ew	ew	2602	0+1274+1369–39; 0+538+698+1369
767	ew	vw	2641	0+1274+1369
797	ew	ew	2671	0+2×698+1274
805		ew	2679	0+698+746+1274–38; 0+538+746+2×698
841	vw	vw	2715	0+698+746+1274
890	ewd	vw	2764	0+2×698+1369
936	ewd	ew	2810	0+698+746+1369
994	ew	ewd	2868	0+2×746+1369; 0+698+1274+903
40038		ew	2912	0+746+903+1274
366		ew	3240	0+698+2×1274; 0+698+746+2×903
417		ewd	3291	0+746+2×1274
461		ewd	3335	0+698+1274+1369
507		ewd	3381	0+746+1274+1369
547		ewd	3421	0+2×698+746+1274
587		ewd	3461	0+3×698+1369; 0+698+2×746+1274
632		ewd	3506	0+2×698+746+1369

[a]Intensity classification: ew = extremely weak, vw = very weak, w = weak, m = medium, s = strong, vs = very strong, d = diffuse, sh = sharp, b = broad.
*Measured from enlarged prints.

lengths from the 0–0 transition, a number of bands were found which appear under different conditions according to their different Boltzmann factors. The separations of these bands from the 0–0 band give obviously the frequencies of vibrations in the ground state, and they should agree with the Raman frequencies. Table II illustrates this agreement. The Raman and infrared data are those of Ferguson, Hudson, Nielsen, and Smith (1953*c*).

TABLE II

VIBRATIONAL FREQUENCIES (IN cm^{-1}) OCCURRING IN ELECTRONIC, RAMAN, AND INFRARED SPECTRA

Electronic			
Upper	Lower	Raman	Infrared
	162	161 α''	
	285	288 α'	286
	344	341 α'	340
	443	442 α'	441
	503	503 α'	
538	588	586 α'	587
698	735	728 α'	728
746	787	781 α'	781
	848?	854 α''	854
903	971	965 α'	963
983?	1081?	1098 α'	1099
	1197	1205 α'	1203
	1240	1250 α'	1250
1274	1320	1308 α'	1312
1369?	1467?	1443 α'	1443
	1514	1518 α'	1522

Towards the violet side of the 0–0 band one observes a number of strong bands, which belong to different groups. The separations of these from the 0–0 band give the frequencies of vibrations in the upper electronic state of the molecule. Prominent bands on the short wave length side of the 0–0 band were found to involve the excited state frequencies 146, 272, 429, 538, 698, 746, 903, 983, 1274, 1369, and possibly 896 and 1445 cm^{-1}. The excited state vibrations 698, 746, 1274, and 1369 are found in several progressions and combinations, and indeed almost all the bands observed towards the farther ultraviolet can be assigned to these combinations and progressions. These frequencies are associated with totally symmetric vibrations (α') in the excited state of the molecule.

In discussing the nature of these various vibrations we shall begin with the identification of the vibrations consisting largely of C—F stretching. There are three α' fundamentals which may be ascribed to fluorine stretching (Ferguson, Hudson, Nielsen, and Smith 1953*c*), i.e. 1204, 1250, and 1308. It may be seen from Table I that all three vibrations show up in the ground state with values 1197, 1240, and 1320 cm^{-1}, the last one with a higher intensity than the other two. A strong reason for choosing the last value for the main C—F bond stretching mode is the occurrence of a medium intense band giving a 1274 vibration in the excited state. Furthermore, a value of 1335 cm^{-1} has been assigned to the C—F stretching vibration in 1,2,4,5-tetrafluoro-

benzene (Ferguson, Hudson, Nielsen, Smith 1953*b*). It will be noticed that the Raman value 1308 is lower than the one derived from ultraviolet absorption, 1320. The Raman spectrum was studied in the liquid state of the molecule and the ultraviolet absorption in the vapor. It may be recalled that in the case of benzene the carbon vibration has the same value in both the liquid and vapor spectrum but the hydrogen vibration is lower in the spectrum of the liquid. Cooper (1954) noticed a similar lowering in the frequency of the totally symmetric fluorine bond stretching vibration in the case of *p*-difluorobenzene where he obtained a value of 1259 cm^{-1} from the ultraviolet absorption data compared to 1245 cm^{-1} in the Raman spectrum of the liquid.

We expect the 1204 and 1250 C—F stretching modes to be lower in the upper electronic state by approximately the same extent as the 1320 vibration. There are a number of weaker bands in the wave-length region in question, some of which have other reasonable explanations, but others like the very weak bands at 1176, 1158, 1091, have more tentative assignments. We do not wish to make suggestions which would only be guesses. There will be mixing between the eigenfunctions of the three C—F stretching modes which will be partly derived from the benzene hydrogen vibrations 3047 ϵ_g^+, 3063 β_{1u}, 3062 α_{1g}, and 3061 ϵ_u^-, together with contributions from some planar C—H bending and ring deformation vibrations, so that correlation with a particular benzene vibration does not seem advisable without normal coordinate treatments of the vibrations.

As was already mentioned, the excited state vibrations 746 and 698 are prominent in the spectrum of 1,2,4-trifluorobenzene. The respective frequencies in the ground state are taken as 787 and 735 (Raman values in the liquid 780.6 and 727.8). The 787 corresponds to the 858.5 vibration in *p*-difluorobenzene, and in the latter case Raman and ultraviolet absorption values agree closely. Delsemme (1950) has assigned the 858.5 cm^{-1} frequency to the symmetric carbon breathing mode, and this is very likely correct. In analogy, we consider the 787 in 1,2,4-trifluorobenzene to be the counterpart of the totally symmetric benzene vibration 992 cm^{-1}.

The origin of the 735 cm^{-1} frequency is not as clear. Although the paper by Ferguson *et al.* (1953*c*) contains a complete analysis with respect to the two vibrational symmetry classes α' and α'', the nature of the vibrations (or "motions") is hardly discussed. Indeed, mixing of vibrational modes derived from different benzene vibrations makes the correlation with individual benzene vibrational modes ambiguous in a number of cases. Even the comparison with the vibrational analyses of *p*-difluorobenzene (Ferguson, Hudson, Nielsen, and Smith 1953*a*) and *p*-tetrafluorobenzene (Ferguson *et al.* 1953*b*) does not remove all ambiguities. It appears that the α' vibrations 964 and 728 (here measured as 971 and 735) may represent vibrational modes related either mainly to the carbon benzene vibration 1010 β_{1u} or to the planar hydrogen vibration 1037 ϵ_u^-. The 964 and 728 appear equally strong in the infrared and Raman spectra and have the same low depolarization factor. We believe that the 971 becomes 903 in the upper electronic state, and the 735 becomes 698. Since relatively small decreases may be expected for either type vibration,

a decision between the possible assignments of the 698 and 903 bands cannot be made from the observed drops. However, the frequent occurrence of the 698 is suggestive of a ring vibration and this would correlate the 735 with the 1010 β_{1u} benzene vibration.

Assignments for a few more bands involving very likely α' vibrations may be suggested. Although numerically the 983 fits closely 235+746, it is rather believed to represent also a fundamental vibration, being possibly the excited state value of the 1081 (Raman value 1098) vibration. The 1369 band also looks like a fundamental, and the 1449 might represent one, although a satisfactory assignment as combination can be offered.

The separations 1274, 746, and 698, by forming progressions and combinations, account for the majority of the bands in the system if the pattern of the first strong group is included, that is, if these vibrations are simply superimposed on the bands of the first group.

In the near ultraviolet benzene spectrum, bands on the long wave-length side from the main bands involve the separations 87 and 161 cm^{-1}. The first is the difference between lower and upper state values of the carbon ring vibration 606 ϵ_g^+, and the second is the corresponding difference of the nonplanar ring bending vibration 404 ϵ_u^+. These vibrations show quite similar decreases in the spectra of the deuterated benzenes (Garforth, Ingold, and Poole 1948). For the halogenated benzenes such a similarity may not, in general, be expected. The benzene 606 splits into two vibrations, suggested as 443 or 503, and 288, in unsymmetric trifluorobenzene. In monofluorobenzene, the corresponding values are 519 α_1 and 617 β_1 respectively. From the low values in unsymmetric ΦF_3 fairly strong v''–v' bands may be expected for these vibrations. Known shifts in the spectra of fluorinated benzenes are, for example: ΦF 617 → 517 (16%) and 519 → 410 (20%) (Wollman), ΦpF_2 452 → 408 (10%) (Cooper). One would expect the percentage decreases to be of the same order in unsymmetric ΦF_3. With this in mind, we have tried a great number of combinations, without being able to offer unambiguous correlations. It is true that for instance the pairs 443 → 394, 503 → 429 show reasonable shifts, and their Δv's fit observation, but they are not the only possibilities, and the important v–v separation of 39 cm^{-1} is not obtainable in an easy, convincing manner. If we assume 285 to decrease by 39 we can explain the intensity of this Δv band but the resulting upper-state vibration of 246 is not observed. If we assume 285 → 274, contrary to the usual lowering of this vibrational mode, we obtain $\Delta v = 11$, which is the separation of the first strong companion on the long wave-length side of many bands. Furthermore, the C—F planar bending mode related to benzene 1037 ϵ_u^- and of value 344 (340–341 infrared, Raman in the liquid) may decrease only slightly in the excited state and may produce the weak band 334, which again gives $\Delta v = 10$. However, it is probable that the "doublet" structure involving the 10 cm^{-1} separation is rotational in origin.

We shall now examine a few other possibilities to explain the structure of the first group by considering out-of-plane vibrations. The 404 ϵ_u^+ benzene vibration assumes the values 161 and 238 in unsymmetric ΦF_3. Bands have

been measured in both locations on the long wave-length side from the 0–0 band. If they cannot be explained in another way—the following discussion shows such possibilities—we must assume that they involve fundamental vibrations and hence represent transitions with a moment perpendicular to the molecular plane. In benzene and substituted benzenes, deuterated and otherwise, the shift of these vibrations in the excited electronic state has been found to be around 40%. It is not certain that this applies to the 1,2,4-compound. If one applies such a percentage decrease here, one may suggest $238 \rightarrow 146$ and $162 \rightarrow 78$ instead of $162 \rightarrow 106$, since the 106 band fits a plausible assignment as $146 - 39$. In this interpretation, there may also be possible the cross-transitions $238 \rightarrow 78$ and $162 \rightarrow 146$ giving Δv's of 160 and 16 cm^{-1}. The bands -162 and 146 show great resemblance in structure and sharpness, suggesting a relationship between them. They look as if they involve the same vibration, which would correspond to an 8% drop and the not-observed $\Delta v = 16$. But this Δv should have been found if this interpretation were correct. Another possibility is that 238 decreases by 39 and gives the very weak diffuse band at 194 which fits also another explanation. Assuming the mentioned possibility to be correct, a band much stronger than 194 should appear at $2 \times (238 - 39) = 398$ cm^{-1}. This would be another way to account for the 394 band. As seen from Table I, the -238 band may also be explained as $0 - 162 - 76$. It is conceivable that this band is actually a superposition of several transitions.

A few remarks may be in order with regard to the possible occurrence of bands resulting from a transition moment perpendicular to the molecular plane. They occur because of excitation of a vibration of appropriate symmetry, in the present case of an out-of-plane (α'') vibration. In the spectra of substituted benzenes such bands are in general very weak, although in some cases moderate intensities have been observed. Their occurrence in unsymmetric ΦF_3 would be easily understandable if the molecule showed deviation from planarity. Benzene derivatives whose substituents are simple atoms are usually considered planar. Bastiansen and Hassel (1947) have found, however, from electron diffraction data, that some steric hindrance is present in *o*-$C_6H_4Cl_2$ causing a small angle (18°) between the chlorine atoms, which lie slightly above and below the molecular plane. Duchesne and Monfils (1954) deduced 20° in 1,2,4-trichlorobenzene from quadrupole spectra. Because of the small size of the fluorine atom one would expect a considerably smaller angle in the fluoro-compound. Indeed, Delbouille (1956) has recently found indication of hexafluorobenzene being planar, whereas Bastiansen and Hassel had found an angle of 12° for C—Cl bending in C_6Cl_6. It is therefore unlikely that any appreciable angular ortho effect is present in 1,2,4-trifluorobenzene, and hence it cannot be used as an argument in favor of perpendicular transitions occurring.

It was noticed that several bands coincide within limits of error with bands of *p*-difluorobenzene (Cooper). We cite as examples the bands 36841 (assignment $0 - 285$) and 37664 (assignment $0 + 538$), which agree closely with 36843 (0–0 band) and 37662 ($0 + 819$) of *p*-$C_6H_4F_2$. Because of a Δv

separation of 38–39 in the 1,2,4-compound and of 40 in the *p*-compound, the respective long wave-length companion bands $0-285-38$ and $0-40$ etc. also show close numerical agreement. However, the strong para-bands $0+1250$, $0+2\times819$, $0+819+1250$ and their -40 companions do not have plausible coincidences in the 1,2,4–spectrum. We therefore conclude that the sample was free of traces of *p*-difluorobenzene and that the mentioned numerical agreements must be accidental. We also checked that the 0–0 band of 1,2,4,5-tetrafluorobenzene (at 36605 cm^{-1})* was missing.

In Table II a collection of vibrational frequencies observed in electronic absorption, Raman, and infrared spectra is given.

In conclusion, we may say that this paper gives an over-all understanding of the lowest singlet absorption spectrum of 1,2,4-trifluorobenzene. Further progress may be sought along the following lines: High resolution observations will reveal fine structure in many bands, so that the vibration type α' or α'' might be fairly easily recognized. Even with our rather low dispersion we have noticed structure in a number of bands. Long absorption columns will permit lower pressure and consequently greater sharpness of the spectrum. Complete correlation of vibrational modes with observed frequencies in fluorinated benzenes would be helpful not only in analysis work like this but also in comparisons among corresponding spectra of different fluorobenzenes and among corresponding spectra of halogenated benzenes with different substituents in the same positions.

ACKNOWLEDGMENT

The writers wish to express their indebtedness to Mrs. N. B. Moran of the Naval Research Laboratory for making the sample available.

REFERENCES

BASTIANSEN, O. and HASSEL, O. 1947. Acta Chem. Scand. **1**, 489.
COOPER, C. D. 1954. J. Chem. Phys. **22**, 503.
DELBOUILLE, L. 1956. J. Chem. Phys. **25**, 182.
DELSEMME, A. H. 1950. J. Chem. Phys. **18**, 1680.
DUCHESNE, J. and MONFILS, A. 1954. J. Chem. Phys. **22**, 1275.
FERGUSON, E. E., HUDSON, R. L., NIELSEN, J. R., and SMITH, D. C. 1953*a*. J. Chem. Phys. **21**, 1457.
——— 1953*b*. J. Chem. Phys. **21**, 1464.
——— 1953*c*. J. Chem. Phys. **21**, 1727.
FINGER, G. C., REED, F. H., BURNESS, D. M., FORT, D. N., and BLOUGH, R. R. 1951. J. Am. Chem. Soc. **73**, 145.
GARFORTH, F. M., INGOLD, C. K., and POOLE, H. G. 1948. J. Chem. Soc. 491.
KOHN, H. and SPONER, H. 1949. J. Opt. Soc. Amer. **39**, 75.
RAO, V. R. and SPONER, H. 1952. Phys. Rev. **87**, 213A.
SASTRI, M. L. N. 1951. Ph.D. Dissertation, Duke University.
SPONER, H. 1954. J. Chem. Phys. **22**, 234.
WOLLMAN, S. H. 1946. J. Chem. Phys. **14**, 123.

*Unpublished measurements by K. Narahari Rao.

TABLES OF CERTAIN CLEBSCH–GORDAN COEFFICIENTS AND OF MATRIX ELEMENTS OF P_2, P_2^2, AND P_2^3 BETWEEN SINGLE-PARTICLE STATES

KAILASH KUMAR*

In the course of an investigation into energy levels in spheroidal nuclei, certain matrix elements were calculated which would be useful to other investigators, and which have not been previously tabulated.

In Table I† we present Clebsch–Gordan vector addition coefficients for the coupling of two angular momenta (j, m) and $(j', -m)$ to give a resultant $(2, 0)$, i.e. $(j\,j'\,m\,-m|2\,0)$. These are tabulated for the ranges $1/2 \leqslant m \leqslant 13/2$ and $1/2 \leqslant j, j' \leqslant 17/2$, with j, j' half odd integers. For $j, j' \leqslant 9/2$ these were taken from Simon's tables (Simon 1954). The remainder were calculated using formulae given in the algebraic tabulation of Sears and Radtke (Sears and Radtke 1954) and from the fundamental formulae.

Tables II, III, and IV† contain the matrix elements of $P_2(\cos\theta)$, $[P_2(\cos\theta)]^2$, and $[P_2(\cos\theta)]^3$ between single-particle states of given l, j, m, compounded from an orbital angular momentum l and spin $1/2$. It can be seen that

$$(l'\ j'\ m|P_2|l\ j\ m) = \int \phi^*_{l'\,j'\,m} P_2 \phi_{l\,j\,m} d\Omega$$

$$= \tfrac{1}{5}(-)^{j+j'+m+\frac{1}{2}}[(2j+1)(2j'+1)]^{\frac{1}{2}}(j\,j'\,-m\ m|2\,0)(j\,j'\,\tfrac{1}{2}\,-\tfrac{1}{2}|2\,0) \text{ if } l+l' \text{ is even.}$$

Otherwise the matrix element is zero. (This equation in a slightly different form was kindly pointed out by Dr. J. M. Kennedy.) This formula was used to calculate the matrix elements of P_2. For a given m, the matrix elements of P_2^2 and P_2^3 were obtained by squaring and cubing the P_2 matrix on the University of Toronto digital computor FERUT.

The matrix elements $(l'\ j'\ m|P_2|l\ j\ m)$ are tabulated for $1/2 \leqslant m \leqslant 13/2$, $1/2 \leqslant j,\ j' \leqslant 17/2$. For P_2^2 and P_2^3 the ranges are $1/2 \leqslant m \leqslant 13/2$, $1/2 \leqslant j, j' \leqslant 13/2$.

The author wishes to express his appreciation of the help given by Professor J. N. P. Hume in connection with the preparation of the problem for FERUT and of the advice of Professor M. A. Preston in connection with the general calculation.

SEARS, B. J. and RADTKE, M. G. 1954. Algebraic Tables of Clebsch–Gordan Coefficients, TPI-75, Chalk River (unpublished).
SIMON, A. 1954. Numerical Table of Clebsch–Gordan Coefficients, ORNL-1718 (unpublished).

RECEIVED DECEMBER 13, 1956.
DEPARTMENT OF PHYSICS,
HAMILTON COLLEGE,
McMASTER UNIVERSITY,
HAMILTON, ONTARIO.

*Now at Mathematics Department, McGill University, Montreal, Que.
†See pages 342–345 for the tables.

TABLE I

CLEBSCH–GORDAN VECTOR ADDITION COEFFICIENTS $(j\,j'\,m\,-m|2\,0)$

Note that $(j\,j'\,m\,-m|2\,0) = (-)^{j+j'}(j'\,j\,-m\,m|2\,0)$

j'	$j = 1/2$	3/2	5/2	7/2	9/2	11/2	13/2	15/2	17/2
					$(jj'\ 1/2\ -1/2\|\ 2\ 0)$				
j		.500000	−.4364357	.3857584	−.3481553	.3193451	−.2964997	.2778594	−.2622963
$j+1$	.7071068	−.2672612	.1543034	−.1040313	.0763381	−.0591312	.0475651	−.0393445	
$j+2$	.7071067	−.5669467	.4879500	−.4351941	.3966644	−.3668997	.3429972		
					$(jj'\ 3/2\ -3/2|\ 2\ 0)$				
j		.50000000	.10910893	−.23145502	.26111645	−.26460029	.25943725	−.25139665	.24262422
$j+1$		.65465358	−.42257712	.29607822	−.22124881	.20483668	−.14012414	.11638250	
$j+2$		.42257712	−.42257712	.39886194	−.37397882	.35160544	−.33210550		
					$(jj'\ 5/2\ -5/2|\ 2\ 0)$				
j			.54554465	−.07715167	−.08703882	.15511052	−.18531232	.19847104	.20327975
$j+1$			.54554472	−.43519413	.34139437	−.27372451	.17515518	−.18834730	
$j+2$			.28867512	−.3256694	.32846934	−.32097036	.31030389		
					$(jj'\ 7/2\ -7/2|\ 2\ 0)$				
j				.54006171	−.17407763	.00912415	.07412493	−.11908262	.14426305
$j+1$				.46056613	−.41391866	.34982518	−.29513397	.25141195	
$j+2$				.21320071	−.25967780	.27486526	−.27754425		
					$(jj'\ 9/2\ -9/2|\ 2\ 0)$				
j					.52223291	−.2281037	.07412493	.01323140	−.06557411
$j+1$					.39666440	−.38516442	.3432326	−.30092732	
$j+2$					.16574838	−.21290765	.23371317		
					$(jj'\ 11/2\ -11/2|\ 2\ 0)$				
j						.50182814	−.25943725	.11908262	−.03278706
$j+1$						.34767674	−.35651204	.33054817	
$j+2$						.13363062	−.17850139		
					$(jj'\ 13/2\ -13/2|\ 2\ 0)$				
j							.48181204	−.27785945	.15082047
$j+1$							.30917346	−.33015769	
$j+2$							.11070186		

TABLE II

MATRIX ELEMENTS OF P_2 BETWEEN SINGLE-PARTICLE STATES
$\langle l' j' m | P_2 | l j m \rangle$
The matrices are symmetric. $l+l'$ must be even

j'	$j = 1/2$	3/2	5/2	7/2	9/2	11/2	13/2	15/2	17/2
					$m = 1/2$				
j	0	.2000000	.22857134	.23809526	.24242424	.24475524	.2461538	.2470587	.24767769
$j+1$	−.2828427	−.06998539	−.03299146	−.0193599	−.01276742	−.00906397	−.00677223	−.00525404	
$j+2$	.3464102	.36365489	.36885551	.37113473	.37234076	.37305714	.37351803		
					$m = 3/2$				
j		−.20000000	.05714284	.14285714	.18181816	.20279713	.21538459	.22352938	.22910198
$j+1$		−.17142850	−.09035079	−.05509922	−.03700350	−.0265366	−.01995059	−.01554167	
$j+2$		.27105234	.3194383	.34015057	.35104623	.35750622	.36165711		
					$m = 5/2$				
j			−.28571419	−.04761904	.06060606	.11888108	.15384613	.17647056	.19195031
$j+1$			−.11664237	−.08098825	−.05709754	−.04195805	−.03199578	−.02515181	
$j+2$			.21821789	.27773177	.30832741	.32635701	.33791554		
					$m = 7/2$				
j				−.33333332	−.12121211	−.0069930	−.06153845	.10588233	.1362228
$j+1$				−.08570991	−.06922722	−.05362319	−.04202058	−.03357384	
$j+2$				.18181816	.24375421	.27947816	.30224086		
					$m = 9/2$				
j					−.36363636	−.17482512	−.06153845	.01176470	.06191946
$j+1$					−.06634148	−.05904019	−.04886877	−.0401857	
$j+2$					.1555846	.21648075	.25450957		
					$m = 11/2$				
j						−.38461526	−.21538459	−.10588233	−.03095973
$j+1$						−.05329387	−.05075952	−.04414125	
$j+2$						.13587326	.1943849		
					$m = 13/2$				
j							−.39999995	−.24705878	−.14241476
$j+1$							−.0440195	−.04408911	
$j+2$							.1205524		

TABLE III

MATRIX ELEMENTS OF P_z^2 BETWEEN SINGLE-PARTICLE STATES

$\langle l' j' m | P_z^2 | l j m \rangle$

The matrices are symmetric. $l+l'$ must be even

Entries consist of a seven figure number, followed by its sign, followed by a power of 10 with its sign, e.g. 1.820332+ 1− = $+1.820332\times10^{-1}$

j'	$j = 1/2$	3/2	5/2	7/2	9/2	11/2	13/2
				$m = 1/2$			
j	2.000000+ 1−	2.571428+ 1−	3.142857+ 1−	3.281385+ 1−	3.339994+ 1−	3.370629+ 1−	3.388731+ 1−
$j+1$	8.081219− 2−	1.399708− 1−	4.798755− 2−	2.621032− 2−	1.678004− 2−	1.172985− 2−	8.684007− 3−
$j+2$	9.897430+ 2−	1.616244+ 1−	1.743680+ 1−	1.794498+ 1−	1.820332+ 1−	1.835361+ 1−	1.844905+ 1−
$j+3$	1.142857− 1−	3.285482− 2−	1.695361− 2−	1.057243− 2−	7.284556− 3−	5.345615− 3−	
$j+4$	1.277753+ 1−	1.349650+ 1−	1.373399+ 1−	1.384545+ 1−	1.390760+ 1−		
				$m = 3/2$			
j		1.428571+ 1−	1.428571+ 1−	2.207791+ 1−	2.627373+ 1−	2.867132+ 1−	3.015221+ 1−
$j+1$		0	8.213705− 2−	5.933762− 2−	4.228972− 2−	3.121952− 2−	2.386435− 2−
$j+2$		0	8.131155+ 2−	1.196134+ 1−	1.404185+ 1−	1.529438+ 1−	1.610618+ 1−
$j+3$		6.969560− 2−	4.255321− 2−	2.836881− 2−	2.023256− 2−	1.515339− 2−	
$j+4$		9.219861+ 2−	1.121376+ 1−	1.216059+ 1−	1.269584+ 1−		
				$m = 5/2$			
j			1.428571+ 1−	9.956705+ 2−	1.561772+ 1−	2.027972+ 1−	2.357055+ 1−
$j+1$			2.120769+ 2−	4.236305− 2−	4.567810− 2−	3.948989− 2−	3.276123− 2−
$j+2$			3.967596− 2−	2.441596+ 2−	6.851719+ 2−	9.773256+ 2−	1.176547+ 1−
$j+3$			4.485500− 2−	3.662398− 2−	2.849936− 2−	2.238675− 2−	
$j+4$			6.728256+ 2−	9.063971+ 2−	1.041886+ 1−		
				$m = 7/2$			
j				1.515151+ 1−	8.624709+ 2−	1.188826+ 1−	1.591938+ 1−
$j+1$				2.637228+ 2−	1.977921− 2−	3.154316− 2−	3.216901− 2−
$j+2$				5.594405− 2−	1.083352− 2−	2.989069+ 2−	6.118232+ 2−
$j+3$				3.064182− 2−	2.959019− 2−	2.559027− 2−	
$j+4$				5.081420+ 2−	7.367248+ 2−		
				$m = 9/2$			
j					1.608392+ 1−	8.531467+ 2−	9.864257+ 2−
$j+1$					2.653659+ 2−	6.945909− 3−	2.057633− 2−
$j+2$					6.223384− 2−	3.241422− 2−	2.060794+ 3−
$j+3$					2.196488− 2−	2.372572− 2−	
$j+4$					3.959777+ 2−		
				$m = 11/2$			
j						1.692307+ 1−	8.959277+ 2−
$j+1$						2.507945+ 2−	4.857503+ 4−
$j+2$						6.394033− 2−	4.564503− 2−
$j+3$						1.635714− 2−	
				$m = 13/2$			
j							1.764706+ 1−
$j+1$							2.316815+ 2−
$j+2$							6.344861− 2−

TABLE IV

MATRIX ELEMENTS OF P_{2^3} BETWEEN SINGLE-PARTICLE STATES

$\langle l' j' m | P_{2^3} | l j m \rangle$

The matrices are symmetric. $l+l'$ must be even. The notation is explained in Table III

j'	$j = 1/2$	3/2	5/2	7/2	9/2	11/2	13/2
				$m = 1/2$			
j	5.714285+ 2−	1.428571+ 1−	1.818181+ 1−	2.055944+ 1−	2.137862+ 1−	2.178880+ 1−	2.202690+ 1−
$j+1$	1.212183− 1−	9.543464− 2−	8.236325− 2−	3.663487− 2−	2.246638− 2−	1.543000− 2−	
$j+2$	1.484615+ 1−	1.873373+ 1−	2.104798+ 1−	2.177867+ 1−	2.213186+ 1−	1.711954+ 1−	
$j+3$	6.233766− 2−	6.444600− 2−	2.543041− 2−	1.492579− 2−	1.002311− 2−		
$j+4$	6.969561+ 2−	9.343728+ 2−	9.888474+ 2−	1.012230+ 1−	1.024770+ 1−		
$j+5$	4.404676− 2−	1.345651− 2−	7.254763− 3−	4.676440− 3−			
$j+6$	4.757596+ 2−	5.034964+ 2−	5.129894+ 2−				
				$m = 3/2$			
j		2.857142− 2−	4.155843+ 2−	8.291703+ 2−	1.278721+ 1−	1.559029+ 1−	1.737903+ 1−
$j+1$		4.675322− 2−	4.359582− 2−	6.357601− 2−	4.944166− 2−	3.770989− 2−	
$j+2$		7.392334+ 2−	1.058837+ 1−	1.457788+ 1−	1.699182+ 1−	1.375476+ 1−	
$j+3$		1.608360− 2−	4.255320− 2−	3.254069− 2−	2.441599− 2−		
$j+4$		2.127659+ 2−	5.382605+ 2−	7.051100+ 2−	8.018420+ 2−		
$j+5$		2.691302− 2−	1.745025− 2−	1.214974− 2−			
$j+6$		3.296158+ 2−	4.055536+ 2−				
				$m = 5/2$			
j			5.194802− 2−	2.996994+ 3−	2.797202+ 2−	6.705056+ 2−	9.985062+ 2−
$j+1$			2.691745− 2−	1.868959− 2−	3.828897− 2−	3.936001− 2−	
$j+2$			5.035796+ 2−	6.409193+ 2−	9.673018+ 2−	8.525777+ 2−	
$j+3$			5.884424− 9−	2.262068− 2−	2.474946− 2−		
$j+4$			2.960661+ 9−	2.513537+ 2−	4.386887+ 2−		
$j+5$			1.679150− 2−	1.465557− 2−			
$j+6$			2.273582+ 2−				
				$m = 7/2$			
j				6.293706− 2−	1.398601− 2−	4.115078+ 4−	2.869083+ 2−
$j+1$				1.977921− 2−	8.726255− 3−	2.212770− 2−	
$j+2$				4.195831+ 2−	4.492727+ 2−	3.857462+ 2−	
$j+3$				5.407360+ 3−	1.067917− 2−		
$j+4$				8.967226− 3−	7.754996+ 3−		
$j+5$				1.096724− 2−			
				$m = 9/2$			
j				6.993007− 2−		2.328259− 2−	1.381282− 2−
$j+1$				1.639025− 2−		4.935251− 3−	
$j+2$				3.843855+ 2−		1.938051+ 2−	
$j+3$				6.936277+ 3−			
$j+4$				1.250456− 2−			
				$m = 11/2$			
j						7.511306− 2−	2.953084− 2−
$j+1$						1.435469− 2−	
$j+2$						2.921308+ 2−	
				$m = 13/2$			
j							7.925695− 2−

CONDUCTIVITY OF α-MANGANESE*

G. K. WHITE AND S. B. WOODS

It is well known that manganese has a complex crystal structure and in many of its physical properties appears somewhat anomalous by comparison with other transition elements (see recent book by Sully (1955), for review of the metallurgy and physical properties of manganese). Measurements by Meissner and Voigt (1930) on the electrical resistance of α-manganese indicated little change as the temperature was reduced from room temperature to liquid helium temperatures, but more recently Patrick (1954) reported a broad resistance minimum at about 90° K., i.e. in the vicinity of the Neel temperature of 100° K. established by the neutron diffraction studies of Shull and Wilkinson (1953).

We have recently made some measurements of electrical and thermal resistance on electrolytic flake manganese in a cryostat which could be controlled at temperatures from 2° K. up to room temperature (White and Woods 1955). Specimen Mn 1 was cut from material supplied by A. D. MacKay Inc., and was annealed *in vacuo* at 600° C. for some hours to remove adsorbed hydrogen, then cooled slowly. Our spectrographic analyses showed that this material was of comparable high purity to that subsequently obtained from Messrs. Johnson Matthey & Mallory Ltd.; the latter material (JM10792) is stated by the suppliers to be of high purity with 10 parts per million of magnesium as the major solid impurity, and was the source of our specimens Mn 2 (unannealed) and Mn 3 (annealed).

Data for Mn 1 are given in Fig. 1. The electrical resistance exhibits a rather shallow minimum in the vicinity of 100° K. and falls rapidly below 50° K.; for $T < 20°$ K., the resistivity, ρ, may be expressed as a sum of a constant term, ρ_0, and a term quadratic in the temperature, thus $\rho = \rho_0 + BT^2$.

Values of the so-called "ideal" electrical resistivity, $\rho_i = \rho - \rho_0$ (assuming Matthiessen's rule to be valid), are plotted in Fig. 2 for the annealed specimens Mn 1 and Mn 3, and the values quoted in the caption for the residual resistivity, ρ_0, indicate that the total resistance falls by a factor of about 10 as the temperature is decreased from room temperature to liquid helium temperatures. In the unannealed specimen Mn 2 there was much less change in the resistivity, which only fell from about 378×10^{-6} ohm cm. (room temperature) to 330×10^{-6} ohm cm. at 4.2° K. The room temperature value for the resistivities of Mn 1 and Mn 3 of about 150×10^{-6} ohm cm. agrees with the value for α-manganese quoted as "probable" by Sully; owing to the rather uncertain geometry of these flakes, the absolute values of resistivity may be in error by as much as 20%.

The thermal conductivity measurements (Fig. 3) for Mn 2 and Mn 3 also appear to be rather unusual. For Mn 2 (unannealed) the conductivity varies approximately linearly with temperature and the data are not very different from those obtained by Rosenberg (1955) on a vacuum-annealed sample. The thermal conductivity, K, of our specimen Mn 2 is many times greater

*Issued as N.R.C. No. 4193.

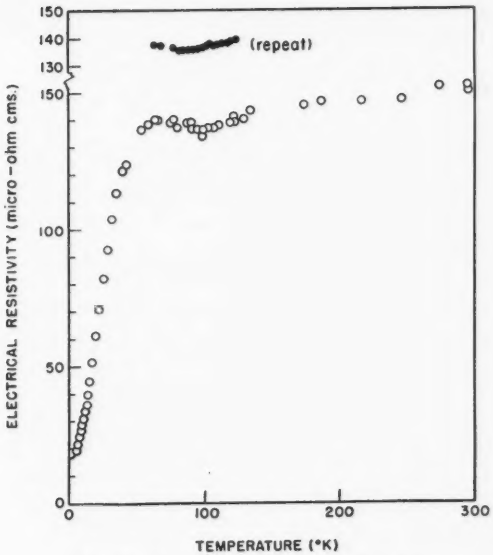

FIG. 1. Electrical resistivity of Mn 1.

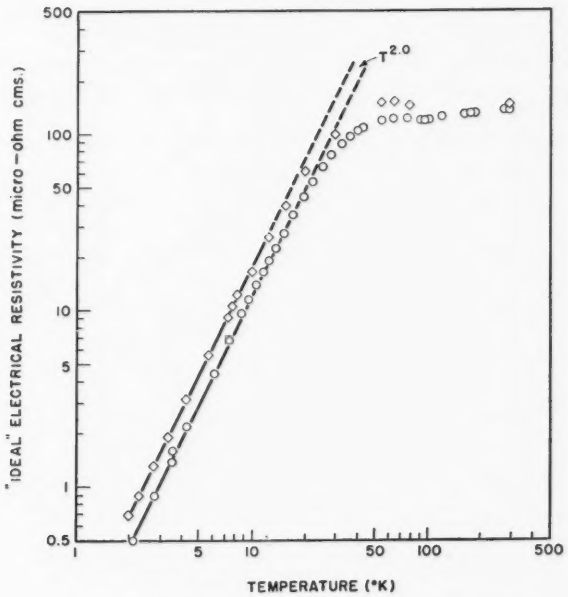

FIG. 2. "Ideal" electrical resistivity of manganese.
○ Mn 1 ($\rho_0 = 16.8 \times 10^{-6}$ ohm cm.)
◇ Mn 3 ($\rho_0 = 11.3 \times 10^{-6}$ ohm cm.)

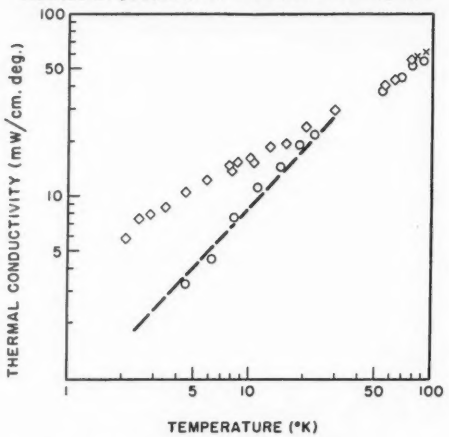

FIG. 3. Thermal conductivity of manganese.
○ Mn 2 —— Rosenberg (1955)
◇ Mn 3 × Reddemann (1935) (β-manganese)

than would be calculated from its residual electrical resistance using the Wiedemann–Franz law:

$$\rho K/T = 2.45\times10^{-8} \text{ watt ohm/deg.}^2,$$

suggesting that a substantial part of the thermal conductivity must be due to conduction by lattice waves. However in Mn 3, the thermal conductivity is comparable with that deduced from the Wiedemann–Franz law, but increases rather more slowly with temperature than expected theoretically. All in all, both the electrical and thermal resistivities of magnesium appear quite anomalous.

We may contrast these anomalous transport properties with those observed for other transition elements (for example Kemp *et al.* 1956), and for the monovalent metals (reviews by Klemens 1956; MacDonald 1956). The electrical resistivity appears to be of particular interest because it is very difficult to understand how any process of scattering of electrons by thermal vibrations or static imperfections can explain the type of temperature dependence shown in Figs. 1 and 2. The possibility of internal cracks in the specimens seems to be discounted, as the surface of a manganese flake was polished, etched, and examined under the microscope and showed no evidence of such cracking.

KEMP, W. R. G., KLEMENS, P. G., and WHITE, G. K. 1956. Australian J. Phys. **9**, 180.
KLEMENS, P. G. 1956. Handb. der Physik, **14**, 198.
MACDONALD, D. K. C. 1956. Handb. der Physik, **14**, 137.
MEISSNER, W. and VOIGT, B. 1930. Ann. Physik, **7**, 892.
PATRICK, L. 1954. Phys. Rev. **93**, 370.
REDDEMANN, H. 1935. Ann. Physik, **22**, 28.
ROSENBERG, H. M. 1955. Trans. Roy. Soc. (London), **247**, 441.
SHULL, C. G. and WILKINSON, M. K. 1953. Revs. Mod. Phys. **25**, 100.
SULLY, A. H. 1955. Manganese (Butterworth Scientific Publications, London).
WHITE, G. K. and WOODS, S. B. 1955. Can. J. Phys. **33**, 58.

RECEIVED OCTOBER 26, 1956.
DIVISION OF PURE PHYSICS,
NATIONAL RESEARCH COUNCIL,
OTTAWA, CANADA.

CANADIAN JOURNAL OF PHYSICS

Notes to Contributors

Manuscripts

(i) ***General.*** Manuscripts, in English or French, should be typewritten, double spaced, on paper 8½×11 in. **The original and one copy are to be submitted.** Tables and captions for the figures should be placed at the end of the manuscript. Every sheet of the manuscript should be numbered.

Style, arrangement, spelling, and abbreviations should conform to the usage of this journal. Names of all simple compounds, rather than their formulas, should be used in the text. Greek letters or unusual signs should be written plainly or explained by marginal notes. Superscripts and subscripts must be legible and carefully placed.

Manuscripts and illustrations should be carefully checked before they are submitted. Authors will be charged for unnecessary deviations from the usual format and for changes made in the proof that are considered excessive or unnecessary.

(ii) ***Abstract.*** An abstract of not more than about 200 words, indicating the scope of the work and the principal findings, is required, except in Notes.

(iii) ***References.*** References should be listed **alphabetically by authors' names,** unnumbered, and typed after the text. The form of the citations should be that used in current issues of this journal; in references to papers in periodicals, titles should not be given and only initial page numbers are required. The names of periodicals should be abbreviated in the form given in the most recent *List of Periodicals Abstracted by Chemical Abstracts.* All citations should be checked with the original articles and each one referred to in the text by the authors' names and the year.

(iv) ***Tables.*** Tables should be numbered in roman numerals and each table referred to in the text. Titles should always be given but should be brief; column headings should be brief and descriptive matter in the tables confined to a minimum. Vertical rules should be used only when they are essential. Numerous small tables should be avoided.

Illustrations

(i) ***General.*** All figures (including each figure of the plates) should be numbered consecutively from 1 up, in arabic numerals, and each figure referred to in the text. The author's name, title of the paper, and figure number should be written in the lower left corner of the sheets on which the illustrations appear. Captions should not be written on the illustrations (see Manuscripts (i)).

(ii) ***Line Drawings.*** Drawings should be carefully made with India ink on white drawing paper, blue tracing linen, or co-ordinate paper ruled in blue only; any co-ordinate lines that are to appear in the reproduction should be ruled in black ink. Paper ruled in green, yellow, or red should not be used unless it is desired to have all the co-ordinate lines show. All lines should be of sufficient thickness to reproduce well. Decimal points, periods, and stippled dots should be solid black circles large enough to be reduced if necessary. Letters and numerals should be neatly made, preferably with a stencil (**do NOT use typewriting**) and be of such size that the smallest lettering will be not less than 1 mm. high when reproduced in a cut 3 in. wide.

Many drawings are made too large; originals should not be more than 2 or 3 times the size of the desired reproduction. In large drawings or groups of drawings the ratio of height to width should conform to that of a journal page but the height should be adjusted to make allowance for the caption.

The original drawings and one set of clear copies (e.g. small photographs) are to be submitted.

(iii) ***Photographs.*** Prints should be made on glossy paper, with strong contrasts. They should be trimmed so that essential features only are shown and mounted carefully, with rubber cement, on white cardboard with no space or only a **very** small space (less than 1 mm.) between them. In mounting, full use of the space available should be made (to reduce the number of cuts required) and the ratio of height to width should correspond to that of a journal page (4⅛×7½ in.); however, allowance must be made for the captions. Photographs or groups of photographs should not be more than 2 or 3 times the size of the desired reproduction.

Photographs are to be submitted in duplicate; if they are to be reproduced in groups one set should be mounted, the duplicate set unmounted.

Reprints

A total of 50 reprints of each paper, without covers, are supplied free. Additional reprints, with or without covers, may be purchased.

Charges for reprints are based on the number of printed pages, which may be calculated approximately by multiplying by 0.6 the number of manuscript pages (double-spaced typewritten sheets, 8½×11 in.) and including the space occupied by illustrations. An additional charge is made for illustrations that appear as coated inserts. The cost per page is given on the reprint requisition which accompanies the galley.

Any reprints required in addition to those requested on the author's reprint requisition form must be ordered officially as soon as the paper has been accepted for publication.

Contents

Printed in Canada *by* University of Toronto Press